



Universiteit Gent
Faculteit Wetenschappen
Vakgroep Fysica en Sterrenkunde

² No title yet

³ No sub-title neither, obviously...

⁴ Alexis Fagot

5



Thesis to obtain the degree of
Doctor of Philosophy in Physics
Academic years 2012-2017



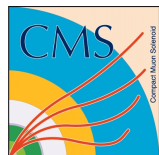


Universiteit Gent
Faculteit Wetenschappen
Vakgroep Fysica en Sterrenkunde

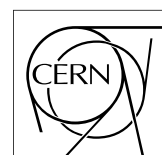
Promotoren: Dr. Michael Tytgat
Prof. Dr. Dirk Ryckbosch

Universiteit Gent
Faculteit Wetenschappen
Vakgroep Fysica en Sterrenkunde
Proeftuinstraat 86, B-9000 Gent, België
Tel.: +32 9 264.65.28
Fax.: +32 9 264.66.97

17



Thesis to obtain the degree of
Doctor of Philosophy in Physics
Academic years 2012-2017



Acknowledgements

¹⁹ Ici on remerciera tous les gens que j'ai pu croiser durant cette aventure et qui m'ont permis de passer
²⁰ un bon moment

²¹ *Gent, ici la super date de la mort qui tue de la fin d'écriture*
²² *Alexis Fagot*

Table of Contents

24	Acknowledgements	i
25	Nederlandse samenvatting	xvii
26	English summary	xix
27	1 Introduction	1-1
28	1.1 A story of High Energy Physics	1-1
29	1.2 Organisation of this study	1-1
30	2 Investigating the TeV scale	2-1
31	2.1 The Standard Model of Particle Physics	2-1
32	2.2 The Large Hadron Collider and the Compact Muon Solenoid	2-1
33	2.3 Muon Phase-II Upgrade	2-1
34	3 Amplification processes in gaseous detectors	3-1
35	3.1 Signal formation	3-1
36	3.2 Gas transport parameters	3-1
37	4 Resistive Plate Chambers	4-1
38	4.1 Principle	4-1
39	4.2 Rate capability of Resistive Plate Chambers	4-3
40	4.2.1 Operation modes	4-3
41	4.3 High time resolution	4-3
42	4.3.1 Electron drift velocity	4-3
43	4.4 Resistive Plate Chambers at CMS	4-3
44	4.4.1 Overview	4-3
45	4.4.2 The present RPC system	4-3
46	4.4.3 Pulse processing of CMS RPCs	4-4
47	5 Longevity studies and Consolidation of the present CMS RPC subsystem	5-1
48	5.1 Testing detectors under extreme conditions	5-1
49	5.1.1 The Gamma Irradiation Facilities	5-3
50	5.1.1.1 GIF	5-3
51	5.1.1.2 GIF++	5-5
52	5.2 Preliminary tests at GIF	5-7
53	5.2.1 Resistive Plate Chamber test setup	5-7
54	5.2.2 Data Acquisition	5-9
55	5.2.3 Geometrical acceptance of the setup layout to cosmic muons	5-9
56	5.2.3.1 Description of the simulation layout	5-10
57	5.2.3.2 Simulation procedure	5-12

58	5.2.3.3	Results	5-13
59	5.2.4	Photon flux at GIF	5-13
60	5.2.4.1	Expectations from simulations	5-13
61	5.2.4.2	Dose measurements	5-18
62	5.2.5	Results and discussions	5-19
63	5.3	Longevity tests at GIF++	5-20
64	5.3.1	Description of the Data Acquisition	5-23
65	5.3.2	RPC current, environmental and operation parameter monitoring	5-24
66	5.3.3	Measurement procedure	5-25
67	5.3.4	Longevity studies results	5-25
68	6	Investigation on high rate RPCs	6-1
69	6.1	Rate limitations and ageing of RPCs	6-1
70	6.1.1	Low resistivity electrodes	6-1
71	6.1.2	Low noise front-end electronics	6-1
72	6.2	Construction of prototypes	6-1
73	6.3	Results and discussions	6-1
74	7	Conclusions and outlooks	7-1
75	7.1	Conclusions	7-1
76	7.2	Outlooks	7-1
77	A	A data acquisition software for CAEN VME TDCs	A-1
78	A.1	GIF++ DAQ file tree	A-1
79	A.2	Usage of the DAQ	A-2
80	A.3	Description of the readout setup	A-3
81	A.4	Data read-out	A-3
82	A.4.1	V1190A TDCs	A-4
83	A.4.2	DataReader	A-6
84	A.4.3	Data quality flag	A-10
85	A.5	Communications	A-12
86	A.5.1	V1718 USB Bridge	A-13
87	A.5.2	Configuration file	A-13
88	A.5.3	WebDCS/DAQ intercommunication	A-17
89	A.5.4	Example of inter-process communication cycle	A-18
90	A.6	Software export	A-18
91	B	Details on the offline analysis package	B-1
92	B.1	GIF++ Offline Analysis file tree	B-1
93	B.2	Usage of the Offline Analysis	B-2
94	B.2.1	Output of the offline tool	B-3
95	B.2.1.1	ROOT file	B-3
96	B.2.1.2	CSV files	B-5
97	B.3	Analysis inputs and information handling	B-6
98	B.3.1	Dimensions file and IniFile parser	B-6
99	B.3.2	TDC to RPC link file and Mapping	B-7
100	B.4	Description of GIF++ setup within the Offline Analysis tool	B-9
101	B.4.1	RPC objects	B-9
102	B.4.2	Trolley objects	B-10
103	B.4.3	Infrastructure object	B-11

104	B.5 Handeling of data	B-12
105	B.5.1 RPC hits	B-13
106	B.5.2 Clusters of hits	B-14
107	B.6 DAQ data Analysis	B-15
108	B.6.1 Determination of the run type	B-16
109	B.6.2 Beam time window calculation for efficiency runs	B-17
110	B.6.3 Data loop and histogram filling	B-18
111	B.6.4 Results calculation	B-19
112	B.6.4.1 Rate normalisation	B-19
113	B.6.4.2 Rate and activity	B-21
114	B.6.4.3 Strip masking tool	B-23
115	B.6.4.4 Output CSV files filling	B-25
116	B.7 Current data Analysis	B-29

List of Figures

117

118 2.1	Absorbed dose in the CMS cavern after an integrated luminosity of 3000 fb. R is the 119 transverse distance from the beamline and Z is the distance along the beamline from 120 the Interaction Point at Z=0.	2-2
121 2.2	A quadrant of the muon system, showing DTs (yellow), RPCs (light blue), and CSCs 122 (green). The locations of new forward muon detectors for Phase-II are contained 123 within the dashed box and indicated in red for GEM stations (ME0, GE1/1, and 124 GE2/1) and dark blue for improved RPC (iRPC) stations (RE3/1 and RE4/1).	2-2
125 2.3	RMS of the multiple scattering displacement as a function of muon p_T for the pro- 126 posed forward muon stations. All of the electromagnetic processes such as bremsstrahlung 127 and magnetic field effect are included in the simulation.	2-3
128 4.1	Different phases of the avalanche development in the RPC gas volume subjected to 129 a constant electric field E_0 . a) An avalanche is initiated by the primary ionisation 130 caused by the passage of a charged particle through the gas volume. b) Due to 131 its growing size, the avalanche starts to locally influence the electric field. c) The 132 electrons, lighter than the cations reach the anode first. d) The ions reach the cathode. 133 While the charges have not been recombined, the electric field in the small region 134 around the avalanche stays affected and locally blind the detector.	4-2
135 4.2	Signals from the RPC strips are shaped by the FEE described on Figure 4.2a. Out- 136 put LVDS signals are then read-out by a TDC module connected to a computer or 137 converted into NIM and sent to scalers. Figure 4.2b describes how these converted 138 signals are put in coincidence with the trigger.	4-5
139 4.3	Description of the principle of a CFD. A comparison of threshold triggering (left) 140 and constant fraction triggering (right) is shown in Figure 4.3a. Constant fraction 141 triggering is obtained thanks to zero-crossing technique as explained in Figure 4.3b. 142 The signal arriving at the input of the CFD is split into three components. A first 143 one is delayed and connected to the inverting input of a first comparator. A sec- 144 ond component is connected to the noninverting input of this first comparator. A 145 third component is connected to the noninverting input of another comparator along 146 with a threshold value connected to the inverting input. Finally, the output of both 147 comparators is fed through an AND gate.	4-6
148 5.1	(5.1a) Extrapolation from 2016 data of single hit rate per unit area in the barrel 149 region. (5.1b) Extrapolation from 2016 data of single hit rate per unit area in the 150 endcap region.	5-2
151 5.2	Background Fluka simulation compared to 2016 Data at $L = 10^{34} cm^{-2}.s^{-1}$ in 152 the fourth endcap disk region. A mismatch in between simulation and data can be 153 observed. [To be understood.]	5-3

154	5.3	Layout of the test beam zone called X5c GIF at CERN. Photons from the radioactive source produce a sustained high rate of random hits over the whole area. The zone is surrounded by 8 m high and 80 cm thick concrete walls. Access is possible through three entry points. Two access doors for personnel and one large gate for material. A crane allows installation of heavy equipment in the area.	5-4
155			
156			
157			
158			
159	5.4	^{137}Cs decays by β^- emission to the ground state of ^{137}Ba (BR = 5.64%) and via the 662 keV isomeric level of ^{137}Ba (BR = 94.36%) whose half-life is 2.55 min.	5-5
160			
161	5.5	Floor plan of the GIF++ facility. When the facility downstream of the GIF++ takes electron beam, a beam pipe is installed along the beam line (z-axis). The irradiator can be displaced laterally (its center moves from $x = 0.65$ m to 2.15 m), to increase the distance to the beam pipe.	5-5
162			
163			
164			
165	5.6	Simulated unattenuated current of photons in the xz plane (Figure 5.6a) and yz plane (Figure 5.6b) through the source at $x = 0.65$ m and $y = 0$ m. With angular correction filters, the current of 662 keV photons is made uniform in xy planes.	5-6
166			
167			
168	5.7	Description of the RPC setup. Dimensions are given in mm. A tent containing RPCs is placed at 1720 mm from the source container. The source is situated in the center of the container. RE-4-2-BARC-161 chamber is 160 mm inside the tent. This way, the distance between the source and the chambers plan is 2060 mm. Figure 5.7a provides a side view of the setup in the xz plane while Figure 5.7b shows a top view in the yz plane.	5-7
169			
170			
171			
172			
173			
174	5.8	RE-4-2-BARC-161 chamber is inside the tent as described in Figure 5.7. In the top right, the two scintillators used as trigger can be seen. This trigger system has an inclination of 10° relative to horizontal and is placed above half-partition B2 of the RPCs. PMT electronics are shielded thanks to lead blocks placed in order to protect them without stopping photons from going through the scintillators and the chamber.	5-8
175			
176			
177			
178			
179	5.9	Hit distributions over all 3 partitions of RE-4-2-BARC-161 chamber is showed on these plots. Top, middle and bottom figures respectively correspond to partitions A, B, and C. These plots show that some events still occur in other half-partitions than B2, which corresponds to strips 49 to 64, in front of which the trigger is placed, contributing to the inefficiency of detection of cosmic muons. In the case of partitions A and C, the very low amount of data can be interpreted as noise. On the other hand, it is clear that a little portion of muons reach the half-partition B1, corresponding to strips 33 to 48.	5-9
180			
181			
182			
183			
184			
185			
186			
187	5.10	Results are derived from data taken on half-partition B2 only. On the 18 th of June 2014, data has been taken on chamber RE-2-BARC-161 at building 904 (Prevessin Site) with cosmic muons providing us a reference efficiency plateau of $(97.54 \pm 0.15)\%$ represented by a black curve. A similar measurement has been done at GIF on the 21 st of July with the same chamber giving a plateau of $(78.52 \pm 0.94)\%$ represented by a red curve.	5-10
188			
189			
190			
191			
192			
193	5.11	Representation of the layout used for the simulations of the test setup. The RPC is represented as a yellow trapezoid while the two scintillators as blue cuboids looking at the sky. A green plane corresponds to the muon generation plane within the simulation. Figure 5.7a shows a global view of the simulated setup. Figure 5.7b shows a zommed view that allows to see the 2 scintillators as well as the full RPC plane.	5-11
194			
195			
196			
197			
198	5.12	γ flux $F(D)$ is plot using values from table 5.1. As expected, the plot shows similar attenuation behaviours with increasing distance for each absorption factors.	5-14
199			

200	5.13	Figure 5.13a shows the linear approximation fit done via formulae 5.7 on data from table 5.2. Figure 5.13b shows a comparison of this model with the simulated flux using a and b given in figure 5.13a in formulae 5.4 and the reference value $D_0 =$ 50cm and the associated flux for each absorption factor F_0^{ABS} from table 5.1	5-16
204	5.14	Dose measurements has been done in a plane corresponding to the tents front side. This plan is 1900 mm away from the source. As explained in the first chapter, a lens-shaped lead filter provides a uniform photon flux in the vertical plan orthogonal to the beam direction. If the second line of measured fluxes is not taken into account because of lower values due to experimental equipments in the way between the source and the tent, the uniformity of the flux is well showed by the results.	5-18
210	5.15	5-19
211	5.16	Evolution of the maximum efficiency for RE2 (5.16a) and RE4 (5.16b) chambers with increasing extrapolated γ rate per unit area at working point. Both irradiated (blue) and non irradiated (red) chambers are shown.	5-21
214	5.17	Evolution of the working point for RE2 (5.17a) and RE4 (5.17b) with increasing extrapolated γ rate per unit area at working point. Both irradiated (blue) and non irradiated (red) chambers are shown.	5-21
217	5.18	Evolution of the maximum efficiency at HL-LHC conditions, i.e. a background hit rate per unit area of 300 Hz/cm^2 , with increasing integrated charge for RE2 (5.18a) and RE4 (5.18b) detectors. Both irradiated (blue) and non irradiated (red) chambers are shown. The integrated charge for non irradiated detectors is recorded during test beam periods and stays small with respect to the charge accumulated in irradiated chambers.	5-22
223	5.19	Comparison of the efficiency sigmoid before (triangles) and after (circles) irradiation for RE2 (5.19a) and RE4 (5.19b) detectors. Both irradiated (blue) and non irradiated (red) chambers are shown.	5-22
226	5.20	Evolution of the Bakelite resistivity for RE2 (5.20a) and RE4 (5.20b) detectors. Both irradiated (blue) and non irradiated (red) chambers are shown.	5-23
228	5.21	Evolution of the noise rate per unit area for the irradiated chamber RE2-2-BARC-9 only.	5-23
230	A.1	(A.1a) View of the front panel of a V1190A TDC module [28]. (A.1b) View of the front panel of a V1718 Bridge module [29]. (A.1c) View of the front panel of a 6U 6021 VME crate [30].	A-3
233	A.2	Module V1190A <i>Trigger Matching Mode</i> timing diagram [28].	A-4
234	A.3	Structure of the ROOT output file generated by the DAQ. The 5 branches (<code>EventNumber</code> , <code>number_of_hits</code> , <code>Quality_flag</code> , <code>TDC_channel</code> and <code>TDC_TimeStamp</code>) are visible on the left panel of the ROOT browser. On the right panel is visible the histogram cor- responding to the variable <code>nHits</code> . In this specific example, there were approximately 50k events recorded to measure the gamma irradiation rate on the detectors. Each event is stored as a single entry in the <code>TTree</code>	A-10
240	A.4	The effect of the quality flag is explained by presenting the content of <code>TBranch</code> <code>number_of_hits</code> of a data file without <code>Quality_flag</code> in Figure A.4a and the con- tent of the same <code>TBranch</code> for data corresponding to a <code>Quality_flag</code> where all TDCs were labelled as <code>GOOD</code> in Figure A.4b taken with similar conditions. It can be noted that the number of entries in Figure A.4b is slightly lower then in Figure A.4a due to the excluded events.	A-12

246 A.5 Using the same data as previously showed in Figure A.4, the effect of the quality 247 flag is explained by presenting the reconstructed hit multiplicity of a data file without 248 <code>Quality_flag</code> in Figure A.5a and the reconstructed content of the same RPC 249 partition for data corresponding to a <code>Quality_flag</code> where all TDCs were labelled as 250 <code>GOOD</code> in Figure A.5b taken with similar conditions. The artificial high content of bin 251 0 is completely suppressed.	A-12
252 A.6 WebDCS DAQ scan page. On this page, shifters need to choose the type of scan 253 (Rate, Efficiency or Noise Reference scan), the gamma source configuration at the 254 moment of data taking, the beam configuration, and the trigger mode. These in- 255 formation will be stored in the DAQ ROOT output. Are also given the minimal 256 measurement time and waiting time after ramping up of the detectors is over before 257 starting the data acquisition. Then, the list of HV points to scan and the number of 258 triggers for each run of the scan are given in the table underneath.	A-14
259 B.1 Example of expected hit time distributions in the cases of efficiency (Figure B.1a) 260 and noise/gamma rate per unit area (Figure B.1b) measurements as extracted from 261 the raw ROOT files. The unit along the x-axis corresponds to ns. The fact that 262 "the" muon peak is not well defined in Figure B.1a is due to the contribution of all 263 the RPCs being tested at the same time that don't necessarily have the same signal 264 arrival time. Each individual peak can have an offset with the ones of other detectors. 265 The inconsistancy in the first 100 ns of both time distributions is an artefact of the 266 TDCs and are systematically rejected during the analysis.	B-16
267 B.2 The effect of the quality flag is explained by presenting the reconstructed hit multi- 268 plicity of a data file without <code>Quality_flag</code> . The artificial high content of bin 0 is the 269 effect of corrupted data.	B-19
270 B.3 Display of the masking tool page on the webDCS. The window on the left allows the 271 shifter to edit <code>ChannelsMapping.csv</code> . To mask a channel, it only is needed to set the 272 3rd field corresponding to the strip to mask to 0. It is not necessary for older mapping 273 file formats to add a 1 for each strip that is not masked as the code is versatile and 274 the default behaviour is to consider missing mask fields as active strips. The effect 275 of the mask is directly visible for noisy channels as the corresponding bin turns red. 276 The global effect of masking strips will be an update of the rate value showed on the 277 histogram that will take into consideration the rejected channels.	B-24

List of Tables

278

279 5.1	Total photon flux ($E\gamma \leq 662$ keV) with statistical error predicted considering a	
280 ^{137}Cs activity of 740 GBq at different values of the distance D to the source along		
281 the x-axis of irradiation field [24].		5-13
282 5.2	Correction factor c is computed thanks to formulae 5.5 taking as reference $D_0 =$	
283 50 cm and the associated flux F_0^{ABS} for each absorption factor available in table 5.1.		5-15
284 5.3	The data at D_0 in 1997 is taken from [24]. In a second step, using Equations 5.8	
285 and 5.9, the flux at D can be estimated in 1997. Then, taking into account the		
286 attenuation of the source activity, the flux at D can be estimated at the time of the		
287 tests in GIF in 2014. Finally, assuming a sensitivity of the RPC to γ $s = 2 \cdot 10^{-3}$,		
288 an estimation of the hit rate per unit area is obtained.		5-17
289 A.1	Inter-process communication cycles in between the webDCS and the DAQ through	
290 file string signals.		A-19

List of Acronyms

List of Acronyms

A

297 **AFL** Almost Full Level

B

302 **BARC** Bhabha Atomic Research Centre
303 **BLT** Block Transfer
304 **BR** Branching Ratio

C

309 **CAEN** Costruzioni Apparecchiature Elettroniche Nucleari S.p.A.
310 **CERN** European Organization for Nuclear Research
311 **CFD** Constant Fraction Discriminator
312 **CMS** Compact Muon Solenoid
313 **CSC** Cathode Strip Chamber

D

318 **DAQ** Data Acquisition
319 **DCS** Detector Control Software
320 **DQM** Data Quality Monitoring
321 **DT** Drift Tube

F

326	FEE	Front-End Electronics
327	FEB	Front-End Board
328		
329	G	
330		
332	GE-/-	Find a good description
333	GE1/1	Find a good description
334	GE2/1	Find a good description
335	GEANT	GEometry ANd Tracking - a series of software toolkit platforms developed by CERN
336		
337	GEM	Gas Electron Multiplier
338	GIF	Gamma Irradiation Facility
339	GIF++	new Gamma Irradiation Facility
340		
341	H	
342		
343		
344	HL-LHC	High Luminosity LHC
345	HV	High Voltage
346		
347	I	
348		
349		
350	iRPC	improved RPC
351	IRQ	Interrupt Request
352		
353	L	
354		
355		
356	LHC	Large Hadron Collider
357	LS1	First Long Shutdown
358	LS3	Third Long Shutdown
359	LV	Low Voltage
360	LVDS	Low-Voltage Differential Signaling
361		
362	M	
363		
364		
365	MC	Monte Carlo
366	MCNP	Monte Carlo N-Particle
367	ME-/-	Find good description
368	ME0	Find good description

369		
370	N	
371		
372		
373	NIM	Nuclear Instrumentation Module logic signals
374		
375	P	
376		
377		
378	PMT	PhotoMultiplier Tube
379		
380	R	
381		
382		
383	RE-/-	Find a good description
384	RE2/2	Find a good description
385	RE3/1	Find a good description
386	RE3/2	Find a good description
387	RE4/1	Find a good description
388	RE4/2	Find a good description
389	RE4/3	Find a good description
390	RMS	Root Mean Square
391	ROOT	a framework for data processing born at CERN
392	RPC	Resistive Plate Chamber
393		
394	S	
395		
396		
397	SPS	Super Proton Synchrotron
398		
399	T	
400		
401		
402	TDC	Time-to-Digital Converter
403		
404	W	
405		
406		
407	webDCS	Web Detector Control System

409

Nederlandse samenvatting –Summary in Dutch–

410

411 Le resume en Neerlandais (j'aurais peut-être de apprendre la langue juste pour ca...).

English summary

⁴¹³ Le meme résume mais en Anglais (on commencera par la hein!).

1

Introduction

414

415

⁴¹⁶ **1.1 A story of High Energy Physics**

⁴¹⁷ **1.2 Organisation of this study**

2

418

419

Investigating the TeV scale

420 2.1 The Standard Model of Particle Physics

421 2.2 The Large Hadron Collider and the Compact Muon Solenoid

422 2.3 Muon Phase-II Upgrade

423 After the more than two years lasting First Long Shutdown (LS1), the Large Hadron Collider (LHC)
424 delivered its very first Run-II proton-proton collisions early 2015. LS1 gave the opportunity to the
425 LHC and to the its experiments to undergo upgrades. The accelerator is now providing collisions
426 at center-of-mass energy of 13 TeV and bunch crossing rate of 40 MHz, with a peak luminosity
427 exceeding its design value. During the first and upcoming second LHC Long Shutdown, the Compact
428 Muon Solenoid (CMS) detector is also undergoing a number of upgrades to maintain a high system
429 performance [1].

430 From the LHC Phase-2 or High Luminosity LHC (HL-LHC) period onwards, i.e. past the Third
431 Long Shutdown (LS3), the performance degradation due to integrated radiation as well as the average
432 number of inelastic collisions per bunch crossing, or pileup, will rise substantially and become a
433 major challenge for the LHC experiments, like CMS that are forced to address an upgrade program
434 for Phase-II [2]. Simulations of the expected distribution of absorbed dose in the CMS detector
435 under HL-LHC conditions, show in figure 5.14 that detectors placed close to the beamline will have
436 to withstand high irradiation, the radiation dose being of the order of a few tens of Gy.

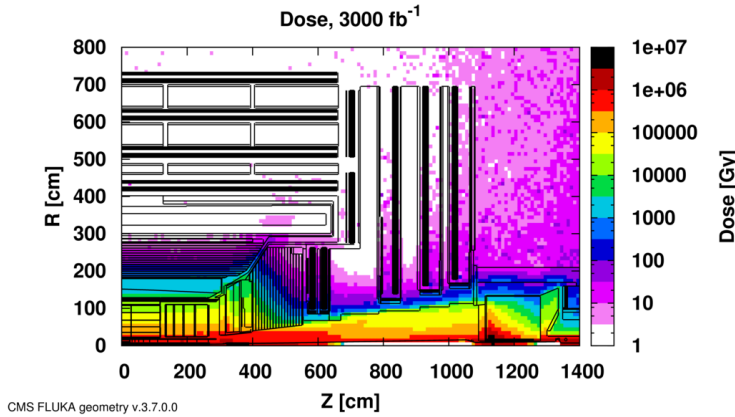


Figure 2.1: Absorbed dose in the CMS cavern after an integrated luminosity of 3000 fb^{-1} . R is the transverse distance from the beamline and Z is the distance along the beamline from the Interaction Point at $Z=0$.

437 The measurement of small production cross-section and/or decay branching ratio processes, such
 438 as the Higgs boson coupling to charge leptons or the $B_s \rightarrow \mu^+ \mu^-$ decay, is of major interest and
 439 specific upgrades in the forward regions of the detector will be required to maximize the physics
 440 acceptance on the largest possible solid angle. To ensure proper trigger performance within the
 441 present coverage, the muon system will be completed with new chambers. In figure 2.2 one can
 442 see that the existing Cathode Strip Chambers (CSCs) will be completed by Gas Electron Multipliers
 443 (GEMs) and Resistive Plate Chambers (RPCs) in the pseudo-rapidity region $1.6 < |\eta| < 2.4$ to
 444 complete its redundancy as originally scheduled in the CMS Technical Proposal [3].

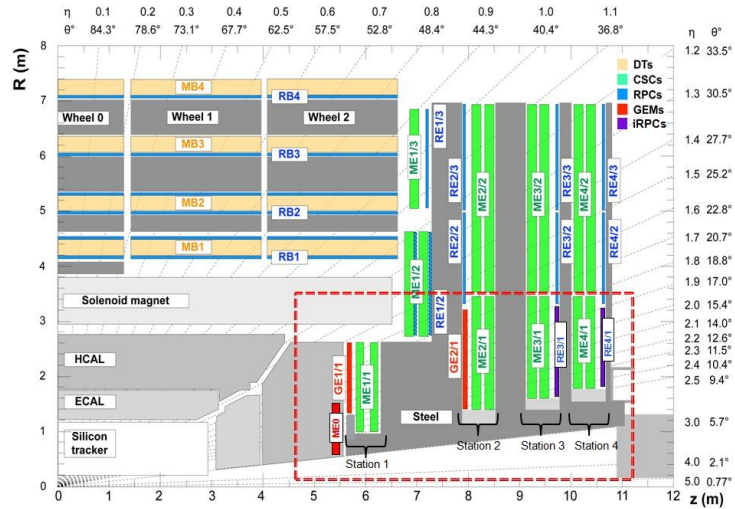


Figure 2.2: A quadrant of the muon system, showing DTs (yellow), RPCs (light blue), and CSCs (green). The locations of new forward muon detectors for Phase-II are contained within the dashed box and indicated in red for GEM stations (ME0, GE1/1, and GE2/1) and dark blue for improved RPC (iRPC) stations (RE3/1 and RE4/1).

445 RPCs are used by the CMS first level trigger for their good timing performances. Indeed, a very

446 good bunch crossing identification can be obtained with the present CMS RPC system, given their
 447 fast response of the order of 1 ns. In order to contribute to the precision of muon momentum mea-
 448 surements, muon chambers should have a spatial resolution less or comparable to the contribution
 449 of multiple scattering [1]. Most of the plausible physics is covered only considering muons with
 450 $p_T < 100$ GeV thus, in order to match CMS requirements, a spatial resolution of $\mathcal{O}(\text{few mm})$ the
 451 proposed new RPC stations, as shown by the simulation in figure 2.3. According to preliminary
 452 designs, RE3/1 and RE4/1 readout pitch will be comprised between 3 and 6 mm and 5 η -partitions
 453 could be considered.

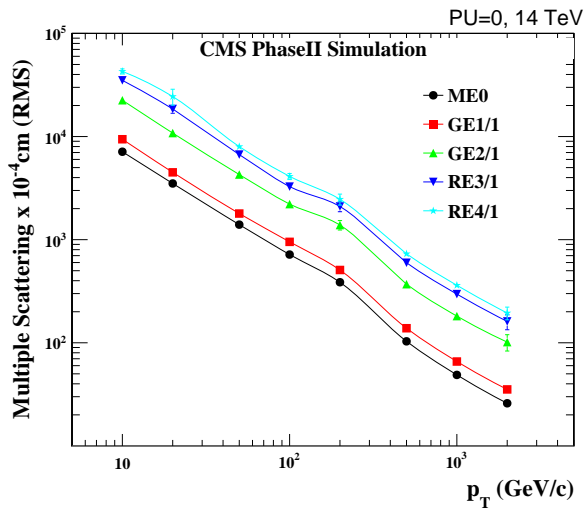


Figure 2.3: RMS of the multiple scattering displacement as a function of muon p_T for the proposed forward muon stations. All of the electromagnetic processes such as bremsstrahlung and magnetic field effect are included in the simulation.

3

454

Amplification processes in gaseous detectors

456 **3.1 Signal formation**

457 **3.2 Gas transport parameters**

4

458

459

Resistive Plate Chambers

460 A Resistive Plate Chamber (RPC) is a gaseous detector using the same physical processes described
461 in Chapter 3. It has been developed in 1981 by Santonico and Cardarelli [4], under the name of
462 *Resistive Plate Counter*, as an alternative to the local-discharge spark counters proposed in 1978
463 by Pestov and Fedotovich [5, 6]. Working with spark chambers implied using high-pressure gas
464 and high mechanical precision which the RPC simplified by formerly using a gas mixture of argon
465 and butane flowed at atmospheric pressure and a constant and uniform electric field propagated
466 in between two parallel electrode plates. Moreover, a significant increase in rate capability was
467 introduced by the use of electrode plate material with high bulk resistivity, preventing the discharge
468 from growing throughout the whole gas gap. Indeed, the effect of using resistive electrodes is that
469 the constant electric field is locally canceled out by the development of the discharge, limiting its
470 growth.

471 Through its development history, different operating modes [7–9] and new detector designs [10–
472 12] have been discovered, leading to further improvement of the rate capability of such a detector.
473 Moreover, the addition of SF_6 into the gas mix improved the stability of operation of the RPC [13,
474 14].

475 The low developing costs and easily achievable large detection areas offered by RPCs, as well
476 as the wide range of possible designs, made them a natural choice to as muon chambers and/or
477 trigger detectors in multipurpose experiments such as CMS [1] or ATLAS [15], time-of-flight detec-
478 tors in ALICE [16], calorimeter with CALICE [17] or even detectors for volcanic muography with
479 ToMuVol [18].

480 4.1 Principle

481 RPCs are composed of two parallel resistive plate electrodes in between which a constant electric
482 field is set. The space in between the electrodes, referred as *gap*, is filled with a dense gas that is
483 used to generate primary ionization into the gas volume. The free charge carriers (electrons and
484 cations) created by the ionization of the gas molecules are then accelerated towards the electrodes

485 by the electric field, as shown in Figure 4.1 taken from the thesis of Lippmann [19].

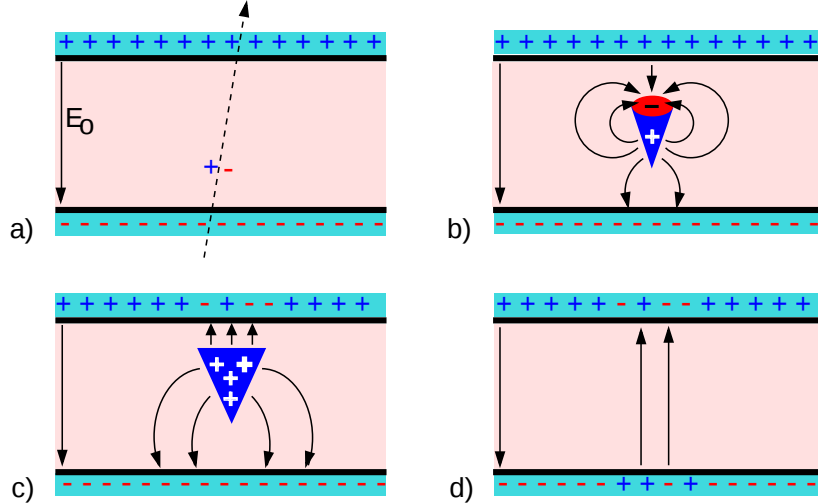


Figure 4.1: Different phases of the avalanche development in the RPC gas volume subjected to a constant electric field E_0 . a) An avalanche is initiated by the primary ionisation caused by the passage of a charged particle through the gas volume. b) Due to its growing size, the avalanche starts to locally influence the electric field. c) The electrons, lighter than the cations reach the anode first. d) The ions reach the cathode. While the charges have not been recombined, the electric field in the small region around the avalanche stays affected and locally blind the detector.

486 RPCs being passive detectors, a current on pick-up copper read-out placed outside of the gas
 487 volume is induced by the charge accumulation during the growth of the avalanche. As a result,
 488 the time resolution of the detector is substantially increased as the output signal is generated while
 489 the electrons are still in movement. The advantage of a constant electric field, over multi-wire
 490 proportional chambers, is that the electrons are being fully accelerated from the moment charge
 491 carriers are freed and feel the full strength of the electric field that doesn't depend on the distance to
 492 the readout and that the output signal doesn't need for the electrons to be physically collected.

493 The typical gas mixture RPCs are operated with is generally composed of 3 gas compounds.

- 494 • Tetrafluoroethane ($C_2F_4H_2$), also referred to as *Freon*, is the principal compound of the RPC
 495 gas mixtures, with a typical fraction above 90%. It is used for it's high effective Townsend
 496 coefficient and the great average fast charge that allows to operate the detector with a high
 497 threshold with respect to argon, for example, that has similar effective Townsend coefficient
 498 but suffers from a lower fast charge. To operate with similar conditions, argon would require a
 499 higher electric field leading to a higher fraction of streamers, thus limiting the rate capability
 500 of the detector [20].
- 501 • Isobutane (C_4H_{10}), only present in a few percent in the gas mixtures, is used for its UV
 502 quenching properties [21] helping to prevent streamers due to UV photon emission during the
 503 avalanche growth.
- 504 • Sulfur hexafluoride, (SF_6), referred to simply as *SF6*, is used in very little quantities for its
 505 high electronegativity. Excess of electrons are being absorbed by the compound and streamers

506 are suppressed [14]. Nevertheless, a fraction of SF_6 higher than 1% will not bring any extra
 507 benefice in terms of streamer cancelation power but will lead to higher operating voltage.

508 **Talk about electrodes resistivity and it's effect on charge recombination and rate capability.**

509 **4.2 Rate capability of Resistive Plate Chambers**

510 **4.2.1 Operation modes**

511 **4.3 High time resolution**

512 **4.3.1 Electron drift velocity**

513 **4.4 Resistive Plate Chambers at CMS**

514 **4.4.1 Overview**

515 The Resistive Plate Chambers (RPC) system, located in both barrel and endcap regions, provides a
 516 fast, independent muon trigger with a looser p_T threshold over a large portion of the pseudorapidity
 517 range ($|\eta| < 1.6$) [\[add reconstruction\]](#).

518 During High-Luminosity LHC (HL-LHC) operations the expected conditions in terms of back-
 519 ground and pile-up will make the identification and correct P_T assignment a challenge for the Muon
 520 system. The goal of RPC upgrade is to provide additional hits to the Muon system with precise timing.
 521 All these informations will be elaborated by the trigger system in a global way enhancing the
 522 performance of the trigger in terms of efficiency and rate control. The RPC Upgrade is based on two
 523 projects: an improved Link Board System and the extension of the RPC coverage up to $|\eta| = 2.4$.
 524 [\[FIXME 2.4 or 2.5?\]](#)

525 The Link Board system, that will be described in section xxx, is responsible to process, syn-
 526 chronize and zero-suppress the signals coming from the RPC front end boards. The Link Board
 527 components have been produced between 2006 and 2007 and will be subjected to aging and failure
 528 in the long term. The upgraded Link Board system will overcome the aging problems described in
 529 section xxx and will allow for a more precise timing information to the RPC hits from 25 to 1 ns [ref
 530 section xxx].

531 The extension of the RPC system up to $|\eta| = 2.1$ was already planned in the CMS TDR [ref
 532 cmstdr] and staged because of budget limitations and expected background rates higher than the rate
 533 capability of the present CMS RPCs in that region. An extensive R&D program has been done in
 534 order to develop an improved RPC that fulfills the CMS requirements. Two new RPC layers in the
 535 innermost ring of stations 3 and 4 will be added with benefits to the neutron-induced background
 536 reduction and efficiency improvement for both trigger and offline reconstruction.

538 **4.4.2 The present RPC system**

539 The RPC system is organized in 4 stations called RB1 to RB4 in the barrel region, and RE1 to RE4
 540 in the endcap region. The innermost barrel stations, RB1 and RB2, are instrumented with 2 layers
 541 of RPCs facing the innermost (RB1in and RB2in) and outermost (RB1out and RB2out) sides of the
 542 DT chambers. Every chamber is then divided from the read-out point of view into 2 or 3 η partitions

543 called “rolls”. The RPC system consist of 480 barrel chambers and 576 endcap chambers. Details
 544 on the geometry are discussed in the paper [ref to geo paper].

545 The CMS RPC chamber is a double-gap, operated in avalanche mode to ensure reliable operation
 546 at high rates. Each RPC gap consists of two 2-mm-thick resistive High-Pressure Laminate (HPL)
 547 plates separated by a 2-mm-thick gas gap. The outer surface of the HPL plates is coated with a thin
 548 conductive graphite layer, and a voltage is applied. The RPCs are operated with a 3-component,
 549 non-flammable gas mixture consisting of 95.2% freon ($C_2H_2F_4$, known as R134a), 4.5% isobutane
 550 ($i-C_4H_{10}$), and 0.3% sulphur hexafluoride (SF_6) with a relative humidity of 40% - 50%. Readout
 551 strips are aligned in η between the 2 gas gaps. [\[Add a sentence on FEBs.\]](#)

552 The discriminated signals coming from the Front End boards feed via twisted cables (10 to 20 m
 553 long) the Link Board System located in UXC on the balconies around the detector. The Link System
 554 consist of the 1376 Link Boards (LBs) and the 216 Control Boards (CBs), placed in 108 Link Boxes.
 555 The Link Box is a custom crate (6U high) with 20 slots (for two CBs and eighteen LBs). The Link
 556 Box contains custom backplane to which the cables from the chambers are connected, as well as the
 557 cables providing the LBs and CBs power supply and the cables for the RPC FEBs control with use
 558 of the I2C protocol (trough the CB). The backplane itself contains only connectors (and no any other
 559 electronic devices).

560 The Link Board has 96 input channels (one channel corresponds to one RPC strip). The input
 561 signals are the ~ 100 ns binary pulses which are synchronous to the RPC hits, but not to the LHC
 562 clock (which drives the entire CMS electronics). Thus the first step of the FEB signals processing
 563 is synchronization, i.e. assignment of the signals to the BXes (25 ns periods). Then the data are
 564 compressed with a simple zero-suppressing algorithm (the input channels are grouped into 8 bit
 565 partitions, only the partitions with at least one nonzero bit are selected for each BX). Next, the non-
 566 empty partitions are time-multiplexed i.e. if there are more than one such partition in a given BX,
 567 they are sent one-by-one in consecutive BXes. The data from 3 neighbouring LBs are concentrated
 568 by the middle LB which contains the optical transmitter for sending them to the USC over a fiber at
 569 1.6 Gbps.

570 The Control Boards provide the communication of the control software with the LBs via the
 571 FEC/CCU system. The CBs are connected into token rings, each ring consists of 12 CBs of one
 572 detector tower and a FEC mezzanine board placed on the CCS board located in the VME crate in
 573 the USC. In total, there are 18 rings in the entire Link System. The CBs also perform automatic
 574 reloading of the LB’s firmware which is needed in order to avoid accumulation of the radiation
 575 induced SEUs in the LBs firmware.

576 Both LBs and CB are based on the Xilinx Spartan III FPGAs, the CB additionally contains
 577 radiation-tolerant (FLASH based) FPGA Actel ProAsicPlus.

578 The High Voltage power system is located in USC, not exposed to radiation and easily accessible
 579 for any reparation. A single HV channel powers 2 RPC chambers both in the barrel and endcap
 580 regions. The Low Voltage boards are located in UXC on the balconies and provide the voltage to the
 581 front end electronics.

582 4.4.3 Pulse processing of CMS RPCs

583 Signals induced by cosmic particle in the RPC strips are shaped by standard CMS RPC Front-End
 584 Electronics (FEE) following the scheme of Figure 4.2. On a first stage, analogic signals are amplified
 585 and then sent to the Constant Fraction Discriminator (CFD) described in Figure 4.3. At the end of
 586 the chain, 100 ns long pulses are sent in the LVDS output. These output signal are sent on one side to

587 a V1190A Time-to-Digital Converter (TDC) module from CAEN and on the other to an OR module
 588 to count the number of detected signals. Trigger and hit coïncidences are monitored using scalers.
 589 The TDC is used to store the data into ROOT files. These files are thus analysed to understand the
 590 detectors performance.

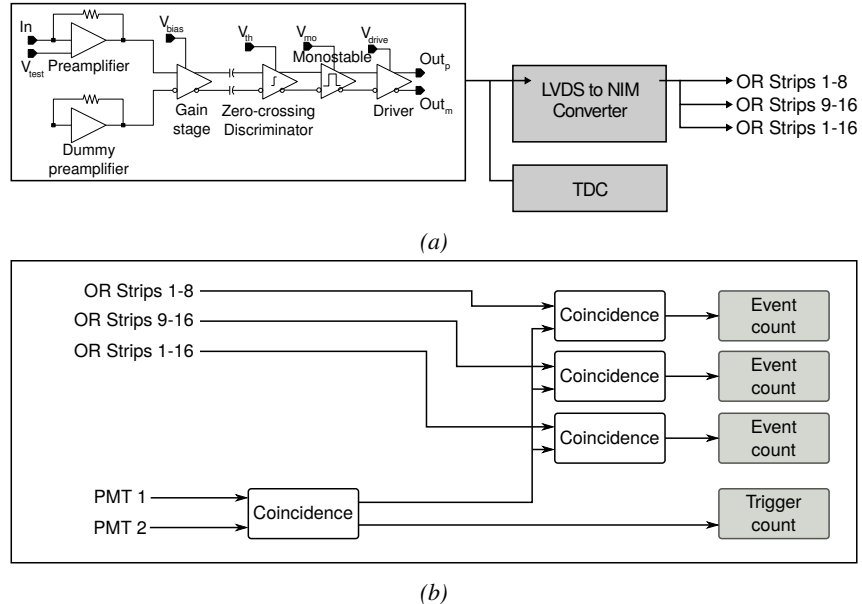
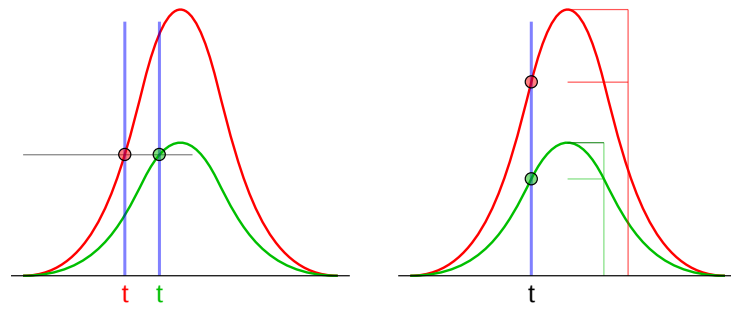
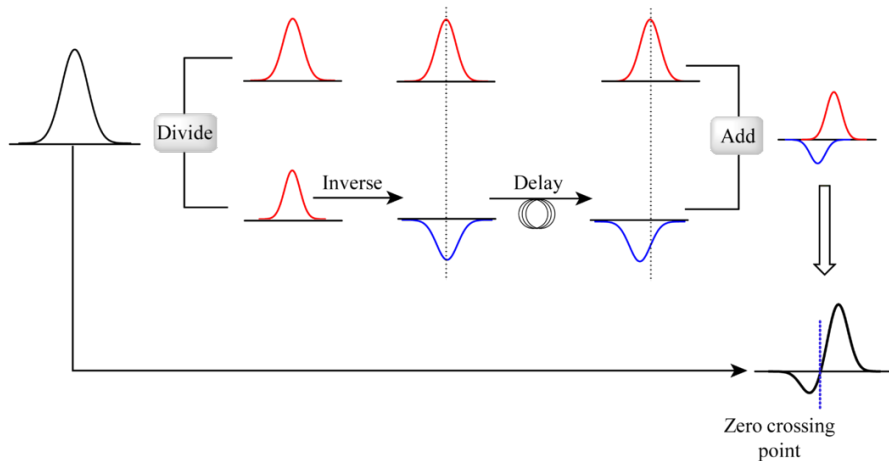


Figure 4.2: Signals from the RPC strips are shaped by the FEE described on Figure 4.2a. Output LVDS signals are then read-out by a TDC module connected to a computer or converted into NIM and sent to scalers. Figure 4.2b describes how these converted signals are put in coincidence with the trigger.



(a)



(b)

Figure 4.3: Description of the principle of a CFD. A comparison of threshold triggering (left) and constant fraction triggering (right) is shown in Figure 4.3a. Constant fraction triggering is obtained thanks to zero-crossing technique as explained in Figure 4.3b. The signal arriving at the input of the CFD is split into three components. A first one is delayed and connected to the inverting input of a first comparator. A second component is connected to the noninverting input of this first comparator. A third component is connected to the noninverting input of another comparator along with a threshold value connected to the inverting input. Finally, the output of both comparators is fed through an AND gate.

5

591

592

593

Longevity studies and Consolidation of the present CMS RPC subsystem

594

5.1 Testing detectors under extreme conditions

595

The upgrade from LHC to HL-LHC will increase the peak luminosity from $10^{34} \text{ cm}^{-2} \text{ s}^{-1}$ to reach $5 \times 10^{34} \text{ cm}^{-2} \text{ s}^{-1}$, increasing in the same way the total expected background to which the RPC system will be subjected to. Composed of low energy gammas and neutrons from $p\text{-}p$ collisions, low momentum primary and secondary muons, puch-through hadrons from calorimeters, and particles produced in the interaction of the beams with collimators, the background will mostly affect the regions of CMS that are the closest to the beam line, i.e. the RPC detectors located in the endcaps.

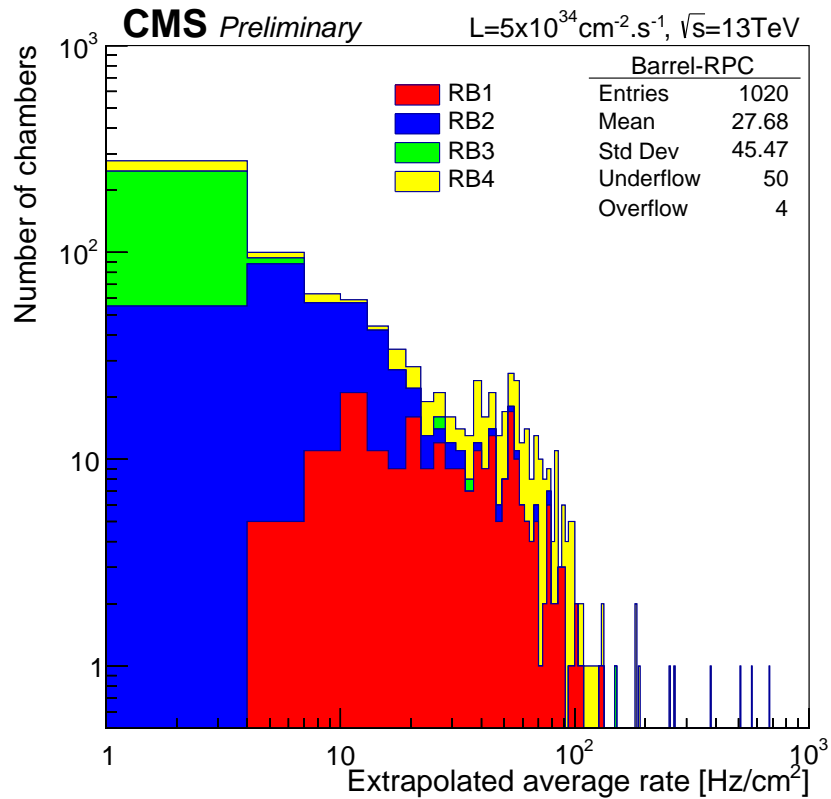
[To update.]

602

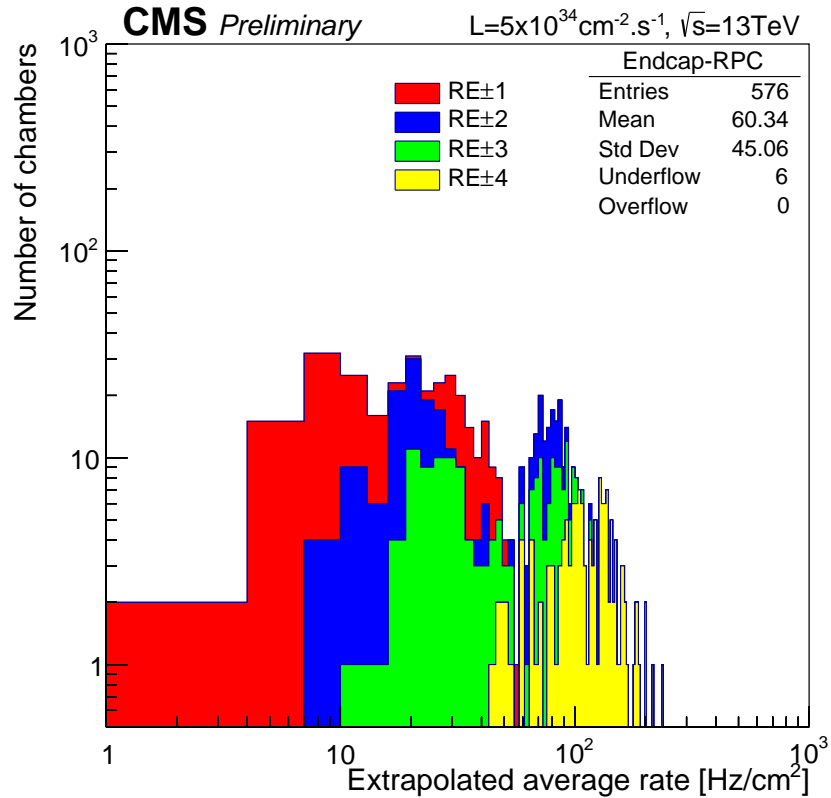
603

The 2016 data allowed to study the values of the background rate in all RPC system. In Figure 5.1, the distribution of the chamber background hit rate per unit area is shown at a luminosity of $5 \times 10^{34} \text{ cm}^{-2} \cdot \text{s}^{-1}$ linearly extrapolating from data collected in 2016 [ref mentioning the linear dependency of rate vs lumi]. The maximum rate per unit area at HL-LHC conditions is expected to be of the order of 600 Hz/cm^2 (including a safety factor 3). Nevertheless, Fluka simulations have conducted in order to understand the background at HL-LHC conditions. The comparison to the data has shown, in Figure 5.2, a discrepancy of a factor 2 even though the order of magnitude is consistent. [Understand mismatch.]

611



(a)



(b)

Figure 5.1: (5.1a) Extrapolation from 2016 data of single hit rate per unit area in the barrel region. (5.1b) Extrapolation from 2016 data of single hit rate per unit area in the endcap region.

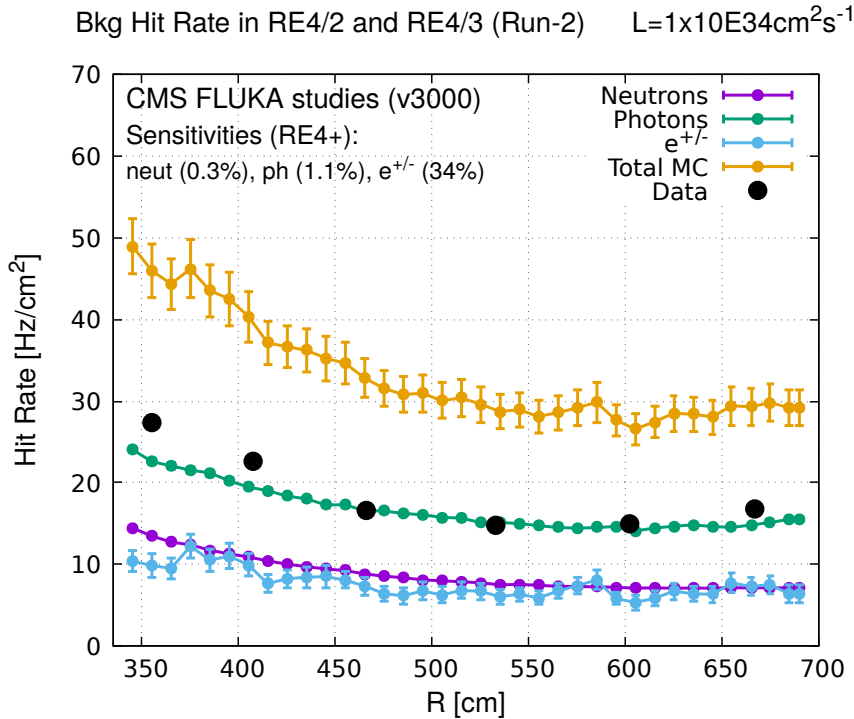


Figure 5.2: Background Fluka simulation compared to 2016 Data at $L = 10^{34}\text{cm}^{-2}\cdot\text{s}^{-1}$ in the fourth endcap disk region. A mismatch in between simulation and data can be observed. [\[To be understood.\]](#)

In the past, extensive long-term tests were carried out at several gamma and neutron facilities certifying the detector performance. Both full size and small prototype RPCs have been irradiated with photons up to an integrated charge of $\sim 0.05C/\text{cm}^2$ and $\sim 0.4C/\text{cm}^2$, respectively [22, 23]. During Run-I, the RPC system provided stable operation and excellent performance and did not show any aging effects for integrated charge of the order of $0.01C/\text{cm}^2$. Projections on currents from 2016 Data, has allowed to determine that the total integrated charge, by the end of HL-LHC, would be of the order of $1C/\text{cm}^2$ (including a safety factor 3). [\[Corresponding figure needed.\]](#)

619

620 5.1.1 The Gamma Irradiation Facilities

621 5.1.1.1 GIF

622 Located in the SPS West Area at the downstream end of the X5 test beam, the Gamma Irradiation
623 Facility (GIF) was a test area in which particle detectors were exposed to a particle beam in presence
624 of an adjustable gamma background [24]. Its goal was to reproduce background conditions these
625 detectors would suffer in their operating environment at LHC. GIF layout is shown in Figure 5.3.
626 Gamma photons are produced by a strong ^{137}Cs source installed in the upstream part of the zone
627 inside a lead container. The source container includes a collimator, designed to irradiate a $6 \times 6\text{ m}^2$
628 area at 5 m maximum to the source. A thin lens-shaped lead filter helps providing with a uniform
629 outgoing flux in a vertical plane, orthogonal to the beam direction. The principal collimator hole
630 provides a pyramidal aperture of $74^\circ \times 74^\circ$ solid angle and provides a photon flux in a pyramidal vol-

ume along the beam axis. The photon rate is controled by further lead filters allowing the maximum rate to be limited and to vary within a range of four orders of magnitude. Particle detectors under test are then placed within the pyramidal volume in front of the source, perpendicularly to the beam line in order to profit from the homogeneous photon flux. Adjusting the background flux of photons can then be done by using the filters and choosing the position of the detectors with respect to the source.

636

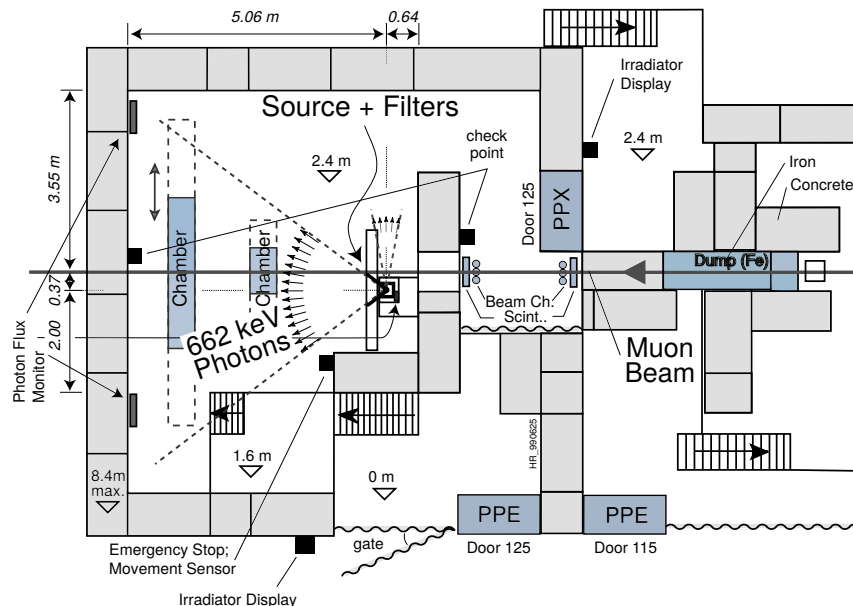


Figure 5.3: Layout of the test beam zone called X5c GIF at CERN. Photons from the radioactive source produce a sustained high rate of random hits over the whole area. The zone is surrounded by 8 m high and 80 cm thick concrete walls. Access is possible through three entry points. Two access doors for personnel and one large gate for material. A crane allows installation of heavy equipment in the area.

637 As described on Figure 5.4, the ^{137}Cs source emits a 662 keV photon in 85% of the decays. An
 638 activity of 740 GBq was measured on the 5th March 1997. To estimate the strength of the flux in
 639 2014, it is necessary to consider the nuclear decay through time assiciated to the Cesium source
 640 whose half-life is well known ($t_{1/2} = (30.05 \pm 0.08)$ y). The GIF tests where done in between the
 641 20th and the 31st of August 2014, i.e. at a time $t = (17.47 \pm 0.02)$ y resulting in an attenuation of
 642 the activity from 740 GBq in 1997 to 494 GBq in 2014.

643

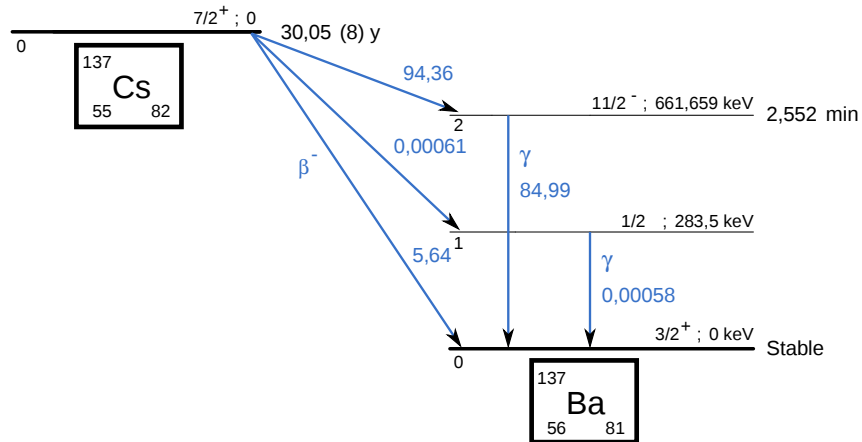


Figure 5.4: ^{137}Cs decays by β^- emission to the ground state of ^{137}Ba ($\text{BR} = 5.64\%$) and via the 662 keV isomeric level of ^{137}Ba ($\text{BR} = 94.36\%$) whose half-life is 2.55 min.

644 5.1.1.2 GIF++

645 The new Gamma Irradiation Facility (GIF++), located in the SPS North Area at the downstream end
 646 of the H4 test beam, has replaced its predecessor during LS1 and has been operational since spring
 647 2015 [25]. Like GIF, GIF++ features a ^{137}Cs source of 662 keV gamma photons, their fluence being
 648 controlled with a set of filters of various attenuation factors. The source provides two separated large
 649 irradiation areas for testing several full-size muon detectors with continuous homogeneous irradiation,
 650 as presented in Figure 5.5.

651

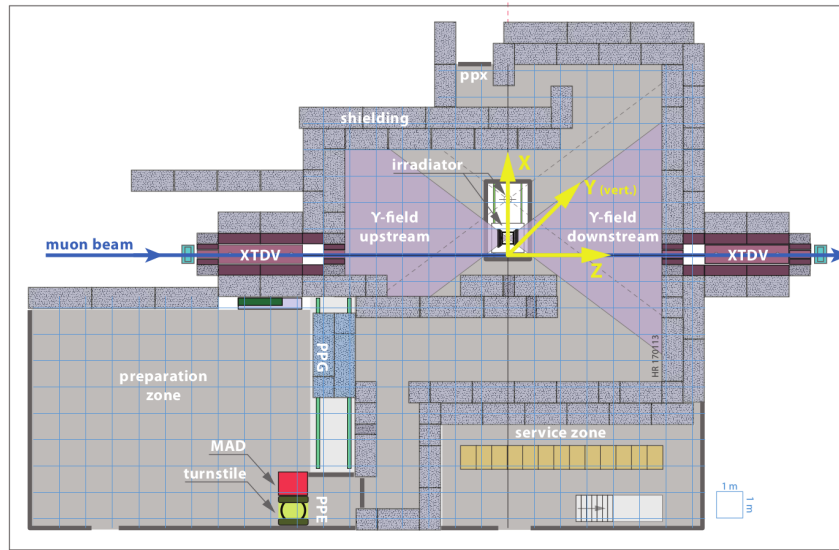


Figure 5.5: Floor plan of the GIF++ facility. When the facility downstream of the GIF++ takes electron beam, a beam pipe is installed along the beam line (z -axis). The irradiator can be displaced laterally (its center moves from $x = 0.65 \text{ m}$ to 2.15 m), to increase the distance to the beam pipe.

652 The source activity was measured to be about 13.5 TBq in March 2016. The photon flux being
 653 far greater than HL-LHC expectations, GIF++ provides an excellent facility for accelerated aging
 654 tests of muon detectors.

655

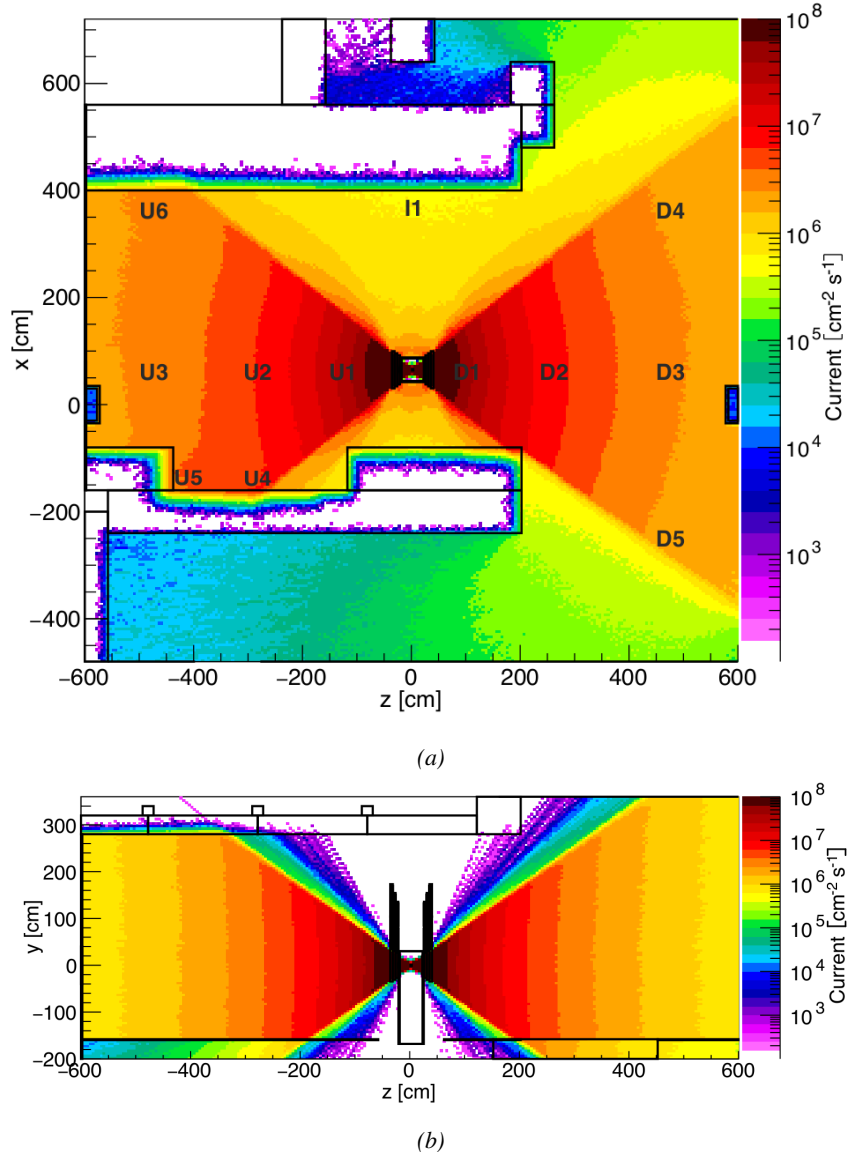


Figure 5.6: Simulated unattenuated current of photons in the xz plane (Figure 5.6a) and yz plane (Figure 5.6b) through the source at $x = 0.65 \text{ m}$ and $y = 0 \text{ m}$. With angular correction filters, the current of 662 keV photons is made uniform in xy planes.

656 The source is situated in the muon beam line with the muon beam being available a few times a
 657 year. The H4 beam, composed of muons with a momentum of about 150 GeV/c, passes through the
 658 GIF++ zone and is used to study the performance of the detectors. Its flux is of 104 particles/ s cm^2

659 focused in an area similar to $10 \times 10 \text{ cm}^2$. Therefore, with properly adjusted filters, one can imitate
 660 the HL-LHC background and study the performance of muon detectors with their trigger/readout
 661 electronics in HL-LHC environment.

662

663 5.2 Preliminary tests at GIF

664 5.2.1 Resistive Plate Chamber test setup

665 During summer 2014, preliminary tests have been conducted in the GIF area on a newly produced
 666 RE4/2 chamber labelled RE-4-2-BARC-161. This chamber has been placed into a trolley covered
 667 with a tent. The position of the RPC inside the tent and of the tent related to the source is described
 668 in Figure 5.7. To test this CMS RPC, three different absorber settings were used. First of all,
 669 measurements were done with fully opened source. Then, to complete this preliminary study, the
 670 gamma flux has been attenuated from a factor 2 and a factor 5. The expected gamma flux at the level
 671 of our detector will be discussed in subsection ??.

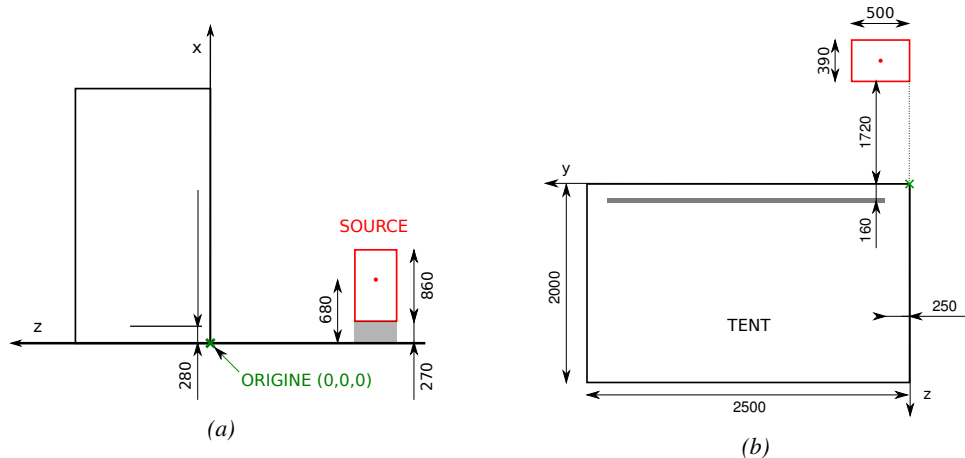


Figure 5.7: Description of the RPC setup. Dimensions are given in mm. A tent containing RPCs is placed at 1720 mm from the source container. The source is situated in the center of the container. RE-4-2-BARC-161 chamber is 160 mm inside the tent. This way, the distance between the source and the chambers plan is 2060 mm. Figure 5.7a provides a side view of the setup in the xz plane while Figure 5.7b shows a top view in the yz plane.



Figure 5.8: RE-4-2-BARC-161 chamber is inside the tent as described in Figure 5.7. In the top right, the two scintillators used as trigger can be seen. This trigger system has an inclination of 10° relative to horizontal and is placed above half-partition B2 of the RPCs. PMT electronics are shielded thanks to lead blocks placed in order to protect them without stopping photons from going through the scintillators and the chamber.

672 At the time of the tests, the beam not being operational anymore, a trigger composed of 2
 673 plastic scintillators has been placed in front of the setup with an inclination of 10 deg with respect to
 674 the detector plane in order to look at cosmic muons. Using this particular trigger layout, shown on
 675 Figure 5.8, leads to a cosmic muon hit distribution into the chamber similar to the one in Figure 5.9.
 676 Measured without gamma irradiation, two peaks can be seen on the profil of partition B, centered
 677 on strips 52 and 59. Section ?? will help us understand that these two peaks are due respectively to
 678 forward and backward coming cosmic particles where forward coming particles are first detected by
 679 the scintillators and then the RPC while the backward coming muons are first detected in the RPC.

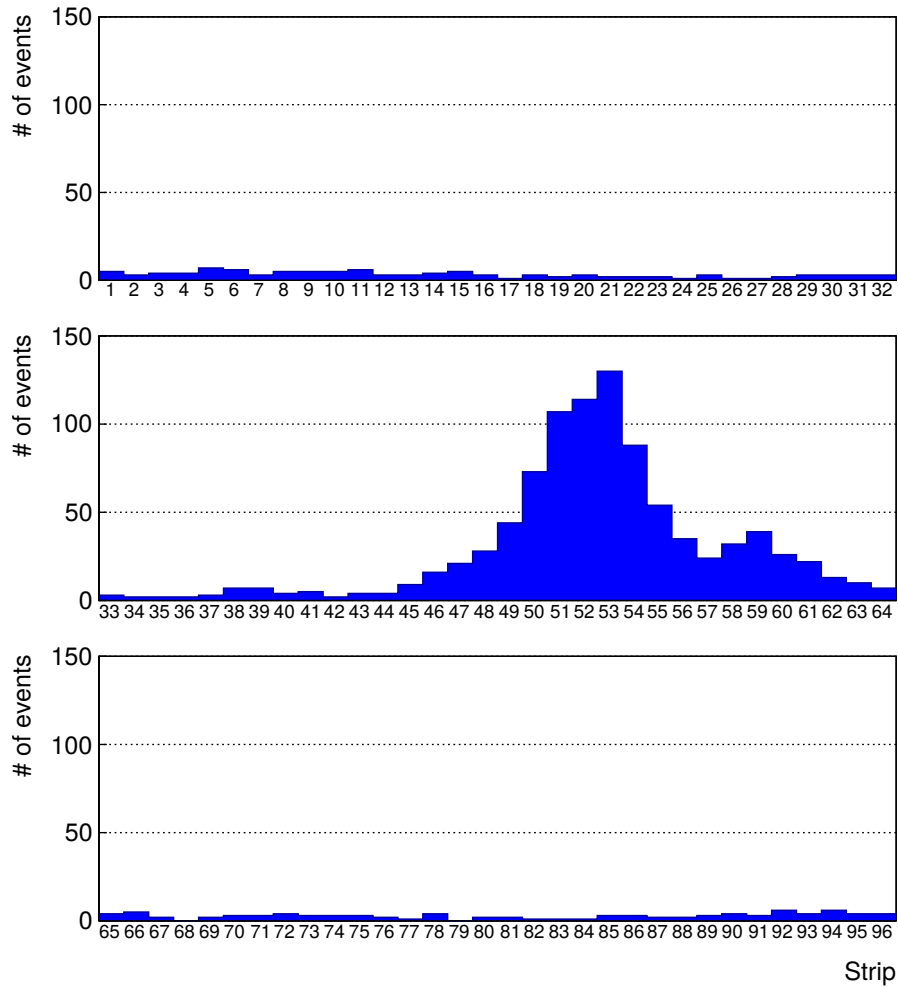


Figure 5.9: Hit distributions over all 3 partitions of RE-4-2-BARC-161 chamber is showed on these plots. Top, middle and bottom figures respectively correspond to partitions A, B, and C. These plots show that some events still occur in other half-partitions than B2, which corresponds to strips 49 to 64, in front of which the trigger is placed, contributing to the inefficiency of detection of cosmic muons. In the case of partitions A and C, the very low amount of data can be interpreted as noise. On the other hand, it is clear that a little portion of muons reach the half-partition B1, corresponding to strips 33 to 48.

680 5.2.2 Data Acquisition

681 5.2.3 Geometrical acceptance of the setup layout to cosmic muons

682 In order to profit from a constant gamma irradiation, the detectors inside of the GIF bunker need
 683 to be placed in a plane orthogonal to the beam line. The muon beam that used to be available was
 684 meant to test the performance of detectors under test. This beam not being active anymore, another
 685 solution to test detector performance had to be used. Thus, it has been decided to use cosmic muons
 686 detected through a telescope composed of two scintillators. Lead blocks were used as shielding to

687 protect the photomultipliers from gammas as can be seen from Figure 5.8.

688 An inclination has been given to the cosmic telescope to maximize the muon flux. A good com-
 689 promise had to be found between good enough muon flux and narrow enough hit distribution to
 690 be sure to contain all the events into only one half partitions as required from the limited available
 691 readout hardware. Nevertheless, a consequence of the misplaced trigger, that can be seen as a loss
 692 of events in half-partition B1 in Figure 5.9, is an inefficiency. Nevertheless, the inefficiency of ap-
 693 proximately 20 % highlighted in Figure 5.10 by comparing the performance of chamber BARC-161
 694 in 904 and at GIF without irradiation seems too important to be explained only by the geometri-
 695 cal acceptance of the setup itself. Simulations have been conducted to show how the setup brings
 696 inefficiency.

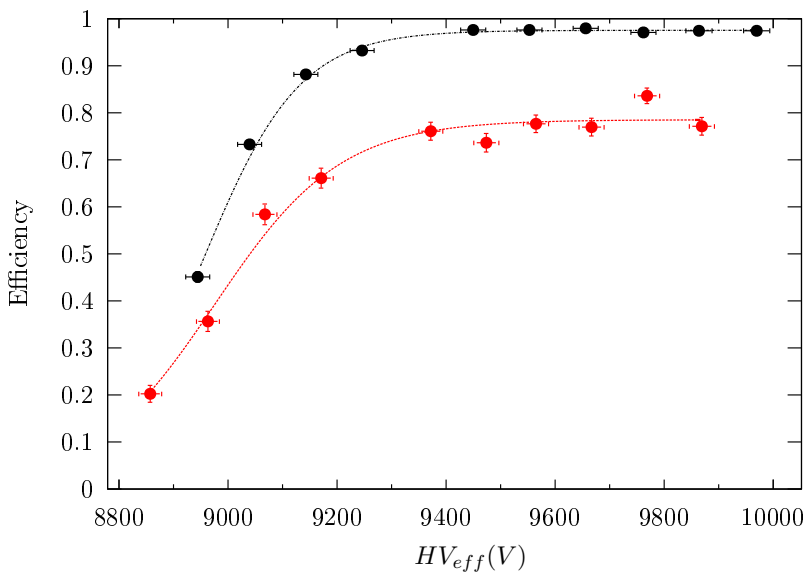


Figure 5.10: Results are derived from data taken on half-partition B2 only. On the 18th of June 2014, data has been taken on chamber RE-2-BARC-161 at building 904 (Prevessin Site) with cosmic muons providing us a reference efficiency plateau of $(97.54 \pm 0.15)\%$ represented by a black curve. A similar measurement has been done at GIF on the 21st of July with the same chamber giving a plateau of $(78.52 \pm 0.94)\%$ represented by a red curve.

697 5.2.3.1 Description of the simulation layout

698 The layout of GIF setup has been reproduced and incorporated into a Monte Carlo (MC) simulation
 699 to study the influence of the disposition of the telescope on the final distribution measured by the
 700 RPC. A 3D view of the simulated layout is given into Figure 5.11. Muons are generated randomly
 701 in a horizontal plane located at a height corresponding to the lowest point of the PMTs. This way,
 702 the needed size of the plane in order to simulate events happening at very big azimuthal angles (i.e.
 703 $\theta \approx \pi$) can be kept relatively small. The muon flux is designed to follow the usual $\cos^2\theta$ distribution
 704 for cosmic particle. The goal of the simulation is to look at muons that pass through the muon
 705 telescope composed of the two scintillators and define their distribution onto the RPC plane. During
 706 the reconstruction, the RPC plane is then divided into its strips and each muon track is assigned to a
 707 strip.

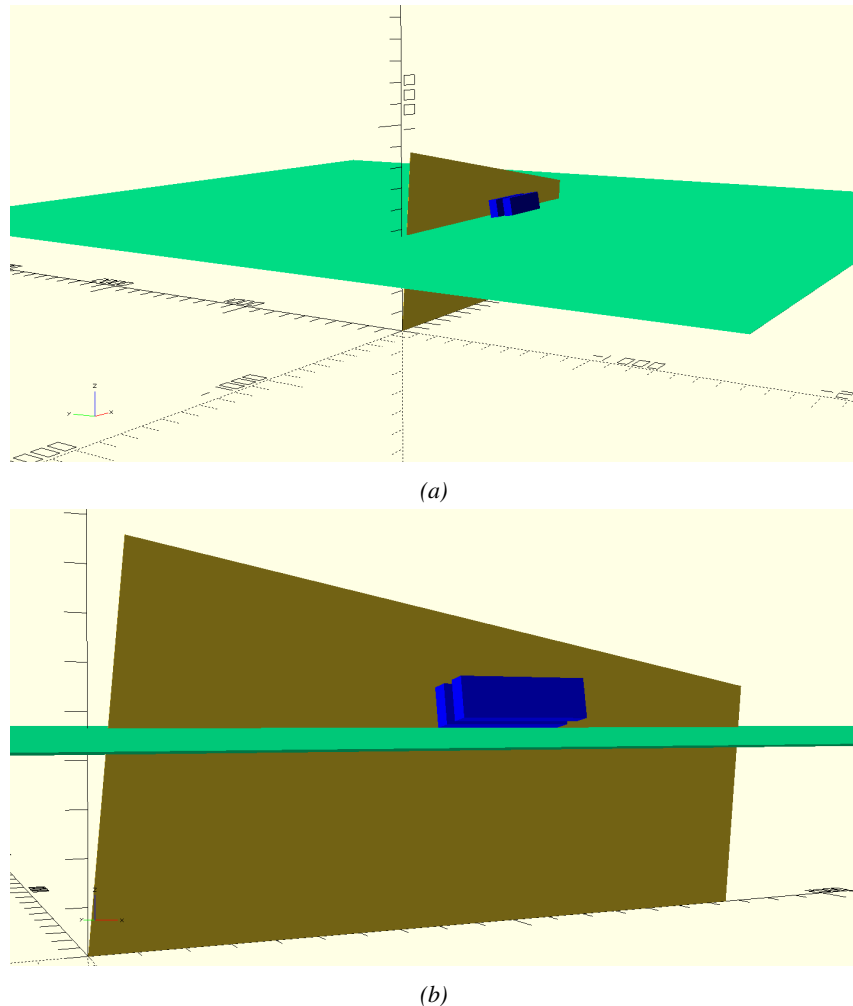


Figure 5.11: Representation of the layout used for the simulations of the test setup. The RPC is represented as a yellow trapezoid while the two scintillators as blue cuboids looking at the sky. A green plane corresponds to the muon generation plane within the simulation. Figure 5.7a shows a global view of the simulated setup. Figure 5.7b shows a zoomed view that allows to see the 2 scintillators as well as the full RPC plane.

708 In order to further refine the quality of the simulation and understand deeper the results the
 709 dependance of the distribution has been studied for a range of telescope inclinations. Moreover,
 710 the threshold applied on the PMT signals has been included into the simulation in the form of a
 711 cut. In the approximation of uniform scintillators, it has been considered that the threshold can be
 712 understood as the minimum distance particles need to travel through the scintillating material to give
 713 a strong enough signal. Particles that travel a distance smaller than the set "threshold" are thus not
 714 detected by the telescope and cannot trigger the data taking. Finally, the FEE threshold also has
 715 been considered in a similar way. The mean momentum of horizontal cosmic rays is higher than
 716 those of vertical ones but the stopping power of matter for momenta ranging from 1 GeV to 1 TeV
 717 stays comparable. It is then possible to assume that the mean number of primary e^- /ion pairs per
 718 unit length will stay similar and thus, depending on the applied discriminator threshold, muons with

719 the shortest path through the gas volume will deposit less charge and induce a smaller signal on the
 720 pick-up strips that could eventually not be detected. These two thresholds also restrain the overall
 721 geometrical acceptance of the system.

722 **5.2.3.2 Simulation procedure**

723 The simulation software has been designed using C++ and the output data is saved into ROOT
 724 histograms. Simulations start for a threshold T_{scint} varying in a range from 0 to 45 mm in steps
 725 of 5 mm, where $T_{scint} = 0$ mm corresponds to the case where there isn't any threshold apply on
 726 the input signal while $T_{scint} = 45$ mm, which is the scintillator thickness, is the case where muons
 727 cannot arrive orthogonally onto the scintillator surface. For a given T_{scint} , a set of RPC thresholds
 728 are considered. The RPC threshold, T_{RPC} varies from 2 mm, the thickness of the gas volume, to
 729 3 mm in steps of 0.25 mm. For each $(T_{scint}; T_{RPC})$ pair, $N_\mu = 10^8$ muons are randomly generated
 730 inside the muon plane described in the previous paragraph with an azimuthal angle θ chosen to follow
 731 a $\cos^2\theta$ distribution.

732 Planes are associated to each surface of the scintillators. Knowing muon position into the muon
 733 plane and its direction allows us, by assuming that muons travel in a straight line, to compute the
 734 intersection of the muon track with these planes. Applying conditions to the limits of the surfaces
 735 of the scintillator faces then gives us an answer to whether or not the muon passed through the
 736 scintillators. In the case the muon has indeed passed through the telescope, the path through each
 737 scintillator is computed and muons whose path was shorter than T_{scint} are rejected and are thus
 738 considered as having not interacted with the setup.

739 On the contrary, if the muon is labeled as good, its position within the RPC plane is computed
 740 and the corresponding strip, determined by geometrical tests in the case the distance through the
 741 gas volume was enough not to be rejected because of T_{RPC} , gets a hit and several histograms
 742 are filled in order to keep track of the generation point on the muon plane, the intersection points
 743 of the reconstructed muons within the telescope, or on the RPC plane, the path traveled through
 744 each individual scintillator or the gas volume, as well as other histograms. Moreover, muons fill
 745 different histograms whether they are forward or backward coming muons. They are discriminated
 746 according to their direction components. When a muon is generated, an (x, y, z) position is assigned
 747 into the muon plane as well as a $(\theta; \phi)$ pair that gives us the direction it's coming from. This way,
 748 muons satisfying the condition $0 \leq \phi < \pi$ are designated as backward coming muons while muons
 749 satisfying $\pi \leq \phi < 2\pi$ as forward coming muons.

750 This simulation is then repeated for different telescope inclinations ranging in between 4 and 20°
 751 and varying in steps of 2° . Due to this inclination and to the vertical position of the detector under
 752 test, the muon distribution reconstructed in the detector plane is asymmetrical. The choice as been
 753 made to chose a skew distribution formula to fit the data built as the multiplication of gaussian and
 754 sigmoidal curves together. A typical gaussian formula is given as 5.1 and has three free parameters
 755 as A_g , its amplitude, \bar{x} , its mean value and σ , its root mean square. Sigmoidal curves as given by
 756 formula 5.2 are functions converging to 0 and A_s as x diverges. The inflection point is given as x_i
 757 and λ is proportional to the slope at $x = x_i$. In the limit where $\lambda \rightarrow \infty$, the sigmoid becomes a
 758 step function.

$$g(x) = A_g e^{-\frac{(x-\bar{x})^2}{2\sigma^2}} \quad (5.1)$$

$$s(x) = \frac{A_s}{1 + e^{-\lambda(x-x_i)}} \quad (5.2)$$

Finally, a possible representation of a skew distribution is given by formula 5.3 and is the product of 5.1 and 5.2. Naturally, here $A_{sk} = A_g \times A_s$ and represents the theoretical maximum in the limit where the skew tends to a gaussian function.

$$sk(x) = g(x) \times s(x) = A_{sk} \frac{e^{\frac{-(x-\bar{x})^2}{2\sigma^2}}}{1 + e^{-\lambda(x-x_i)}} \quad (5.3)$$

5.2.3.3 Results

Influence of T_{scint} on the muon distribution

Influence of T_{RPC} on the muon distribution

Influence of the telescope inclination on the muon distribution

Comparison to data taken at GIF without irradiation

5.2.4 Photon flux at GIF

5.2.4.1 Expectations from simulations

In order to understand and evaluate the γ flux in the GIF area, simulations had been conducted in 1999 and published by S. Agosteo et al [24]. Table 5.1 presented in this article gives us the γ flux for different distances D to the source. This simulation was done using GEANT and a Monte Carlo N-Particle (MCNP) transport code, and the flux F is given in number of γ per unit area and unit time along with the estimated error from these packages expressed in %.

Nominal ABS	Photon flux F [$s^{-1}cm^{-2}$]			
	at $D = 50$ cm	at $D = 155$ cm	at $D = 300$ cm	at $D = 400$ cm
1	$0.12 \cdot 10^8 \pm 0.2\%$	$0.14 \cdot 10^7 \pm 0.5\%$	$0.45 \cdot 10^6 \pm 0.5\%$	$0.28 \cdot 10^6 \pm 0.5\%$
2	$0.68 \cdot 10^7 \pm 0.3\%$	$0.80 \cdot 10^6 \pm 0.8\%$	$0.25 \cdot 10^6 \pm 0.8\%$	$0.16 \cdot 10^6 \pm 0.6\%$
5	$0.31 \cdot 10^7 \pm 0.4\%$	$0.36 \cdot 10^6 \pm 1.2\%$	$0.11 \cdot 10^6 \pm 1.2\%$	$0.70 \cdot 10^5 \pm 0.9\%$

Table 5.1: Total photon flux ($E\gamma \leq 662$ keV) with statistical error predicted considering a ^{137}Cs activity of 740 GBq at different values of the distance D to the source along the x -axis of irradiation field [24].

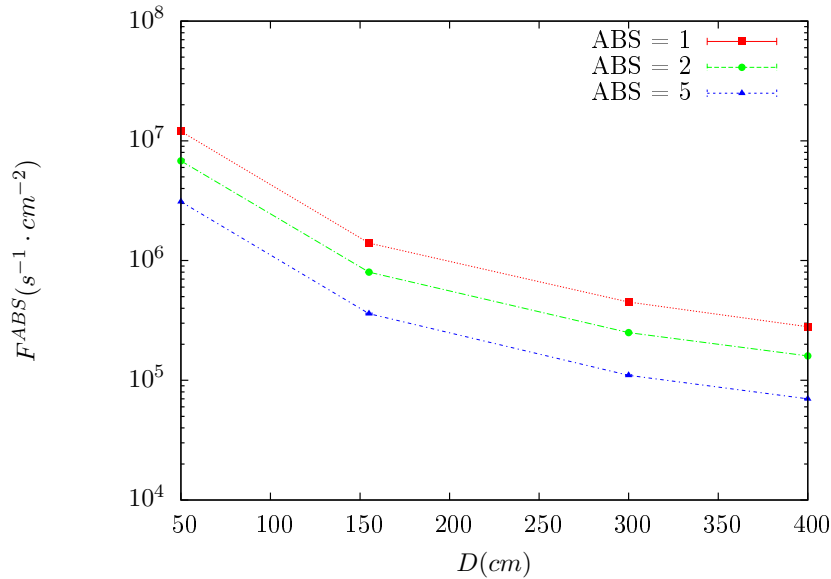


Figure 5.12: γ flux $F(D)$ is plot using values from table 5.1. As expected, the plot shows similar attenuation behaviours with increasing distance for each absorption factors.

The simulation doesn't directly provide us with an estimated flux at the level of our RPC. First of all, it is needed to extract the value of the flux from the available data contained in the original paper and then to estimate the flux in 2014 at the time the experimentation took place. Figure 5.12 that contains the data from Table 5.1. In the case of a pointlike source emitting isotropic and homogeneous gamma radiations, the gamma flux F at a distance D to the source with respect to a reference point situated at D_0 where a known flux F_0 is measured will be expressed like in Equation 5.4, assuming that the flux decreases as $1/D^2$, where c is a fitting factor.

$$F^{ABS} = F_0^{ABS} \times \left(\frac{cD_0}{D} \right)^2 \quad (5.4)$$

By rewriting Equation 5.4, it comes that :

$$c = \frac{D}{D_0} \sqrt{\frac{F^{ABS}}{F_0^{ABS}}} \quad (5.5)$$

$$\Delta c = \frac{c}{2} \left(\frac{\Delta F^{ABS}}{F^{ABS}} + \frac{\Delta F_0^{ABS}}{F_0^{ABS}} \right) \quad (5.6)$$

Finally, using Equation 5.5 and the data in Table 5.1 with $D_0 = 50$ cm as reference point, we can build Table 5.2. It is interesting to note that c for each value of D doesn't depend on the absorption factor.

Nominal ABS	Correction factor c		
	at $D = 155$ cm	at $D = 300$ cm	at $D = 400$ cm
1	$1.059 \pm 0.70\%$	$1.162 \pm 0.70\%$	$1.222 \pm 0.70\%$
2	$1.063 \pm 1.10\%$	$1.150 \pm 1.10\%$	$1.227 \pm 0.90\%$
5	$1.056 \pm 1.60\%$	$1.130 \pm 1.60\%$	$1.202 \pm 1.30\%$

Table 5.2: Correction factor c is computed thanks to formulae 5.5 taking as reference $D_0 = 50$ cm and the associated flux F_0^{ABS} for each absorption factor available in table 5.1.

785 For the range of D/D_0 values available, it is possible to use a simple linear fit to get the evolution
 786 of c . The linear fit will then use only 2 free parameters, a and b , as written in Equation 5.7. This gives
 787 us the results showed in Figure 5.13. Figure 5.13b confirms that using only a linear fit to extract c is
 788 enough as the evolution of the rate that can be obtained superimposes well on the simulation points.

$$c \left(\frac{D}{D_0} \right) = a \frac{D}{D_0} + b \quad (5.7)$$

$$F^{ABS} = F_0^{ABS} \left(a + \frac{bD_0}{D} \right)^2 \quad (5.8)$$

$$\Delta F^{ABS} = F^{ABS} \left[\frac{\Delta F_0^{ABS}}{F_0^{ABS}} + 2 \frac{\Delta a + \Delta b \frac{D_0}{D}}{a + \frac{bD_0}{D}} \right] \quad (5.9)$$

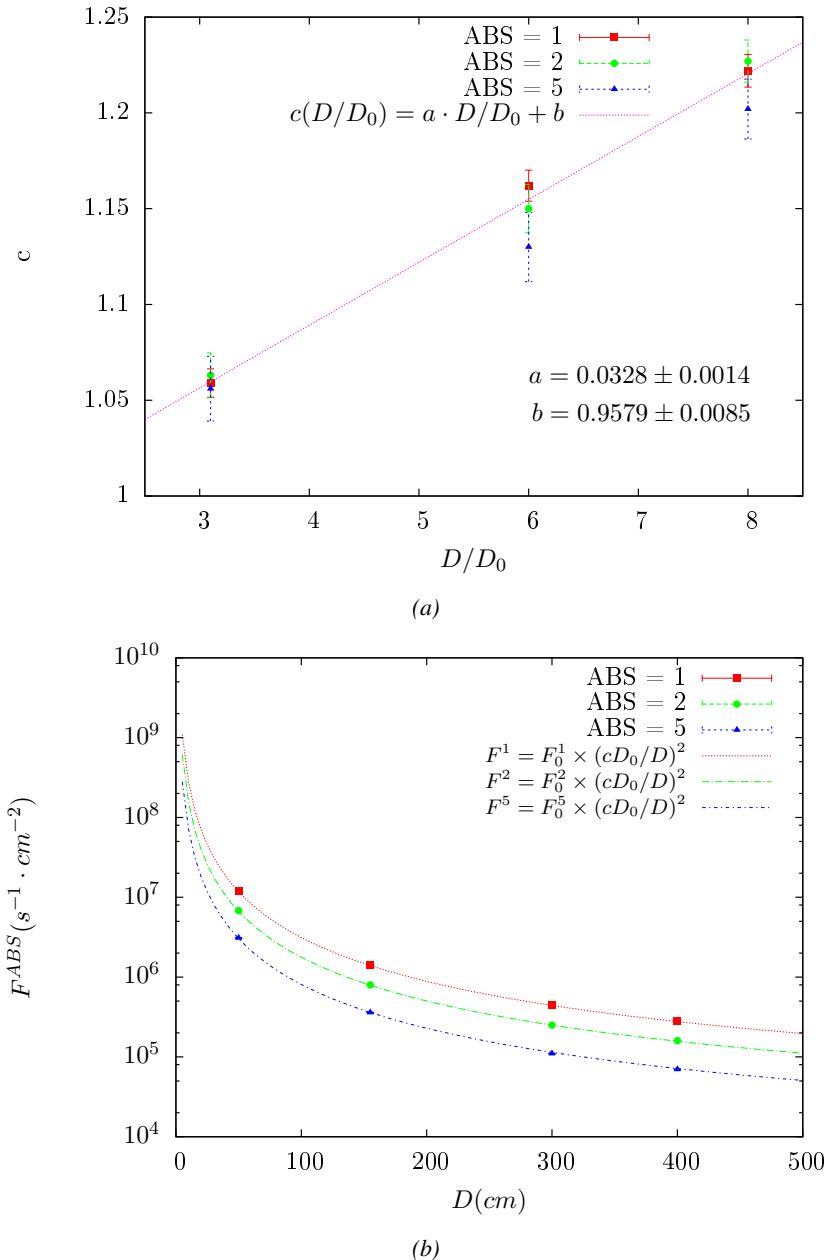


Figure 5.13: Figure 5.13a shows the linear approximation fit done via formulae 5.7 on data from table 5.2. Figure 5.13b shows a comparison of this model with the simulated flux using a and b given in figure 5.13a in formulae 5.4 and the reference value $D_0 = 50\text{cm}$ and the associated flux for each absorption factor F_0^{ABS} from table 5.1

In the case of the 2014 GIF tests, the RPC plane is located at a distance $D = 206\text{ cm}$ to the source. Moreover, to estimate the strength of the flux in 2014, it is necessary to consider the nuclear decay through time associated to the Cesium source whose half-life is well known ($t_{1/2} = (30.05 \pm 0.08)\text{ y}$). The very first source activity measurement has been done on the 5th of March 1997 while the GIF

793 tests where done in between the 20th and the 31st of August 2014, i.e. at a time $t = (17.47 \pm 0.02)$ y
 794 resulting in an attenuation of the activity from 740 GBq in 1997 to 494 GBq in 2014. All the needed
 795 information to extrapolate the flux through our detector in 2014 has now been assembled, leading
 796 to the Table 5.3. It is interesting to note that for a common RPC sensitivity to γ of $2 \cdot 10^{-3}$, the
 797 order of magnitude of the estimated hit rate per unit area is of the order of the kHz for the fully
 798 opened source. Moreover, taking profit of the two working absorbers, it will be possible to scan
 799 background rates at 0 Hz, \sim 300 Hz as well as \sim 600 Hz. Without source, a good estimate of the
 800 intrinsic performance will be available. Then at 300 Hz, the goal will be to show that the detectors
 801 fulfill the performance certification of CMS RPCs. Then a first idea of the performance of the
 802 detectors at higher background will be provided with absorption factors 2 (\sim 600 Hz) and 1 (no
 803 absorption). *[Here I will also put a reference to the plot showing the estimated background rate at
 804 the level of RE3/1 in the case of HL-LHC but this one being in another chapter, I will do it later.]*

Nominal ABS	Photon flux F [$s^{-1}cm^{-2}$]			Hit rate/unit area [$Hz cm^{-2}$] at $D^{2014} = 206$ cm
	at $D_0^{1997} = 50$ cm	at $D_0^{1997} = 206$ cm	at $D^{2014} = 206$ cm	
1	$0.12 \cdot 10^8 \pm 0.2\%$	$0.84 \cdot 10^6 \pm 0.3\%$	$0.56 \cdot 10^6 \pm 0.3\%$	1129 ± 32
2	$0.68 \cdot 10^7 \pm 0.3\%$	$0.48 \cdot 10^6 \pm 0.3\%$	$0.32 \cdot 10^6 \pm 0.3\%$	640 ± 19
5	$0.31 \cdot 10^7 \pm 0.4\%$	$0.22 \cdot 10^6 \pm 0.3\%$	$0.15 \cdot 10^6 \pm 0.3\%$	292 ± 9

Table 5.3: The data at D_0 in 1997 is taken from [24]. In a second step, using Equations 5.8 and 5.9, the flux at D can be estimated in 1997. Then, taking into account the attenuation of the source activity, the flux at D can be estimated at the time of the tests in GIF in 2014. Finally, assuming a sensitivity of the RPC to γ $s = 2 \cdot 10^{-3}$, an estimation of the hit rate per unit area is obtained.

805 **5.2.4.2 Dose measurements**

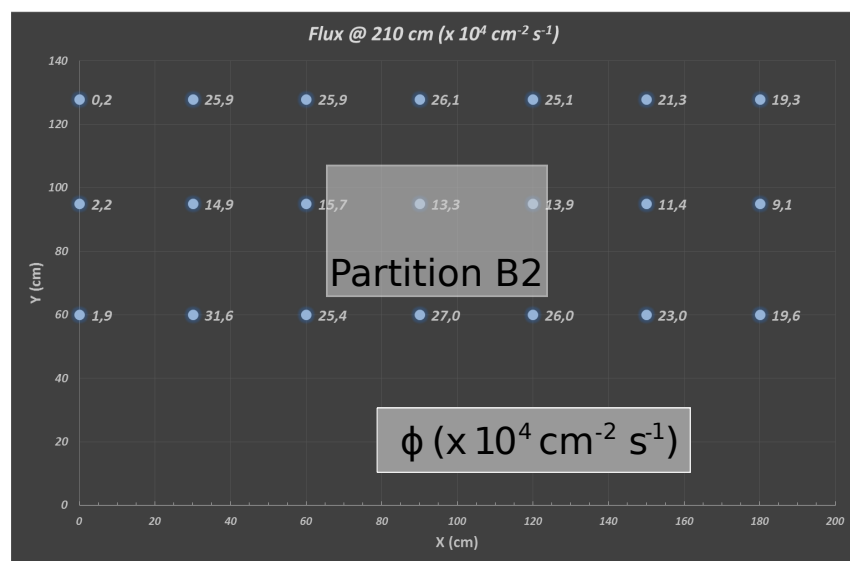


Figure 5.14: Dose measurements has been done in a plane corresponding to the tents front side. This plan is 1900 mm away from the source. As explained in the first chapter, a lens-shaped lead filter provides a uniform photon flux in the vertical plan orthogonal to the beam direction. If the second line of measured fluxes is not taken into account because of lower values due to experimental equipments in the way between the source and the tent, the uniformity of the flux is well showed by the results.

806 **5.2.5 Results and discussions**

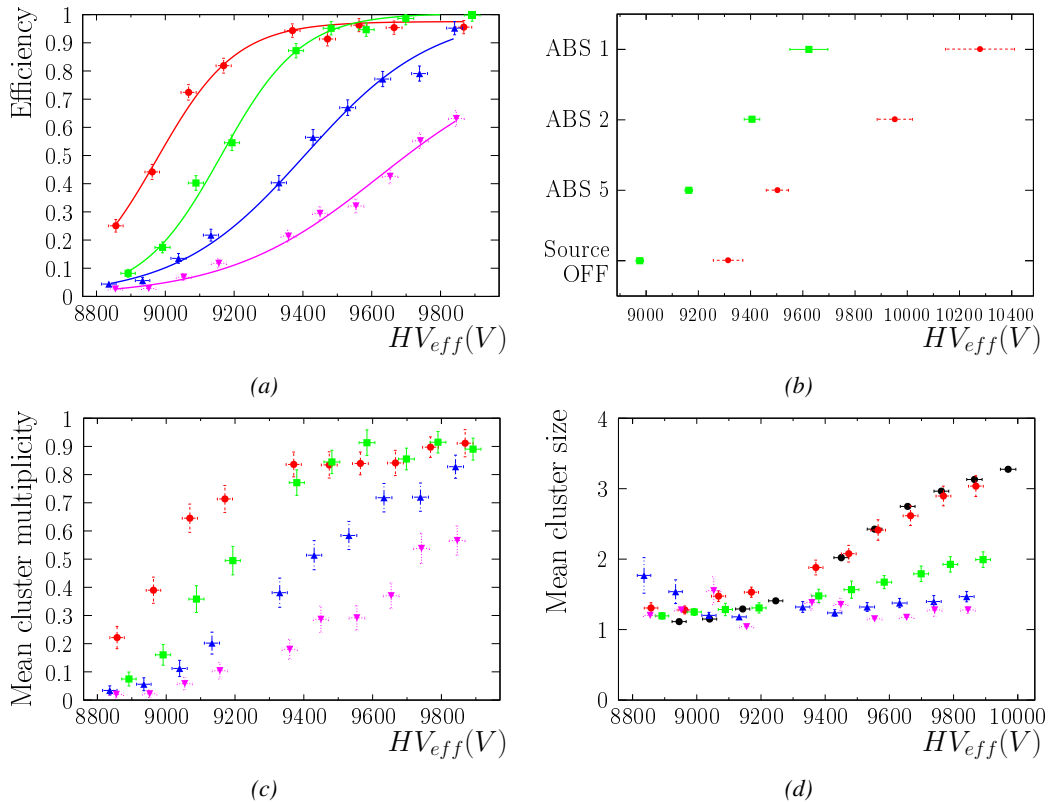


Figure 5.15

⁸⁰⁷ 5.3 Longevity tests at GIF++

⁸⁰⁸ Longevity studies imply a monitoring of the performance of the detectors probed using a high inten-
⁸⁰⁹ sity muon beam in a irradiated environment by periodically measuring their rate capability, the dark
⁸¹⁰ current running through them and the bulk resistivity of the Bakelite composing their electrodes.
⁸¹¹ GIF++, with its very intense ^{137}Cs source, provides the perfect environment to perform such kind
⁸¹² of tests. Assuming a maximum acceleration factor of 3, it is expected to accumulate the equivalent
⁸¹³ charge in 1.7 years.

⁸¹⁴ As the maximum background is found in the endcap, the choice naturally was made to focus the
⁸¹⁵ GIF++ longevity studies on endcap chambers. Most of the RPC system was installed in 2007. Nev-
⁸¹⁶ ertheless, the large chambers in the fourth endcap (RE4/2 and RE4/3) have been installed during
⁸¹⁷ LS1 in 2014. The Bakelite of these two different productions having different properties, four spare
⁸¹⁸ chambers of the present system were selected, two RE2,3/2 spares and two RE4/2 spares. Having
⁸¹⁹ two chambers of each type allows to always keep one of them non irradiated as reference, the per-
⁸²⁰ formance evolution of the irradiated chamber being then compared through time to the performance
⁸²¹ of the non irradiated one.

⁸²² The performance of the detectors under different level of irradiation is measured periodically dur-
⁸²³ ing dedicated test beam periods using the H4 muon beam. In between these test beam periods, the
⁸²⁴ two RE2,3/2 and RE4/2 chambers selected for this study are irradiated by the ^{137}Cs source in order
⁸²⁵ to accumulate charge and the gamma background is monitored, as well as the currents. The two
⁸²⁶ remaining chambers are kept non-irradiated as reference detectors. Due to the limited gas flow in
⁸²⁷ GIF++, the RE4 chamber remained non-irradiated until end of November 2016 where a new mass
⁸²⁸ flow controller has been installed allowing for bigger volumes of gas to flow in the system.

⁸²⁹ Figures 5.16 and 5.17 give us for different test beam periods, and thus for increasing integrated
⁸³⁰ charge through time, a comparison of the maximum efficiency, obtained using a sigmoid-like func-
⁸³¹ tion, and of the working point of both irradiated and non irradiated chambers [26]. No aging is yet
⁸³² to see from this data, the shifts in γ rate per unit area in between irradiated and non irradiated detec-
⁸³³ tors and RE2 and RE4 types being easily explained by a difference of sensitivity due to the various
⁸³⁴ Bakelite resistivities of the HPL electrodes used for the electrode production.

⁸³⁵ Collecting performance data at each test beam period allows us to extrapolate the maximum effi-
⁸³⁶ ciency for a background hit rate of $300\text{ Hz}/\text{cm}^2$ corresponding to the expected HL-LHC conditions.
⁸³⁷ Aging effects could emerge from a loss of efficiency with increasing integrated charge over time,
⁸³⁸ thus Figure 5.18 helps us understand such degradation of the performance of irradiated detectors in
⁸³⁹ comparison with non irradiated ones. The final answer for an eventual loss of efficiency is given in
⁸⁴⁰ Figure 5.19 by comparing for both irradiated and non irradiated detectors the efficiency sigmoids
⁸⁴¹ before and after the longevity study. Moreover, to complete the performance information, the Bake-
⁸⁴² lite resistivity is regularly measured thanks to Ag scans (Figure 5.20) and the noise rate is monitored
⁸⁴³ weekly during irradiation periods (Figure 5.21). At the end of 2016, no signs of aging were observed
⁸⁴⁴ and further investigation is needed to get closer to the final integrated charge requirements proposed
⁸⁴⁵ for the longevity study of the present CMS RPC sub-system.

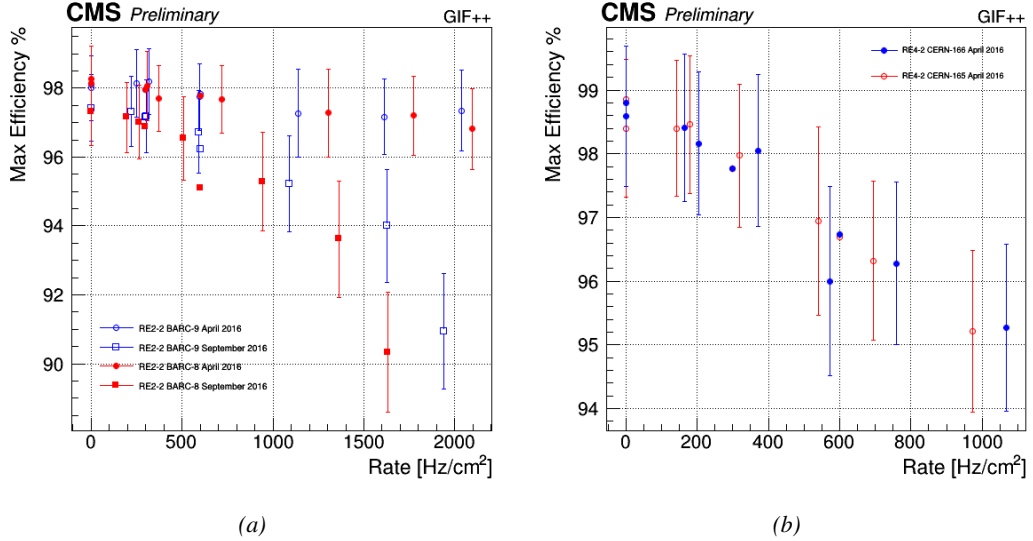


Figure 5.16: Evolution of the maximum efficiency for RE2 (5.16a) and RE4 (5.16b) chambers with increasing extrapolated γ rate per unit area at working point. Both irradiated (blue) and non irradiated (red) chambers are shown.

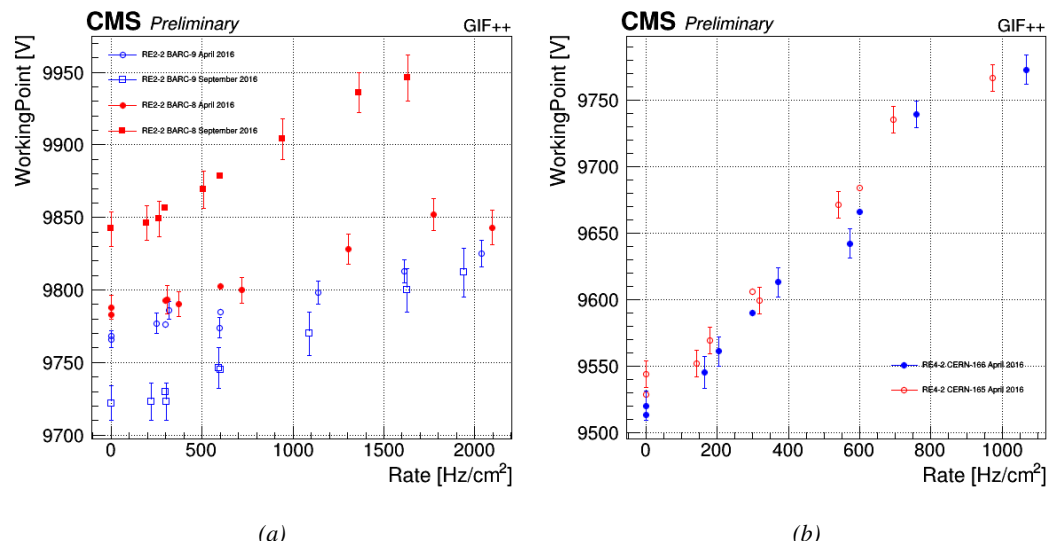


Figure 5.17: Evolution of the working point for RE2 (5.17a) and RE4 (5.17b) with increasing extrapolated γ rate per unit area at working point. Both irradiated (blue) and non irradiated (red) chambers are shown.

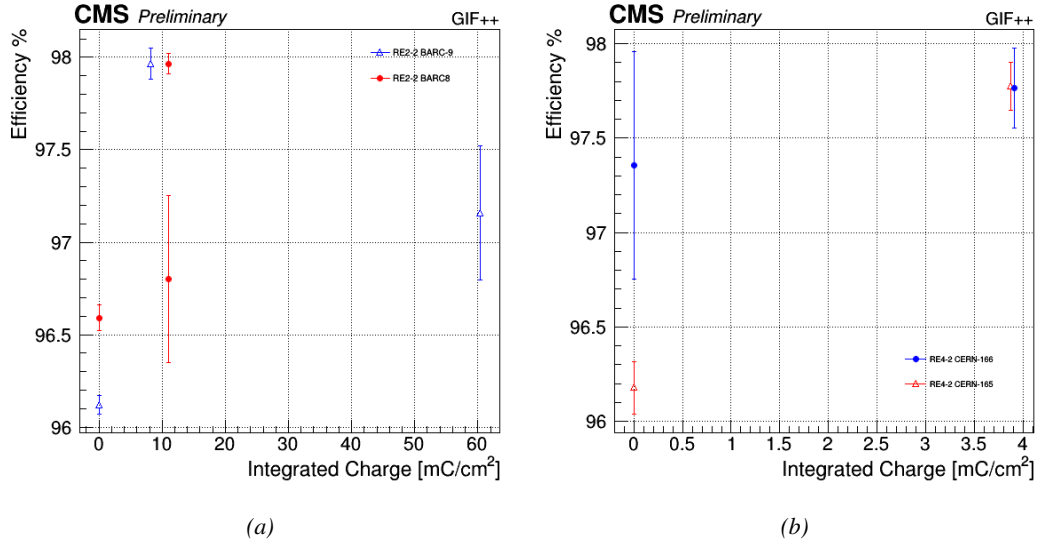


Figure 5.18: Evolution of the maximum efficiency at HL-LHC conditions, i.e. a background hit rate per unit area of $300 \text{ Hz}/\text{cm}^2$, with increasing integrated charge for RE2 (5.18a) and RE4 (5.18b) detectors. Both irradiated (blue) and non irradiated (red) chambers are shown. The integrated charge for non irradiated detectors is recorded during test beam periods and stays small with respect to the charge accumulated in irradiated chambers.

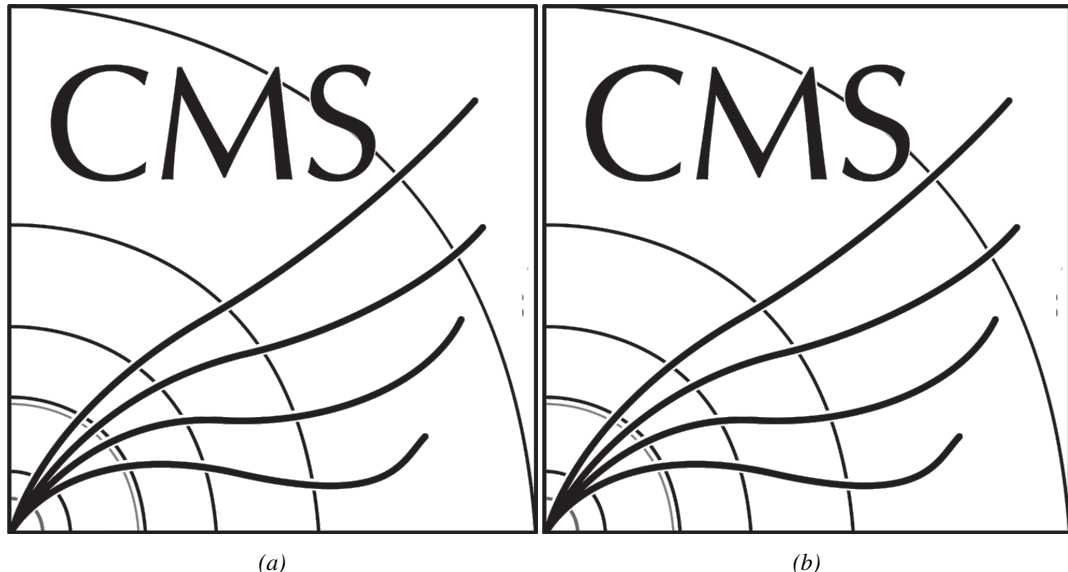


Figure 5.19: Comparison of the efficiency sigmoid before (triangles) and after (circles) irradiation for RE2 (5.19a) and RE4 (5.19b) detectors. Both irradiated (blue) and non irradiated (red) chambers are shown.

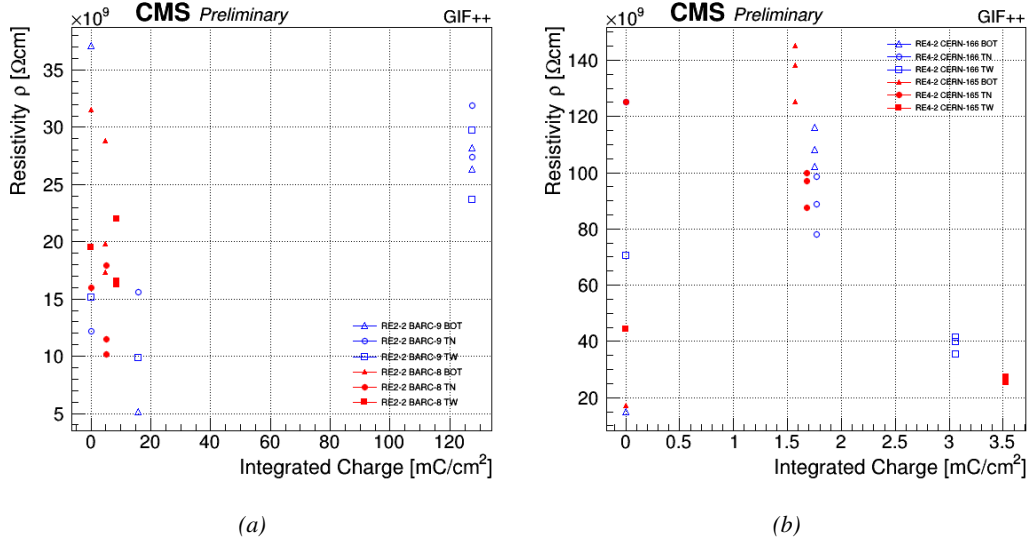


Figure 5.20: Evolution of the Bakelite resistivity for RE2 (5.20a) and RE4 (5.20b) detectors. Both irradiated (blue) and non-irradiated (red) chambers are shown.

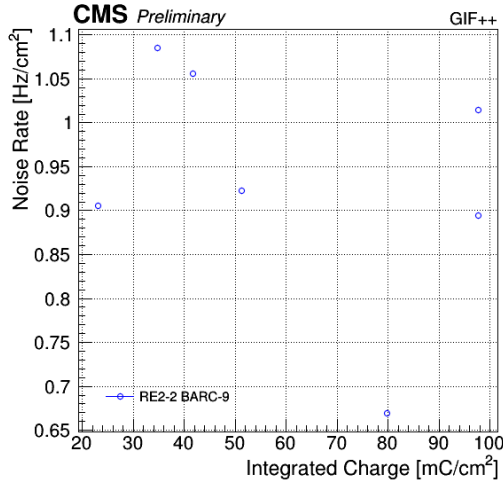


Figure 5.21: Evolution of the noise rate per unit area for the irradiated chamber RE2-2-BARC-9 only.

5.3.1 Description of the Data Acquisition

For the longevity studies, four spare chambers of the present system are used. Two spare RPCs of the RE2,3 stations as well as two spare RPCs from the new RE4 stations have been mounted in a Trolley. Six RE4 gaps are also placed in the trolley. The trolley is placed inside the GIFT++ in the upstream region of the bunker, taking the cesium source as a reference. The trolley is oriented for the detection surface of the chambers to be orthogonal to the beam line. The system can be moved along the orthogonal plane in order to have the beam in all η -partitions. For the aging the trolley is

854 moved outside the beam line and is placed in a distance of 5.2 m to the source, which irradiates the
 855 bunker using an attenuation filter of 2.2 which corresponds to a fluence of 10^7 gamma/cm^2 .

856 During GIF++ operation, the data collected can be divided into different categories as several
 857 parameters are monitored in addition to the usual RPC performance data. On one hand, to know
 858 the performance of a chamber, it is need to measure its efficiency and to know the background
 859 conditions in which it is operated. To do this, the hit signals from the chamber are recorded and
 860 stored in a ROOT file via a Data Acquisition (DAQ) software. On the other hand, it is also very
 861 important to monitor parameters such as environmental pressure and temperature, gas temperature
 862 and humidity, RPC HV, LV, and currents, or even source and beam status. This is done through the
 863 GIF++ web Detector Control Software (DCS) that stores this information in a database.

864 Two different types of tests are conducted on RPCs via the DAQ. Indeed, the performance of the
 865 detectors is measured periodically during dedicated test beam periods using the H4 muon beam. In
 866 between these test beam periods, when the beam is not available, the chambers are irradiated by the
 867 ^{137}Cs in order to accumulate deposited charge and the gamma background is measured.

868 RPCs under test are connected through LVDS cables to V1190A Time-to-Digital Converter
 869 (TDC) modules manufactured by CAEN. These modules, located in the rack area outside of the
 870 bunker, get the logic signals sent by the chambers and save them into their buffers. Due to the
 871 limited size of the buffers, the collected data is regularly erased and replaced. A trigger signal is
 872 needed for the TDC modules to send the useful data to the DAQ computer via a V1718 CAEN USB
 873 communication module.

874 In the case of performance test, the trigger signal used for data acquisition is generated by the
 875 coincidence of three scintillators. A first one is placed upstream outside of the bunker, a second one
 876 is placed downstream outside of the bunker, while a third one is placed in front of the trolley, close by
 877 the chambers. Every time a trigger is sent to the TDCs, i.e. every time a muon is detected, knowing
 878 the time delay in between the trigger and the RPC signals, signals located in the right time window
 879 are extracted from the buffers and saved for later analysis. Signals are taken in a time window of
 880 400 ns centered on the muon peak (here we could show a time spectrum). On the other hand, in the
 881 case of background rate measurement, the trigger signal needs to be "random" not to measure muons
 882 but to look at gamma background. A trigger pulse is continuously generated at a rate of 300 Hz using
 883 a dual timer. To integrate an as great as possible time, all signals contained within a time window of
 884 10us prior to the random trigger signal are extracted form the buffers and saved for further analysis
 885 (here another time spectrum to illustrate could be useful, maybe even place both spectrum together
 886 as a single Figure).

887 The signals sent to the TDCs correspond to hit collections in the RPCs. When a particle hits
 888 a RPC, it induce a signal in the pickup strips of the RPC readout. If this signal is higher than the
 889 detection threshold, a LVDS signal is sent to the TDCs. The data is then organised into 4 branches
 890 keeping track of the event number, the hit multiplicity for the whole setup, and the time and channel
 891 profile of the hits in the TDCs.

892 **5.3.2 RPC current, environmental and operation parameter monitoring**

893 In order to take into account the variation of pressure and temperature between different data taking
 894 periods the applied voltage is corrected following the relationship :

$$895 \quad HV_{eff} = HV_{app} \times \left(0.2 + 0.8 \cdot \frac{P_0}{P} \times \frac{T}{T_0} \right) \quad (5.10)$$

895 where T_0 (=293 K) and P_0 (=990 mbar) are the reference values.

896 **5.3.3 Measurement procedure**

897 Insert a short description of the online tools (DAQ, DCS, DQM).

898 Insert a short description of the offline tools : tracking and efficiency algorithm.

899 Identify long term aging effects we are monitoring the rates per strip.

900 **5.3.4 Longevity studies results**

6

901

902

Investigation on high rate RPCs

903 **6.1 Rate limitations and ageing of RPCs**

904 **6.1.1 Low resistivity electrodes**

905 **6.1.2 Low noise front-end electronics**

906 **6.2 Construction of prototypes**

907 **6.3 Results and discussions**

7

908

909

Conclusions and outlooks

910 **7.1 Conclusions**

911 **7.2 Outlooks**

References

912

- 913 [1] CERN. Geneva. LHC Experiments Committee. *The CMS muon project : Technical Design*
914 *Report*. Tech. rep. CERN-LHCC-97-032. CMS Collaboration, 1997.
- 915 [2] CERN. Geneva. LHC Experiments Committee. *Technical Proposal for the Phase-II Upgrade*
916 *of the CMS Detector*. Tech. rep. CERN-LHCC-2015-010. CMS Collaboration, 2015.
- 917 [3] CERN. Geneva. LHC Experiments Committee. *CMS, the Compact Muon Solenoid : technical*
918 *proposal*. Tech. rep. CERN-LHCC-94-38. CMS Collaboration, 1994.
- 919 [4] R. Santonico and R. Cardarelli. “Development of resistive plate counters”. In: *Nucl. Instr.*
920 *Meth. Phys. Res.* 187 (1981), pp. 377–380.
- 921 [5] Yu.N. Pestov and G.V. Fedotovich. *A picosecond time-of-flight spectrometer fot eh VEPP-2M*
922 *based on local-discharge spark counter*. Tech. rep. SLAC-TRANS-0184. SLAC, 1978.
- 923 [6] W.W. Ash, ed. *Spark Counter With A Localized Discharge*. Vol. SLAC-R-250. 1982, pp. 127–
924 131.
- 925 [7] I. Crotty et al. “The non-spark mode and high rate operation of resistive parallel plate cham-
926 bers”. In: *NIMA* 337 (1993), pp. 370–381.
- 927 [8] I. Crotty et al. “Further studies of avalanche mode operation of resistive parallel plate cham-
928 bers”. In: *NIMA* 346 (1994), pp. 107–113.
- 929 [9] R. Cardarelli et al. “Avalanche and streamer mode operation of resistive plate chambers”. In:
930 *NIMA* 382 (1996), pp. 470–474.
- 931 [10] E. Cerron Zeballos et al. “A new type of resistive plate chamber: The multigap RPC”. In:
932 *NIMA* 374 (1996), pp. 132–135.
- 933 [11] M.C.S.Williams. “The development of the multigap resistive plate chamber”. In: *Nucl. Phys.*
934 *B* 61 (1998), pp. 250–257.
- 935 [12] H. Czyrkowski et al. “New developments on resistive plate chambers for high rate operation”.
936 In: *NIMA* 419 (1998), pp. 490–496.
- 937 [13] P. Camarri et al. “Streamer suppression with SF6 in RPCs operated in avalanche mode”. In:
938 *NIMA* 414 (1998), pp. 317–324.
- 939 [14] E. Cerron Zeballos et al. “Effect of adding SF6 to the gas mixture in a multigap resistive plate
940 chamber”. In: *NIMA* 419 (1998), pp. 475–478.
- 941 [15] CERN. Geneva. LHC Experiments Committee. *ATLAS muon spectrometer: Technical design*
942 *report*. Tech. rep. CERN-LHCC-97-22. ATLAS Collaboration, 1997.
- 943 [16] CERN. Geneva. LHC Experiments Committee. *ALICE Time-Of-Flight system (TOF) : Tech-*
944 *nical Design Report*. Tech. rep. CERN-LHCC-2000-012. ALICE Collaboration, 2000.
- 945 [17] The CALICE collaboration. “First results of the CALICE SDHCAL technological proto-
946 type”. In: *JINST* 11 (2016).

- 947 [18] PoS, ed. *Density Imaging of Volcanoes with Atmospheric Muons using GRPCs*. International
948 Europhysics Conference on High Energy Physics - HEP 2011. 2011.
- 949 [19] C. Lippmann. “Detector Physics of Resistive Plate Chambers”. PhD thesis. Johann Wolfgang
950 Goethe-Universität, 2003.
- 951 [20] M. Abbrescia et al. “Properties of C2H2F4-based gas mixture for avalanche mode operation
952 of resistive plate chambers”. In: *NIMA* 398 (1997), pp. 173–179.
- 953 [21] G. Battistoni et al. “Sensitivity of streamer mode to single ionization electrons”. In: *NIMA*
954 235 (1985), pp. 91–97.
- 955 [22] M. Abbrescia et al. “Study of long-term performance of CMS RPC under irradiation at the
956 CERN GIF”. In: *NIMA* 533 (2004), pp. 102–106.
- 957 [23] H.C. Kim et al. “Quantitative aging study with intense irradiation tests for the CMS forward
958 RPCs”. In: *NIMA* 602 (2009), pp. 771–774.
- 959 [24] S. Agosteo et al. “A facility for the test of large-area muon chambers at high rates”. In: *NIMA*
960 452 (2000), pp. 94–104.
- 961 [25] PoS, ed. *CERN GIF ++ : A new irradiation facility to test large-area particle detectors for
962 the high-luminosity LHC program*. Vol. TIPP2014. 2014, pp. 102–109.
- 963 [26] M. Abbrescia et al. “Cosmic ray tests of double-gap resistive plate chambers for the CMS
964 experiment”. In: *NIMA* 550 (2005), pp. 116–126.
- 965 [27] A. Fagot. *GIF++ DAQ v4.0*. 2017. URL: https://github.com/afagot/GIF_DAQ.
- 966 [28] CAEN. *Mod. V1190-VX1190 A/B, 128/64 Ch Multihit TDC*. 14th ed. 2016.
- 967 [29] CAEN. *Mod. V1718 VME USB Bridge*. 9th ed. 2009.
- 968 [30] W-Ie-Ne-R. *VME 6021-23 VXI*. 5th ed. 2016.
- 969 [31] Wikipedia. *INI file*. 2017. URL: https://en.wikipedia.org/wiki/INI_file.
- 970 [32] S. Carrillo A. Fagot. *GIF++ Offline Analysis v6*. 2017. URL: [https://github.com/afagot/GIF_OfflineAnalysis](https://github.com/
971 afagot/GIF_OfflineAnalysis).

A

972

973

A data acquisition software for CAEN VME TDCs

974

975 Certifying detectors in the perspective of HL-LHC required to develop tools for the GIF++ experiment.
976 Among them was the C++ Data Acquisition (DAQ) software that allows to make the communications
977 in between a computer and TDC modules in order to retrieve the RPC data [27]. In this
978 appendix, details about this software, as of how the software was written, how it functions and how
979 it can be exported to another similar setup, will be given.

980 A.1 GIF++ DAQ file tree

981 GIF++ DAQ source code is fully available on github at https://github.com/afagot/GIF_DAQ. The software requires 3 non-optional dependencies:

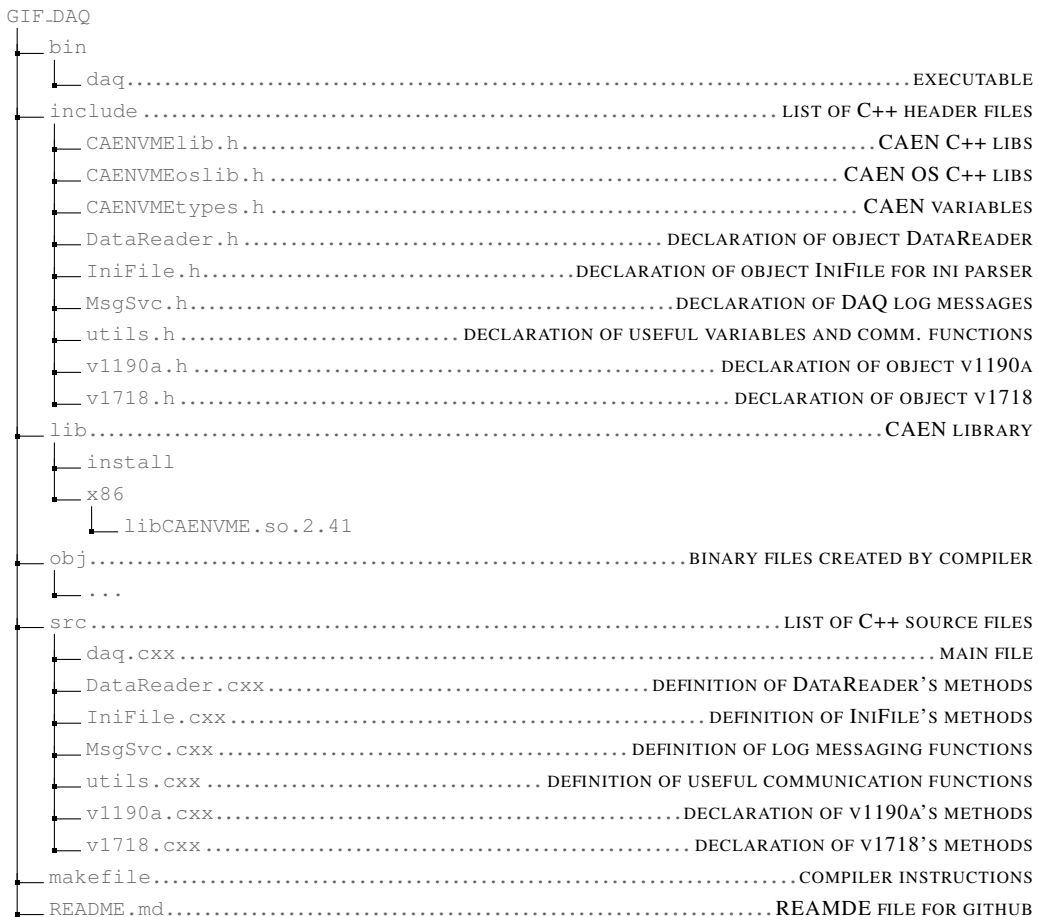
- 983 • CAEN USB Driver, to mount the VME hardware,
984 • CAEN VME Library, to communicate with the VME hardware, and
985 • ROOT, to organize the collected data into a TTree.

986 The CAEN VME library will not be packaged by distributions and will need to be installed man-
987 ually. To compile the GIF++ DAQ project via a terminal, from the DAQ folder use the command:

988 `make`

990 The source code tree is provided below along with comments to give an overview of the files' con-
991 tent. The different objects created for this project (`v1718`, `v1190a`, `IniFile` & `DataReader`) will be
992 described in details in the following sections.

993



994 A.2 Usage of the DAQ

995 GIF++ DAQ, as used in GIF++, is not a standalone software. Indeed, the system being more complexe,
 996 the DAQ only is a sub-layer of the software architecture developped to control and monitor
 997 the RPCs that are placed into the bunker for performance study in an irradiated environment. The top
 998 layer of GIF++ is a Web Detector Control System (webDCS) application. The DAQ is only called
 999 by the webDCS when data needs to be acquired. The webDCS operates the DAQ through command
 1000 line. To start the DAQ, the webDCS calls:

```
1001
1002     bin/daq /path/to/the/log/file/in/the/output/data/folder
```

1003 where /path/to/the/log/file/in/the/output/data/folder is the only argument required. This
 1004 log file is important for the webDCS as this file contains all the content of the communication of the
 1005 webDCS and the different systems monitored by the webDCS. Its content is constantly displayed
 1006 during data taking for the users to be able to follow the operations. The communication messages
 1007 are normally sent to the webDCS log file via the functions declared in file MsgSvc.h, typically
 1008 MSG_INFO(string message).

1009

1010 A.3 Description of the readout setup

1011 The CMS RPC setup at GIF++ counts 5 V1190A Time-to-Digital Converter (TDC) manufactured
 1012 by CAEN [28]. V1190A are VME units accepting 128 independent Multi-Hit/Multi-Event TDC
 1013 channels whose signals are treated by 4 100 ps high performance TDC chips developed by CERN
 1014 / ECP-MIC Division. The communication between the computer and the TDCs to transfer data is
 1015 done via a V1718 VME master module also manufactured by CAEN and operated from a USB
 1016 port [29]. These VME modules are all hosted into a 6U VME 6021 powered crate manufactured by
 1017 W-Ie-Ne-R than can accommodate up to 21 VME bus cards [30]. These 3 components of the DAQ
 1018 setup are shown in Figure A.1.

1019

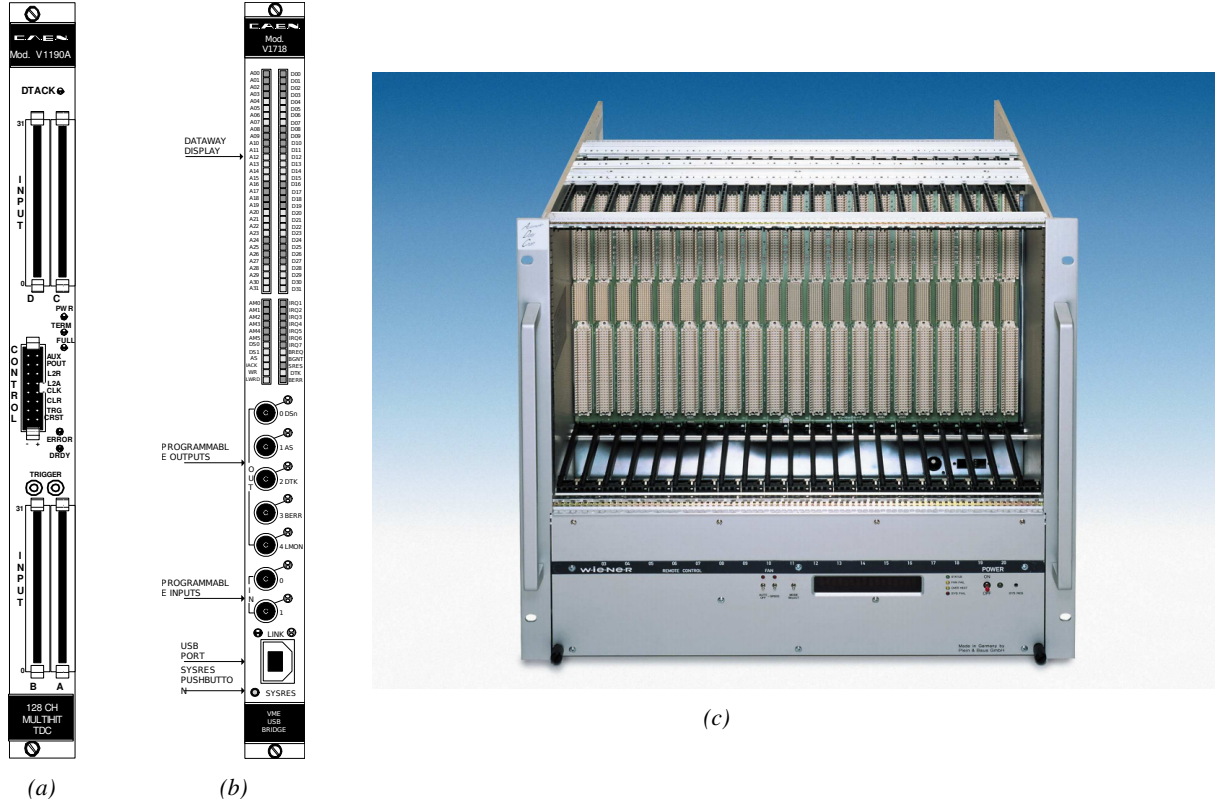


Figure A.1: (A.1a) View of the front panel of a V1190A TDC module [28]. (A.1b) View of the front panel of a V1718 Bridge module [29]. (A.1c) View of the front panel of a 6U 6021 VME crate [30].

1020

A.4 Data read-out

1021 To efficiently perform a data readout algorithm, C++ objects to handle the VME modules (TDCs
 1022 and VME bridge) have been created along with objects to store data and read the configuration file

1023 that comes as an input of the DAQ software.

1024

1025 A.4.1 V1190A TDCs

1026 The DAQ used at GIF takes profit of the *Trigger Matching Mode* offered by V1190A modules.
 1027 This setting is enabled through the method `v1190a::SetTrigMatching (int ntdcs)` where `ntdcs`
 1028 is the total number of TDCs in the setup this setting needs to be enabled for (Source Code A.1). A
 1029 trigger matching is performed in between a trigger time tag, a trigger signal sent into the TRIGGER
 1030 input of the TDC visible on Figure A.1a, and the channel time measurements, signals recorded from
 1031 the detectors under test in our case. Control over this data acquisition mode, explained through
 1032 Figure A.2, is offered via 4 programmable parameters:

- 1033 • **match window:** the matching between a trigger and a hit is done within a programmable time
 1034 window. This is set via the method

1035 `void v1190a::SetTrigWindowWidth(Uint windowHeight, int ntdcs)`

- 1036 • **window offset:** temporal distance between the trigger tag and the start of the trigger matching
 1037 window. This is set via the method

1038 `void v1190a::SetTrigWindowWidth(Uint windowHeight, int ntdcs)`

- 1039 • **extra search margin:** an extended time window is used to ensure that all matching hits are
 1040 found. This is set via the method

1041 `void v1190a::SetTrigSearchMargin(Uint searchMargin, int ntdcs)`

- 1042 • **reject margin:** older hits are automatically rejected to prevent buffer overflows and to speed
 1043 up the search time. This is set via the method

1044 `void v1190a::SetTrigRejectionMargin(Uint rejectMargin, int ntdcs)`

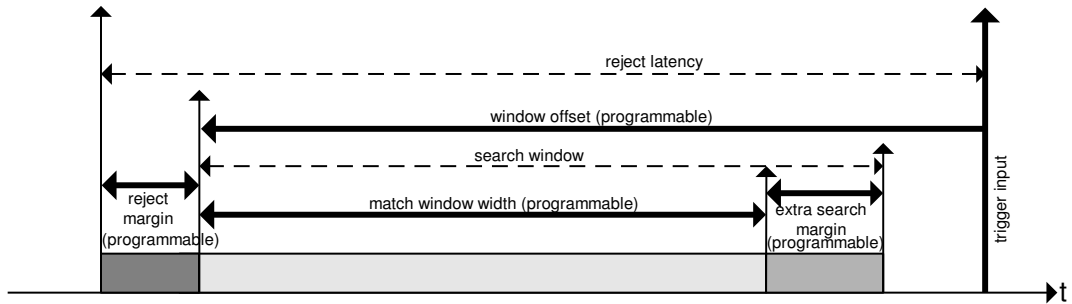


Figure A.2: Module V1190A Trigger Matching Mode timing diagram [28].

1045 Each of these 4 parameters are given in number of clocks, 1 clock being 25 ns long. It is easy to
 1046 understand at this level that there are 3 possible functioning settings:

- 1047 • **1:** the match window is entirely contained after the trigger signal,

- 1048 • **2:** the match window overlaps the trigger signal, or

- 1049 • **3:** the match window is entirely contained before the trigger signal as displayed on Figure A.2.

1050 In both the first and second cases, the sum of the window width and of the offset can be set to
1051 a maximum of 40 clocks, which corresponds to 1 μ s. Evidently, the offset can be negative, allowing
1052 for a longer match window, with the constraint of having the window ending at most 1 μ s after the
1053 trigger signal. In the third case, the maximum negative offset allowed is of 2048 clocks (12 bit) cor-
1054 responding to 51.2 μ s, the match window being strictly smaller than the offset. In the case of GIF++,
1055 the choice has been made to use this last setting by delaying the trigger signal. During the studies
1056 performed in GIF++, both the efficiency of the RPCs, probed using a muon beam, and the noise or
1057 gamma background rate are monitored. The extra search and reject margins are left unused.
1058 To probe the efficiency of RPC detectors, the trigger time tag is provided by the coïncidence of
1059 scintillators when a bunch of muons passes through GIF++ area is used to trigger the data acquisi-
1060 tion. For this measurement, it is useful to reduce the match window width only to contain the muon
1061 information. Indeed, the delay in between a trigger signal and the detection of the corresponding
1062 muon in the RPC being very contant (typically a few tens of ns due to jitter and cable length), the
1063 muon signals are very localised in time. Thus, due to a delay of approximalety 325 ns in between
1064 the muons and the trigger, the settings where chosen to have a window width of 24 clocks (600 ns)
1065 centered on the muon peak thanks to a negative offset of 29 clocks (725 ns).
1066 On the otherhand, monitoring the rates don't require for the DAQ to look at a specific time window.
1067 It is important to integrate enough time to have a robust measurement of the rate as the number of
1068 hits per time unit. The triggerring signal is provided by a pulse generator at a frequency of 300 Hz
1069 to ensure that the data taking occurs in a random way, with respect to beam physics, to probe only
1070 the irradiation spectrum on the detectors. The match window is set to 400 clocks (10 μ s) and the
1071 negative offset to 401 clocks as it needs to exceed the value of the match window.

```

1072
1073 class v1190a
{
    private :
        long             Handle;
        vector<Data32>   Address;
        CVDataWidth      DataWidth;
        CVAddressModifier AddressModifier;

    public:
        v1190a(long handle, IniFile *inifile, int ntdcs);
        ~v1190a();
        Data16 write_op_reg(Data32 address, int code, string error);
        Data16 read_op_reg(Data32 address, string error);
        void Reset(int ntdcs);
        void Clear(int ntdcs);
        void TestWR(Data16 value,int ntdcs);
        void CheckTDCStatus(int ntdcs);
        void CheckCommunication(int ntdcs);
        void SetTDCTestMode(Data16 mode,int ntdcs);
        void SetTrigMatching(int ntdcs);
        void SetTrigTimeSubtraction(Data16 mode,int ntdcs);
        void SetTrigWindowWidth(Uint windowHeight,int ntdcs);
        void SetTrigWindowOffset(Uint windowOffset,int ntdcs);
        void SetTrigSearchMargin(Uint searchMargin,int ntdcs);
        void SetTrigRejectionMargin(Uint rejectMargin,int ntdcs);
        void GetTrigConfiguration(int ntdcs);
        void SetTrigConfiguration(IniFile *inifile,int ntdcs);
        void SetTDCDetectionMode(Data16 mode,int ntdcs);
        void SetTDCResolution(Data16 lsb,int ntdcs);
        void SetTDCDeadTime(Data16 time,int ntdcs);
        void SetTDCHeadTrailer(Data16 mode,int ntdcs);
        void SetTDCEventSize(Data16 size,int ntdcs);
        void SwitchChannels(IniFile *inifile,int ntdcs);
        void SetIRQ(Data32 level, Data32 count,int ntdcs);
        void SetBlockTransferMode(Data16 mode,int ntdcs);
        void Set(IniFile *inifile,int ntdcs);
        void CheckStatus(CVErrorCodes status) const;
        int ReadBlockD32(Uint tdc, const Data16 address,
                         Data32 *data, const Uint words, bool ignore_berr);
        Uint Read(RAWData *DataList,int ntdcs);
};

1074
```

Source Code A.1: Description of C++ object v1190a.

1075 The v1190a object, defined in the DAQ software as in Source Code A.1, offers the possibility to
1076 concatenate all TDCs in the readout setup into a single object containing a list of hardware addresses
1077 (addresses to access the TDCs' buffer through the VME crate) and each constructor and method acts
1078 on the list of TDCs.

1079

1080 A.4.2 DataReader

1081 Enabled thanks to v1190a::SetBlockTransferMode(Data16 mode, int ntdcs), the data transfer
1082 is done via Block Transfer (BLT). Using BLT allows to tranfer a fixed number of events called a
1083 *block*. This is used together with an Almost Full Level (AFL) of the TDCs' output buffers, defined

1084 through `v1190a::SetIRQ(Data32 level, Data32 count, int ntdcs)`. This AFL gives the maximum amount of 32735 words (16 bits, corresponding to the depth of a TDC output buffer) that can
 1085 written in a buffer before an Interrupt Request (IRQ) is generated and seen by the VME Bridge,
 1086 stopping the data acquisition to transfer the content of each TDC buffers before resuming. For each
 1087 trigger, 6 words or more are written into the TDC buffer:

- 1089 • a **global header** providing information of the event number since the beginning of the data
 1090 acquisition,
- 1091 • a **TDC header**,
- 1092 • the **TDC data** (*if any*), 1 for each hit recorded during the event, providing the channel and the
 1093 time stamp associated to the hit,
- 1094 • a **TDC error** providing error flags,
- 1095 • a **TDC trailer**,
- 1096 • a **global trigger time tag** that provides the absolute trigger time relatively to the last reset,
 1097 and
- 1098 • a **global trailer** providing the total word count in the event.

1099 As previously described in Section 4.4.3, CMS RPC FEEs provide us with 100 ns long LVDS
 1100 output signals that are injected into the TDCs' input. Any avalanche signal that gives a signal above
 1101 the FEEs threshold is thus recorded by the TDCs as a hit within the match window. Each hit is
 1102 assigned to a specific TDC channel with a time stamp, with a precision of 100 ps. The reference
 1103 time, $t_0 = 0$, is provided by the beginning of the match window. Thus for each trigger, coming from
 1104 a scintillator coïncidence or the pulse generator, a list of hits is stored into the TDCs' buffers and
 1105 will then be transferred into a ROOT Tree.

1106 When the BLT is used, it is easy to understand that the maximum number of words that have
 1107 been set as ALF will not be a finite number of events or, at least, the number of events that would
 1108 be recorded into the TDC buffers will not be a multiple of the block size. In the last BLT cycle to
 1109 transfer data, the number of events to transfer will most probably be lower than the block size. In that
 1110 case, the TDC can add fillers at the end of the block but this option requires to send more data to the
 1111 computer and is thus a little slower. Another solution is to finish the transfer after the last event by
 1112 sending a bus error that states that the BLT reached the last event in the pile. This method has been
 1113 chosen in GIF++.

1115 Due to irradiation, an event in GIF++ can count up to 300 words per TDC. A limit of 4096 words
 1116 (12 bits) has been set to generate IRQ which represent from 14 to almost 700 events depending on
 1117 the average of hits collected per event. Then the block size has been set to 100 events with enabled
 1118 bus errors. When an AFL is reached for one of the TDCs, the VME bridge stops the acquisition by
 1119 sending a BUSY signal.

1121

1122 The data is then transferred one TDC at a time into a structure called `RAWData` (Source Code A.2).

```
1123
1124 struct RAWData{
1125     vector<int>           *EventList;
1126     vector<int>           *NHitsList;
1127     vector<int>           *QFlagList;
1128     vector<vector<int> >   *Channellist;
1129     vector<vector<float> > *TimeStampList;
1130 };
1131 
```

1125 *Source Code A.2: Description of data holding C++ structure `RAWData`.*

1126 In order to organize the data transfer and the data storage, an object called `DataReader` was
 1127 created (Source Code A.3). On one hand, it has `v1718` and `v1190a` objects as private members for
 1128 communication purposes, such as VME modules settings via the configuration file `*iniFile` or data
 1129 read-out through `v1190a::Read()` and on the other hand, it contains the structure `RAWData` that allows
 1130 to organise the data in vectors reproducing the tree structure of a ROOT file.

```
1131
1132 class DataReader
1133 {
1134     private:
1135         bool      StopFlag;
1136         IniFile *iniFile;
1137         Data32  MaxTriggers;
1138         v1718   *VME;
1139         int       nTDCs;
1140         v1190a  *TDCs;
1141         RAWData TDCData;
1142
1143     public:
1144         DataReader();
1145         virtual ~DataReader();
1146         void      SetIniFile(string inifilename);
1147         void      SetMaxTriggers();
1148         Data32  GetMaxTriggers();
1149         void      SetVME();
1150         void      SetTDC();
1151         int       GetQFlag(Uint it);
1152         void      Init(string inifilename);
1153         void      FlushBuffer();
1154         void      Update();
1155         string  GetFileName();
1156         void      WriteRunRegistry(string filename);
1157         void      Run();
1158 };
1159 
```

1133 *Source Code A.3: Description of C++ object `DataReader`.*

1134 Each event is transferred from `TDCData` and saved into branches of a ROOT `TTree` as 3 integers
 1135 that represent the event ID (`EventCount`), the number of hits read from the TDCs (`nHits`), and the
 1136 quality flag that provides information for any problem in the data transfer (`qflag`), and 2 lists of
 1137 `nHits` elements containing the fired TDC channels (`TDCCh`) and their respective time stamps (`TDCTS`),
 1138 as presented in Source Code A.4. The ROOT file file is named using information contained into
 1139 the configuration file, presented in section A.5.2. The needed information is extracted using method
 1140 `DataReader::GetFileName()` and allow to build the output filename format `ScanXXXXXX_HVX_DAQ.root`

1141 where ScanXXXXXX is a 6 digit number representing the scan number into GIFT++ database and HVX
 1142 the HV step within the scan that can be more than a single digit. An example of ROOT data file is
 1143 provided with Figure A.3.

```
1144
RAWData TDCData;
TFile *outputFile = new TFile(outputFileName.c_str(),"recreate");
TTree *RAWDataTree = new TTree("RAWData","RAWData");

int EventCount = -9;
int nHits = -8;
int qflag = -7;
vector<int> TDCCh;
vector<float> TDCTS;

RAWDataTree->Branch("EventNumber",&EventCount, "EventNumber/I");
RAWDataTree->Branch("number_of_hits",&nHits,"number_of_hits/I");
RAWDataTree->Branch("Quality_flag",&qflag,"Quality_flag/I");
RAWDataTree->Branch("TDC_channel",&TDCCh);
RAWDataTree->Branch("TDC_TimeStamp",&TDCTS);

1145
//...
//Here read the TDC data using v1190a::Read() and place it into
//TDCData for as long as you didn't collect the requested amount
//of data.
//...

for(Uint i=0; i<TDCData.EventList->size(); i++){
    EventCount = TDCData.EventList->at(i);
    nHits = TDCData.NHitsList->at(i);
    qflag = TDCData.QFlagList->at(i);
    TDCCh = TDCData.ChannelList->at(i);
    TDCTS = TDCData.TimeStampList->at(i);
    RAWDataTree->Fill();
}
```

1146 *Source Code A.4: Highlight of the data transfer and organisation within DataReader::Run() after the data has been collected into TDCData.*

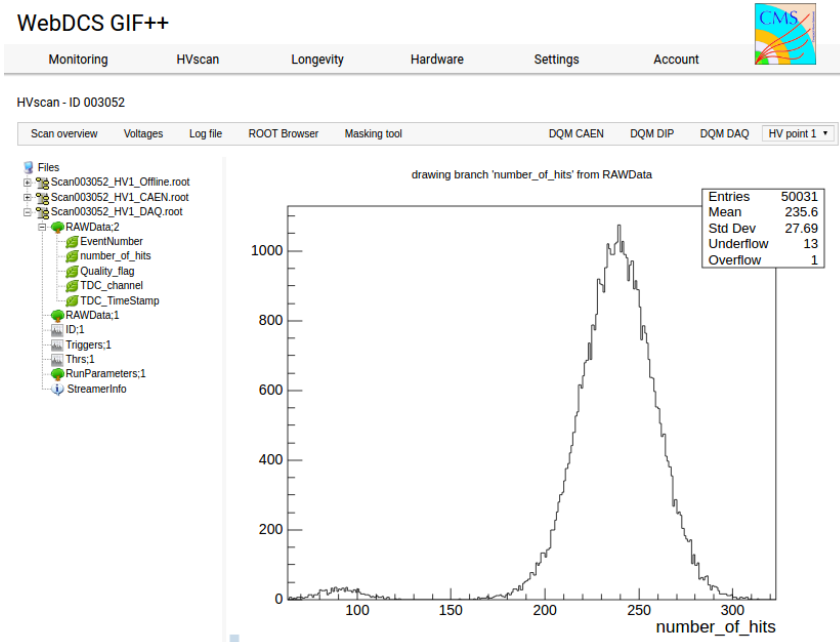


Figure A.3: Structure of the ROOT output file generated by the DAQ. The 5 branches (EventNumber, number_of_hits, Quality_flag, TDC_channel and TDC_TimeStamp) are visible on the left panel of the ROOT browser. On the right panel is visible the histogram corresponding to the variable nHits. In this specific example, there were approximately 50k events recorded to measure the gamma irradiation rate on the detectors. Each event is stored as a single entry in the TTree.

1147 A.4.3 Data quality flag

1148 Among the parameters that are recorded for each event, the quality flag, defined in Source Code A.5,
 1149 is determined on the fly by checking the data recorded by every single TDC. From method `v1190a::Read()`,
 1150 it can be understood that the content of each TDC buffer is readout one TDC at a time. Entries are
 1151 created in the data list for the first TDC and then, when the second buffer is readout, events corre-
 1152 sponding to entries that have already been created to store data for the previous TDC are added to
 1153 the existing list element. On the contrary, when an event entry has not been yet created in the data
 1154 list, a new entry is created.

```
1155
 1156 typedef enum _QualityFlag {
 1157     GOOD      = 1,
 1158     CORRUPTED = 0
 1159 } QualityFlag;
```

1157 *Source Code A.5: Definition of the quality flag `enum`.*

1158 It is possible that each TDC buffer contains a different number of events. In cases where the first
 1159 element in the buffer list is an event for corresponds to a new entry, the difference in between the
 1160 entry from the buffer and the last entry in the data list is recorded and checked. If it is greater than 1,
 1161 what should never be the case, the quality flag is set to CORRUPTED for this TDC and an empty entry
 1162 is created in the place of the missing ones. Missing entries are believe to be the result of a bad hold

1163 on the TDC buffers at the moment of the readout. Indeed, the software hold is effective only on 1
 1164 TDC at a time and no solution as been found yet to completely block the writting in the buffers when
 1165 an IRQ is received.

1166 At the end of each BLT cycle, the ID of the last entry stored for each TDC buffer is not recorded.
 1167 When starting the next cycle, if the first entry in the pile corresponds to an event already existing
 1168 in the list, the readout will start from this list element and will not be able to check the difference
 1169 in between this entry's ID and the one of the last entry that was recorded for this TDC buffer in
 1170 the previous cycle. In the case events were missing, the flag stays at its initial value of 0, which is
 1171 similar to CORRUPTED and it is assumed that then this TDC will not contribute to `number_of_hits`,
 1172 `TDC_channel` or `TDC_TimeStamp`.

1173 Finally, since there will be 1 `RAWData` entry per TDC for each event (meaning `nTDCs` entries,
 1174 referring to `DataReader` private attribute), the individual flags of each TDC will be added together.
 1175 The final format is an integer composed `nTDCs` digits where each digit is the flag of a specific TDC.
 1176 This is constructed using powers of 10 like follows:

```
1177 TDC 0: QFlag = 100 × _QualityFlag
1178 TDC 1: QFlag = 101 × _QualityFlag
1179 ...
1180 TDC N: QFlag = 10N × _QualityFlag
```

1181 and the final flag to be with N digits:

```
1182 QFlag = n....3210
```

1183 each digit being 1 or 0. Below is given an example with a 4 TDCs setup.

1184 If all TDCs were good : `QFlag = 1111`,

1185 but if TDC 2 was corrupted : `QFlag = 1011`.

1186 When data taking is over and the data contained in the dynamical `RAWData` structure is transferred
 1187 to the ROOT file, all the 0s are changed into 2s by calling the method `DataReader::GetQFlag()`.
 1188 This will help translating the flag without knowing the number of TDCs beforehand. Indeed, a flag
 1189 111 could be due to a 3 TDC setup with 3 good individual TDC flags or to a more than 3 TDC setup
 1190 with TDCs those ID is greater than 2 being CORRUPTED, thus giving a 0.

1191 The quality flag has been introduced quite late, in October 2017 only, to the list of GIFT++ DAQ
 1192 parameters to be recorded into the output ROOT file. Before this addition, the missing data, corrupting
 1193 the quality for the offline analysis, was contributing to artificially fill data with lower multiplicity.
 1194 Looking at `TBranch number_of_hits` provides an information about the data of the full GIFT++
 1195 setup. When a TDC is not able to transfer data for a specific event, the effect is a reduction of the
 1196 total number of hits recorded in the full setup, this is what can be seen from Figure A.4. After offline
 1197 reconstruction detector by detector, the effect of missing events can be seen in the artificially filled
 1198 bin at multiplicity 0 shown in Figure A.5. Nonetheless, for data with high irradiation levels, as it is
 1199 the case for Figure A.5a, discarding the fake multiplicity 0 data can be done easily during the offline
 1200 analysis. At lower radiation, the missing events contribution becomes more problematic as the multi-
 1201 tiplicity distribution overlaps the multiplicity 0 and that in the same time the proportion of missing

events decreases. Attempts to fit the distribution with a Poisson or skew distribution function were not conclusive and this very problem has been at the origin of the quality flag that allows to give a non ambiguous information about each event quality.

1205

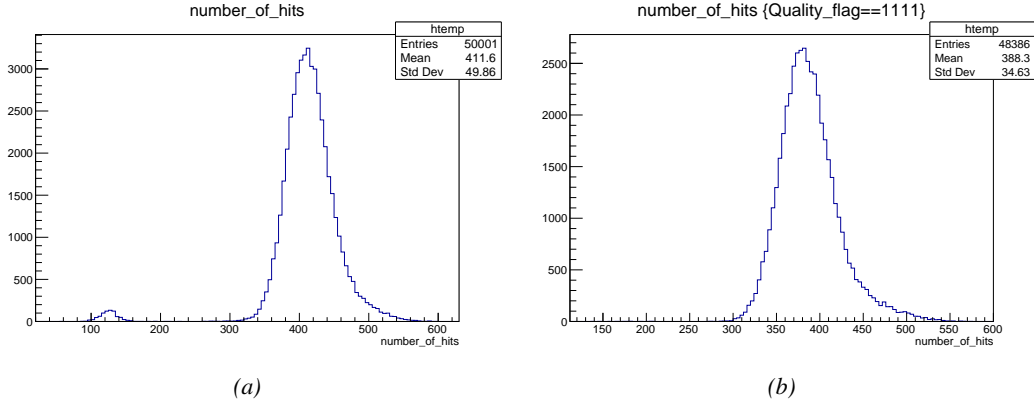


Figure A.4: The effect of the quality flag is explained by presenting the content of TBranch `number_of_hits` of a data file without `Quality_flag` in Figure A.4a and the content of the same TBranch for data corresponding to a `Quality_flag` where all TDCs were labelled as `GOOD` in Figure A.4b taken with similar conditions. It can be noted that the number of entries in Figure A.4b is slightly lower than in Figure A.4a due to the excluded events.

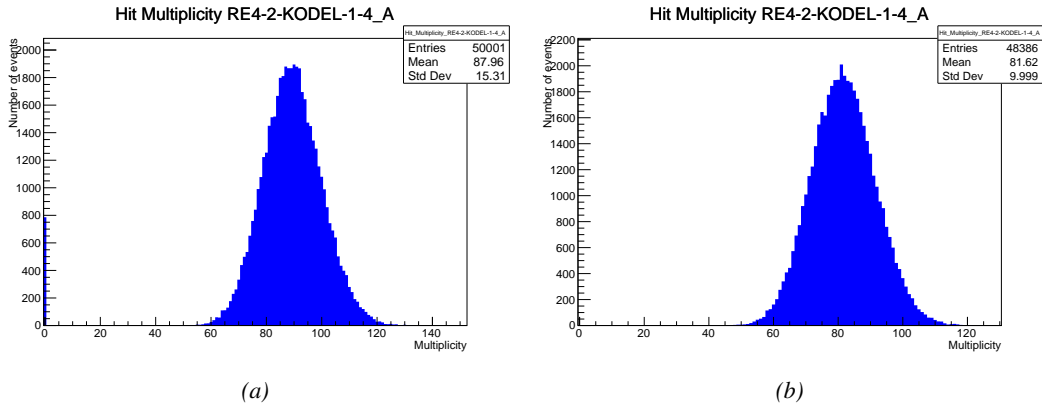


Figure A.5: Using the same data as previously showed in Figure A.4, the effect of the quality flag is explained by presenting the reconstructed hit multiplicity of a data file without `Quality_flag` in Figure A.5a and the reconstructed content of the same RPC partition for data corresponding to a `Quality_flag` where all TDCs were labelled as `GOOD` in Figure A.5b taken with similar conditions. The artificial high content of bin 0 is completely suppressed.

1206

A.5 Communications

1207
1208

To ensure data readout and dialog in between the machine and the TDCs or in between the webDCS and the DAQ, different communication solutions were used. First of all, it is important to have a

1209 module to allow the communication in between the TDCs and the computer from which the DAQ
 1210 operates. When this communication is effective, shifters using the webDCS to control data taking
 1211 can thus send instructions to the DAQ.

1212

1213 A.5.1 V1718 USB Bridge

1214 In the previous section, the data transfer has been discussed. The importance of the `v1718` object
 1215 (Source Code A.6), used as private member of `DataReader`, was not explicated. VME master
 1216 modules are used for communication purposes as they host the USB port that connects the pow-
 1217 ered crate buffer to the computer where the DAQ is installed. From the source code point of view,
 1218 this object is used to control the communication status, by reading the returned error codes with
 1219 `v1718::CheckStatus()`, or to check for IRQs coming from the TDCs through `v1718::CheckIRQ()`.
 1220 Finally, to ensure that triggers are blocked at the hardware level, a NIM pulse is sent out of one of the
 1221 5 programmable outputs (`v1718::SendBUSY()`) to the VETO of the coincidence module where the
 1222 trigger signals originate from. As long as this signal is ON, no trigger can reach the TDCs anymore.
 1223

```
1224 class v1718{
1225     private:
1226         int             Handle;
1227         Data32          Data;           // Data
1228         CVIRQLevels    Level;         // Interrupt level
1229         CVAddressModifier AM;          // Addressing Mode
1230         CVDataWidth     DataSize;       // Data Format
1231         Data32          BaseAddress;   // Base Address
1232
1233     public:
1234         v1718(IniFile *inifile);
1235         ~v1718();
1236         long            GetHandle(void) const;
1237         int             SetData(Data16 data);
1238         Data16          GetData(void);
1239         int             SetLevel(CVIRQLevels level);
1240         CVIRQLevels    GetLevel(void);
1241         int             SetAM(CVAddressModifier am);
1242         CVAddressModifier GetAM(void);
1243         int             SetDatasize(CVDataWidth datasize);
1244         CVDataWidth     GetDataSize(void);
1245         int             SetBaseAddress(Data16 baseaddress);
1246         Data16          GetBaseAddress(void);
1247         void            CheckStatus(CVErrorCodes status) const;
1248         void            CheckIRQ();
1249         void            SetPulsers();
1250         void            SendBUSY(BusyLevel level);
1251     };
1252
```

1225 *Source Code A.6: Description of C++ object v1718.*

1226 A.5.2 Configuration file

1227 The DAQ software takes as input a configuration file written using INI standard [31]. This file is
 1228 partly filled with the information provided by the shifters when starting data acquisition using the
 1229 webDCS, as shown by Figure A.6. This information is written in section [`General`] and will later

1230 be stored in the ROOT file that contains the DAQ data as can be seen from Figure A.3. Indeed,
 1231 another `TTree` called `RunParameters` as well as the 2 histograms `ID`, containing the scan number,
 1232 start and stop time stamps, and `Triggers`, containing the number of triggers requested by the shifter,
 1233 are available in the data files. Moreover, `ScanID` and `HV` are then used to construct the file name
 1234 thanks to the method `DataReader::GetFileName()`.

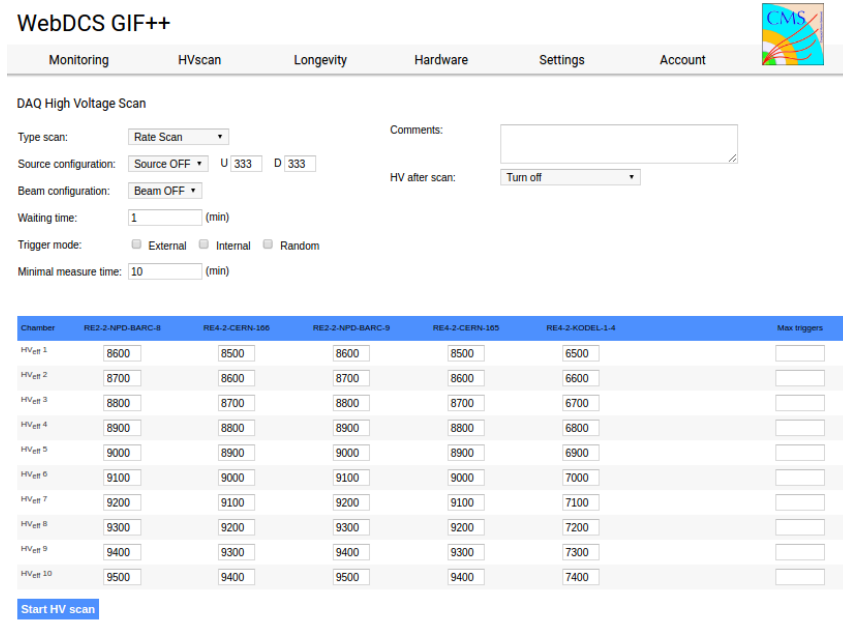


Figure A.6: WebDCS DAQ scan page. On this page, shifters need to choose the type of scan (Rate, Efficiency or Noise Reference scan), the gamma source configuration at the moment of data taking, the beam configuration, and the trigger mode. These information will be stored in the DAQ ROOT output. Are also given the minimal measurement time and waiting time after ramping up of the detectors is over before starting the data acquisition. Then, the list of HV points to scan and the number of triggers for each run of the scan are given in the table underneath.

1235 The rest of the information is written beforehand in the configuration file template, as explicated
 1236 in Source Code A.7, and contains the hardware addresses to the different VME modules in the
 1237 setup as well as settings for the TDCs. As the TDC settings available in the configuration file are not
 1238 supposed to be modified, an improvement would be to remove them from the configuration file and
 1239 to hardcode them inside of the DAQ code itself or to place them into a different INI file that would
 1240 host only the TDC settings to lower the probability for a bad manipulation of the configuration file
 1241 that can be modified from one of webDCS' menus.

1242

```
[General]
TdcS=4
ScanID=$scanid
HV=$HV
RunType=$runtype
MaxTriggers=$maxtriggers
Beam=$beam
[VMEInterface]
Type=V1718
BaseAddress=0xFF0000
Name=VmeInterface
[TDC0]
Type=V1190A
BaseAddress=0x00000000
Name=Tdc0
StatusA00-15=1
StatusA16-31=1
StatusB00-15=1
StatusB16-31=1
StatusC00-15=1
StatusC16-31=1
StatusD00-15=1
StatusD16-31=1
[TDC1]
Type=V1190A
BaseAddress=0x11110000
Name=Tdc1
StatusA00-15=1
StatusA16-31=1
StatusB00-15=1
StatusB16-31=1
StatusC00-15=1
StatusC16-31=1
StatusD00-15=1
StatusD16-31=1
[TDC2]
Type=V1190A
BaseAddress=0x22220000
Name=Tdc2
StatusA00-15=1
StatusA16-31=1
StatusB00-15=1
StatusB16-31=1
StatusC00-15=1
StatusC16-31=1
StatusD00-15=1
StatusD16-31=1
[TDC3]
Type=V1190A
BaseAddress=0x44440000
Name=Tdc3
StatusA00-15=1
StatusA16-31=1
StatusB00-15=1
StatusB16-31=1
StatusC00-15=1
StatusC16-31=1
StatusD00-15=1
StatusD16-31=1
[TDCSettings]
TriggerExtraSearchMargin=0
TriggerRejectMargin=0
TriggerTimeSubtraction=0b1
TdcDetectionMode=0b01
TdcResolution=0b10
TdcDeadTime=0b00
TdcHeadTrailer=0b1
TdcEventSize=0b1001
TdcTestMode=0b0
BLTMode=1
```

Source Code A.7: INI configuration file template for 4 TDCs. In section [General], the number of TDCs is explicitated and information about the ongoing run is given. Then, there are sections for each and every VME modules. There buffer addresses are given and for the TDCs, the list of channels to enable is given. Finally, in section [TDCSettings], a part of the TDC settings are given.

1245 In order to retrieve the information of the configuration file, the object `IniFile` has been developed
 1246 to provide an INI parser, presented in Source Code A.8. It contains private methods returning a
 1247 boolean to check the type of line written in the file, whether a comment, a group header or a key line
 1248 (`IniFile::CheckIfComment()`, `IniFile::CheckIfGroup()` and `IniFile::CheckIfToken()`). The
 1249 key may sometimes be referred to as *token* in the source code. Moreover, the private element
 1250 `FileData` is a map of `const string` to `string` that allows to store the data contained inside the
 1251 configuration file via the public method `IniFile::GetFileData()` following the formatting (see
 1252 method `IniFile::Read()`):

```
1253
 1254     string group, token, value;
 1255     // Get the field values for the 3 strings.
 1256     // Then concatenate group and token together as a single string
 1257     // with a dot separation.
 1258     token = group + "." + token;
 1259     FileData[token] = value;
```

1255 More methods have been written to translate the different keys into the right variable format
 1256 when used by the DAQ. For example, to get a `float` value out of the configuration file data, knowing
 1257 the group and the key needed, the method `IniFile::floatType()` can be used. It takes 3 arguments
 1258 being the group name and key name (both `string`), and a default `float` value used as exception in
 1259 the case the expected combination of group and key cannot be found in the configuration file. This
 1260 default value is then used and the DAQ continues on working after sending an alert in the log file for
 1261 further debugging.

```

1262 typedef map< const string, string > IniFileData;
1263
class IniFile{
    private:
        bool          CheckIfComment (string line);
        bool          CheckIfGroup(string line, string& group);
        bool          CheckIfToken(string line, string& key, string& value);
        string         FileName;
        IniFileData   FileData;
        int           Error;

    public:
        IniFile();
        IniFile(string filename);
        virtual      ~IniFile();

        // Basic file operations
        void          SetFileName(string filename);
        int           Read();
        int           Write();
        IniFileData GetFileData();

        // Data readout methods
        Data32         addressType (string groupname, string keyname, Data32
→     defaultvalue);
        long          intType     (string groupname, string keyname, long
→     defaultvalue);
        long long    longType    (string groupname, string keyname, long long
→     defaultvalue );
        string         stringType  (string groupname, string keyname, string
→     defaultvalue );
        float         floatType   (string groupname, string keyname, float
→     defaultvalue );

        // Error methods
        string         GetErrorMsg();
    };

```

1264 *Source Code A.8: Description of C++ object `IniFile` used as a parser for INI file format.*

1265 A.5.3 WebDCS/DAQ intercommunication

1266 When shifters send instructions to the DAQ via the configuration file, it is the webDCS itself that
 1267 gives the start command to the DAQ and then the 2 softwares use inter-process communication
 1268 through file to synchronise themselves. This communication file is represented by the variable **const**
 1269 string __runstatuspath.

1270 On one side, the webDCS sends commands or status that are readout by the DAQ:

- 1271 • INIT, status sent when launching a scan and read via function `CtrlRunStatus(...)`,
- 1272 • START, command to start data taking and read via function `CheckSTART()`,
- 1273 • STOP, command to stop data taking at the end of the scan and read via function `CheckSTOP()`,
 1274 and
- 1275 • KILL, command to kill data taking sent by user and read via function `CheckKILL()`

1276 and on the other, the DAQ sends status that are controled by the webDCS:

- 1277 ● `DAQ_RDY`, sent with `SendDAQReady()` to signify that the DAQ is ready to receive commands
1278 from the webDCS,
- 1279 ● `RUNNING`, sent with `SendDAQRunning()` to signify that the DAQ is taking data,
- 1280 ● `DAQ_ERR`, sent with `SendDAQError()` to signify that the DAQ didn't receive the expected com-
1281 mand from the webDCS or that the launch command didn't have the right number of argu-
1282 ments,
- 1283 ● `RD_ERR`, sent when the DAQ wasn't able to read the communication file, and
- 1284 ● `WR_ERR`, sent when the DAQ wasn't able to write into the communication file.

1285 **A.5.4 Example of inter-process communication cycle**

1286 Under normal conditions, the webDCS and the DAQ processes exchange commands and status via
1287 the file hosted at the address `__runstatuspath`, as explained in subsection A.5.3. An example of
1288 cycle is given in Table A.1. In this example, the steps 3 to 5 are repeated as long as the webDCS tells
1289 the DAQ to take data. A data taking cycle is the equivalent as what is called a *Scan* in GIFT++ jargon,
1290 referring to a set a runs with several HV steps. Each repetition of steps 3 to 5 is then equivalent to a
1291 single *Run*.

1292

1293 At any moment during the data taking, for any reason, the shifter can decide that the data taking
1294 needs to be stopped before it reached the end of the scheduled cycle. Thus at any moment on the
1295 cycle, the content of the inter-process communication file will be changed to `KILL` and the DAQ will
1296 shut down right away. The DAQ checks for `KILL` signals every 5s after the TDCs configuration is
1297 over. So far, the function `CheckKILL()` has been used only inside of the data taking loop of method
1298 `DataReader::Run()` and thus, if the shifter decides to KILL the data taking during the TDC con-
1299 figuration phase or the HV ramping in between 2 HV steps, the DAQ will not be stopped smoothly
1300 and a *force kill* command will be sent to stop the DAQ process that is still awake on the computer.
1301 Improvements can be brought on this part of the software to make sure that the DAQ can safely
1302 shutdown at any moment.

1303

1304 **A.6 Software export**

1305 In section A.2 was discussed the fact that the DAQ as written in its last version is not a standalone
1306 software. It is possible to make it a standalone program that could be adapted to any VME setup
1307 using V1190A and V1718 modules by creating a GUI for the software or by printing the log mes-
1308 sages that are normally printed in the webDCS through the log file, directly into the terminal. This
1309 method was used by the DAQ up to version 3.0 moment where the webDCS was completed. Also, it
1310 is possible to check branches of DAQ v2.X to have example of communication through a terminal.

1311

1312 DAQ v2.X is nonetheless limited in it's possibilities and requires a lot of offline manual interven-
1313 tions from the users. Indeed, there is no communication of the software with the detectors' power
1314 supply system that would allow for a user a predefine a list of voltages to operate the detectors at

step	actions of webDCS	status of DAQ	<code>__runstatuspath</code>
1	launch DAQ ramp voltages ramping over wait for currents stabilization	readout of IniFile configuration of TDCs	INIT
2		configuration done send DAQ ready wait for START signal	DAQ_RDY
3	waiting time over send START		START
4	wait for run to end monitor DAQ run status	data taking ongoing check for KILL signal	RUNNING
5		run over send DAQ_RDY wait for next DCS signal	DAQ_RDY
6	ramp voltages ramping over wait for currents stabilization		DAQ_RDY
3	waiting time over send START		START
4	wait for run to end monitor DAQ run status	update IniFile information data taking ongoing check for KILL signal	RUNNING
5		run over send DAQ_RDY wait for next DCS signal	DAQ_RDY
7	send command STOP	DAQ shuts down	STOP

Table A.1: Inter-process communication cycles in between the webDCS and the DAQ through file string signals.

1315 and loop over to take data without any further manual intervention. In v2.X, the data is taken for a
1316 single detector setting and at the end of each run, the softwares asks the user if he intends on taking
1317 more runs. If so, the software invites the user to set the operating voltages accordingly to what is
1318 necessary and to manual update the configuration file in consequence. This working mode can be a
1319 very first approach before an evolution and has been successfully used by colleagues from different
1320 collaborations.

1321

1322 For a more robust operation, it is recommended to develop a GUI or a web application to inter-
1323 face the DAQ. Moreover, to limit the amount of manual interventions, and thus the probability to
1324 make mistakes, it is also recommended to add an extra feature into the DAQ by installing the HV
1325 Wrapper library provided by CAEN of which an example of use in a similar DAQ software devel-
1326 opped by a master student of UGent, and called TinyDAQ, is provided on UGent's github. Then, this
1327 HV Wrapper will help you communicating with and give instructions to a CAEN HV powered crate
1328 and can be added into the DAQ at the same level where the communication with the user was made
1329 in DAQ v2.X. In case you are using another kind of power system for your detectors, it is stringly
1330 adviced to use HV modules or crates that can be remotely controled via a using C++ libraries.

1331

B

1332

1333

Details on the offline analysis package

1334 The data collected in GIF++ thanks to the DAQ described in Appendix A is difficult to interpret by
1335 a human user that doesn't have a clear idea of the raw data architecture of the ROOT data files. In
1336 order to render the data human readable, a C++ offline analysis tool was designed to provide users
1337 with detector by detector histograms that give a clear overview of the parameters monitored during
1338 the data acquisition [32]. In this appendix, details about this software in the context of GIF++, as of
1339 how the software was written and how it functions will be given.

1340 B.1 GIF++ Offline Analysis file tree

1341 GIF++ Offline Analysis source code is fully available on github at https://github.com/aafagot/GIF_OfflineAnalysis. The software requires ROOT as non-optionnal dependency
1342 as it takes ROOT files in input and write an output ROOT file containing histograms. To compile the
1343 GIF++ Offline Analysis project is compiled with cmake. To compile, first a build/ directory must
1344 be created to compile from there:

```
1346 mkdir build  
1347 cd build  
1348 cmake ..  
1349 make  
1350 make install
```

1348 To clean the directory and create a new build directory, the bash script cleandir.sh can be used:

```
1349  
1350 ./cleandir.sh
```

1351 The source code tree is provided below along with comments to give an overview of the files' con-
1352 tent. The different objects created for this project (`Infrastructure`, `Trolley`, `RPC`, `Mapping`, `RPCHit`,
1353 `RPCCluster` and `Inifile`) will be described in details in the following sections.

1354

```

GIF_OfflineAnalysis
├── bin
│   └── offlineanalysis ..... EXECUTABLE
├── build..... CMAKE COMPILATION DIRECTORY
└── ...
    ├── include..... LIST OF C++ HEADER FILES
    │   ├── Cluster.h..... DECLARATION OF OBJECT RPCCLUSTER
    │   ├── Current.h..... DECLARATION OF GETCURRENT ANALYSIS MACRO
    │   ├── GIFTrolley.h..... DECLARATION OF OBJECT TROLLEY
    │   ├── Infrastructure.h..... DECLARATION OF OBJECT INFRASTRUCTURE
    │   ├── IniFile.h..... DECLARATION OF OBJECT INI FILE FORINI PARSER
    │   ├── Mapping.h..... DECLARATION OF OBJECT MAPPING
    │   ├── MsgSvc.h..... DECLARATION OF OFFLINE LOG MESSAGES
    │   ├── OfflineAnalysis.h..... DECLARATION OF DATA ANALYSIS MACRO
    │   ├── RPCTracker.h..... DECLARATION OF OBJECT RPC
    │   ├── RPCHit.h..... DECLARATION OF OBJECT RPCHIT
    │   ├── types.h..... DEFINITION OF USEFUL VARIABLE TYPES
    │   └── utils.h..... DECLARATION OF USEFUL FUNCTIONS
    ├── obj..... BINARY FILES CREATED BY COMPILER
    └── ...
        ├── src..... LIST OF C++ SOURCE FILES
        │   ├── Cluster.cc..... DEFINITION OF OBJECT RPCCLUSTER
        │   ├── Current.cc..... DEFINITION OF GETCURRENT ANALYSIS MACRO
        │   ├── GIFTrolley.cc..... DEFINITION OF OBJECT TROLLEY
        │   ├── Infrastructure.cc..... DEFINITION OF OBJECT INFRASTRUCTURE
        │   ├── IniFile.cc..... DEFINITION OF OBJECT INI FILE FORINI PARSER
        │   ├── main.cc..... MAIN FILE
        │   ├── Mapping.cc..... DEFINITION OF OBJECT MAPPING
        │   ├── MsgSvc.cc..... DEFINITION OF OFFLINE LOG MESSAGES
        │   ├── OfflineAnalysis.cc..... DEFINITION OF DATA ANALYSIS MACRO
        │   ├── RPCTracker.cc..... DEFINITION OF OBJECT RPC
        │   ├── RPCHit.cc..... DEFINITION OF OBJECT RPCHIT
        │   └── utils.cc..... DEFINITION OF USEFUL FUNCTIONS
        ├── cleandir.sh..... BASH SCRIPT TO CLEAN BUILD DIRECTORY
        ├── CMakeLists.txt..... SET OF INSTRUCTIONS FOR CMAKE
        ├── config.h.in..... DEFINITION OF VERSION NUMBER
        └── README.md..... README FILE FOR GITHUB

```

1355

B.2 Usage of the Offline Analysis

1356

In order to use the Offline Analysis tool, it is necessary to know the Scan number and the HV Step of the run that needs to be analysed. This information needs to be written in the following format:

1358

1359

```
Scan00XXXX_HVY
```

1360

1361

where XXXX is the scan ID and Y is the high voltage step (in case of a high voltage scan, data will be taken for several HV steps). This format corresponds to the base name of data files in the database

1362 of the GIF++ webDCS. Usually, the offline analysis tool is automatically called by the webDCS at
 1363 the end of data taking or by a user from the webDCS panel if an update of the tool was brought.
 1364 Nonetheless, an expert can locally launch the analysis for tests on the GIF++ computer, or a user can
 1365 get the code on its local machine from github and download data from the webDCS for its own anal-
 1366 ysis. To launch the code, the following command can be used from the `GIF_OfflineAnalysis` folder:

1367
 1368 `bin/offlineanalysis /path/to/Scan00XXXX_HVY`

1369 where, `/path/to/Scan00XXXX_HVY` refers to the local data files. Then, the offline tool will by itself
 1370 take care of finding all available ROOT data files present in the folder, as listed below:

- 1371
 - 1372 ● `Scan00XXXX_HVY_DAQ.root` containing the TDC data as described in Appendix ?? (events, hit
 and timestamp lists), and
 - 1373 ● `Scan00XXXX_HVY_CAEN.root` containing the CAEN mainframe data recorded by the monitor-
 ing tool webDCS during data taking (HVs and currents of every HV channels). This file is
 created independently of the DAQ.

1376 **B.2.1 Output of the offline tool**

1377 **B.2.1.1 ROOT file**

1378 The analysis gives in output ROOT datafiles that are saved into the data folder and called using the
 1379 naming convention `Scan00XXXX_HVY_Offline.root`. Inside those, a list of `TH1` histograms can be
 1380 found. Its size will vary as a function of the number of detectors in the setup as each set of histograms
 1381 is produced detector by detector. For each partition of each chamber, can be found:

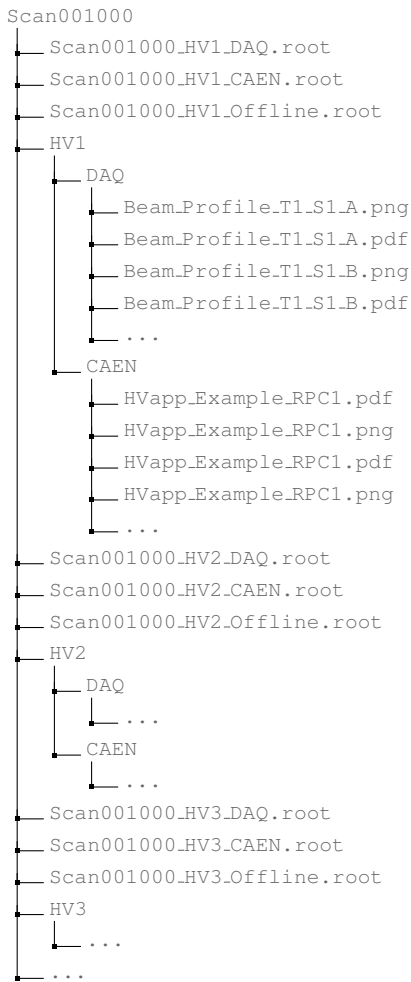
- 1382
 - 1383 ● `Time_Profile_Tt_Sc_p` shows the time profile of all recorded events (number of events per
 time bin),
 - 1384 ● `Hit_Profile_Tt_Sc_p` shows the hit profile of all recorded events (number of events per chan-
 nel),
 - 1386 ● `Hit_Multiplicity_Tt_Sc_p` shows the hit multiplicity (number of hits per event) of all recorded
 events (number of occurrences per multiplicity bin),
 - 1388 ● `Strip_Mean_Noise_Tt_Sc_p` shows noise/gamma rate per unit area for each strip in a se-
 lected time range. After filters are applied on `Time_Profile_Tt_Sc_p`, the filtered version
 of `Hit_Profile_Tt_Sc_p` is normalised to the total integrated time and active detection area
 of a single channel,
 - 1392 ● `Strip_Activity_Tt_Sc_p` shows noise/gamma activity for each strip (normalised version of
 previous histogram - strip activity = strip rate / average partition rate),
 - 1394 ● `Strip_Homogeneity_Tt_Sc_p` shows the *homogeneity* of a given partition ($\text{homogeneity} = \exp(-\text{strip rates standard deviation}(\text{strip rates in partition}/\text{average partition rate}))$),
 - 1396 ● `mask_Strip_Mean_Noise_Tt_Sc_p` shows noise/gamma rate per unit area for each masked
 strip in a selected time range. Offline, the user can control the noise/gamma rate and decide to
 mask the strips that are judged to be noisy or dead. This is done via the *Masking Tool* provided
 by the webDCS,

- 1400 ● `mask_Strip_Activity_Tt_Sc_p` shows noise/gamma activity per unit area for each masked
1401 strip with respect to the average rate of active strips,
- 1402 ● `NoiseCSize_H_Tt_Sc_p` shows noise/gamma cluster size, a cluster being constructed out of
1403 adjacent strips giving a signal at the *same time* (hits within a time window of 25 ns),
- 1404 ● `NoiseCMult_H_Tt_Sc_p` shows noise/gamma cluster multiplicity (number of reconstructed
1405 clusters per event),
- 1406 ● `Chip_Mean_Noise_Tt_Sc_p` shows the same information than `Strip_Mean_Noise_Tt_Scp` us-
1407 ing a different binning (1 chip corresponds to 8 strips),
- 1408 ● `Chip_Activity_Tt_Sc_p` shows the same information than `Strip_Activity_Tt_Scp` using
1409 chip binning,
- 1410 ● `Chip_Homogeneity_Tt_Sc_p` shows the homogeneity of a given partition using chip binning,
- 1411 ● `Beam_Profile_Tt_Sc_p` shows the estimated beam profile when taking efficiency scan. This
1412 is obtained by filtering `Time_Profile_Tt_Sc_p` to only consider the muon peak where the
1413 noise/gamma background has been subtracted. The resulting hit profile corresponds to the
1414 beam profile on the detector channels,
- 1415 ● `L0_Efficiency_Tt_Sc_p` shows the level 0 efficiency that was estimated **without** muon track-
1416 ing,
- 1417 ● `MuonCSize_H_Tt_Sc_p` shows the level 0 muon cluster size that was estimated **without** muon
1418 tracking, and
- 1419 ● `MuonCMult_H_Tt_Sc_p` shows the level 0 muon cluster multiplicity that was estimated **without**
1420 muon tracking.

1421 In the histogram labels, *t* stands for the trolley number (1 or 3), *c* for the chamber slot label in
1422 trolley *t* and *p* for the partition label (A, B, C or D depending on the chamber layout) as explained
1423 in Chapter 5.3.

1424 In the context of GIF++, an extra script called by the webDCS is called to extract the histograms
1425 from the ROOT files. The histograms are then stored in PNG and PDF formats into the correspond-
1426 ing folder (a single folder per HV step, so per ROOT file). the goal is to then display the histograms
1427 on the Data Quality Monitoring (DQM) page of the webDCS in order for the users to control the
1428 quality of the data taking at the end of data taking. An example of histogram organisation is given
1429 below:

1431



1432 *Here can put some screens from the webDCS to show the DQM and the plots available to users.*
 1433

1434 **B.2.1.2 CSV files**

1435 Moreover, up to 3 CSV files can be created depending on which ones of the 3 input files were in the
 1436 data folder:

- 1437 ● `Offline-Corrupted.csv` , is used to keep track of the amount of data that was corrupted and
 1438 removed from old data format files that don't contain any data quality flag.
- 1439 ● `Offline-Current.csv` , contains the summary of the currents and voltages applied on each
 1440 RPC HV channel.
- 1441 ● `Offline-L0-EffC1.csv` , is used to write the efficiencies, cluster size and cluster multiplicity
 1442 of efficiency runs. Note that `L0` refers here to *Level 0* and means that the results of efficiency and
 1443 clusterization are a first approximation calculated without performing any muon tracking in

1444 between the different detectors. This offline tool provides the user with a preliminar calculation
 1445 of the efficiency and of the muon event parameters. Another analysis software especially
 1446 dedicated to muon tracking is called on selected data to retrieve the results of efficiency and
 1447 muon clusterization using a tracking algorithm to discriminate noise or gamma from muons
 1448 as muons are the only particles that pass through the full setup, leaving hits than can be used
 1449 to reconstruct their tracks.

- 1450 ● `Offline-Rate.csv`, is used to write the noise or gamma rates measured in the detector readout
 1451 partitions.

1452 Note that these 4 CSV files are created along with their *headers* (`Offline-[...]-Header.csv`
 1453 containing the names of each data columns) and are automatically merged together when the offline
 1454 analysis tool is called from the webDCS, contrary to the case where the tool is runned locally from
 1455 the terminal as the merging bash script is then not called. Thus, the resulting files, used to make
 1456 official plots, are:

- 1457 ● `Corrupted.csv`,
 1458 ● `Current.csv`,
 1459 ● `L0-EffCl.csv`.
 1460 ● `Rate.csv`.

1461 **B.3 Analysis inputs and information handling**

1462 The usage of the Offline Analysis tool as well as its output have been presented in the previous section.
 1463 It is now important to dig further and start looking at the source code and the inputs necessary
 1464 for the tool to work. Indeed, other than the raw ROOT data files that are analysed, more information
 1465 needs to be imported inside of the program to perform the analysis such as the description of the
 1466 setup inside of `GIF++` at the time of data taking (number of trolleys, of RPCs, dimensions of the
 1467 detectors, etc...) or the mapping that links the TDC channels to the coresponding RPC channels in
 1468 order to translate the TDC information into human readable data. 2 files are used to transmit all this
 1469 information:
 1470

- 1471 ● `Dimensions.ini`, that provides the necessary setup and RPC information, and
 1472 ● `ChannelsMapping.csv`, that gives the link between the TDC and RPC channels as well as the
 1473 *mask* for each channel (masked or not?).

1474 **B.3.1 Dimensions file and InFile parser**

1475 This input file, present in every data folder, allows the analysis tool to know of the number of active
 1476 trolleys, the number of active RPCs in those trolleys, and the details about each RPCs such as
 1477 the number of RPC gaps, the number of pseudo-rapidity partitions (for CMS-like prototypes), the
 1478 number of strips per partion or the dimensions. To do so, there are 3 types of groups in the INI file
 1479 architecture. A first general group, appearing only once at the head of the document, gives information
 1480 about the number of active trolleys as well as their IDs, as presented in Source Code B.1. For

1481 each active trolley, a group similar to Source Code B.2 can be found containing information about
 1482 the number of active detectors in the trolley and their IDs. Each trolley group as a `Tt` name format,
 1483 where `t` is the trolley ID. Finally, for each detector stored in slots of an active trolley, there is a group
 1484 providing information about their names and dimensions, as shown in Source Code B.3. Each slot
 1485 group as a `TtSs` name format, where `s` is the slot ID of trolley `t` where the active RPC is hosted.

```
1486 [General]
1487 nTrolleys=2
1488 TrolleysID=13
```

1488 *Source Code B.1: Example of `[General]` group as might be found in `Dimensions.ini`. In Gif++, only 2 trolleys are available to hold RPCs and place them inside of the bunker for irradiation. The IDs of the trolleys are written in a single string as "13" and then read character by character by the program.*

```
1489 [T1]
1490 nSlots=4
1491 SlotsID=1234
```

1490 *Source Code B.2: Example of trolley group as might be found in `Dimensions.ini`. In this example, the file tells that there are 4 detectors placed in the holding slots of the trolley `T1` and that their IDs, written as a single string variable, are 1, 2, 3 and 4.*

```
1491 [T1S1]
1492 Name=RE2-2-NPD-BARC-8
1493 Partitions=3
1494 Gaps=3
1495 Gap1=BOT
1496 Gap2=TN
1497 Gap3=TW
1498 AreaGap1=11694.25
1499 AreaGap2=6432
1500 AreaGap3=4582.82
1501 Strips=32
1502 ActiveArea-A=157.8
1503 ActiveArea-B=121.69
1504 ActiveArea-C=93.03
```

1502 *Source Code B.3: Example of slot group as might be found in `Dimensions.ini`. In this example, the file provides information about a detector named `RE2-2-NPD-BARC-8`, having 3 pseudo-rapidity readout partitions and stored in slot `S1` of trolley `T1`. This is a CMS RE2-2 type of detector. This information will then be used for example to compute the rate per unit area calculation.*

1493 This information is readout and stored in a C++ object called `IniFile`, that parses the information
 1494 in the INI input file and stores it into a local buffer for later use. This INI parser is the exact same
 1495 one that was previously developed for the Gif++ DAQ and described in Appendix A.5.2.

1496 B.3.2 TDC to RPC link file and Mapping

1497 The same way the INI dimension file information is stored using `map`, the channel mapping and mask
 1498 information is stored and accessed through `map`. First of all, the mapping CSV file is organised into
 1499 3 columns separated by tabulations (and not by commas, as expected for CSV files as it is easier using
 1500 streams to read tab or space separated data using C++):

1501

1502 RPC_channel TDC_channel mask

1503 using as formatting for each field:

1504
1505 TSCCC TCCC M

1506 TSCCC is a 5-digit integer where τ is the trolley ID, s the slot ID in which the RPC is held insite
1507 the trolley τ and ccc is the RPC channel number, or *strip* number, that can take values up to
1508 3-digits depending on the detector,

1509 TCCC is a 4 digit integer where τ is the TDC ID, ccc is the TDC channel number that can take values
1510 in between 0 and 127, and

1511 M is a 1-digit integer indicating if the channel should be considered ($M = 1$) or discarded ($M = 0$)
1512 during analysis.

1513 This mapping and masking information is readout and stored thanks to the object `Mapping`, pre-
1514 sented in Source Code B.4. Similarly to `IniFile` objects, this class has private methods. The first
1515 one, `Mapping::CheckIfNewLine()` is used to find the newline character '`\n`' or return character
1516 '`\r`' (depending on which kind of operating system interacted with the file). This is used for the
1517 simple reason that the masking information has been introduced only during the year 2017 but the
1518 channel mapping files exist since 2015 and the very beginning of data taking at GIF++. This means
1519 that in the older data folders, before the upgrade, the channel mapping file only had 2 columns, the
1520 RPC channel and the TDC channel. For compatibility reasons, this method helps controling the
1521 character following the readout of the 2 first fields of a line. In case any end of line character is
1522 found, no mask information is present in the file and the default $M = 1$ is used. On the contrary, if
1523 the next character was a tabulation or a space, the mask information is present.

1524 Once the 3 fields have been readout, the second private method `Mapping::CheckIfTDCCh()` is
1525 used to control that the TDC channel is an existing TDC channel. Finally, the information is stored
1526 into 3 different maps (`Link`, `ReverseLink` and `Mask`) thanks to the public method `Mapping::Read()`.
1527 `Link` allows to get the RPC channel by knowing the TDC channel while `ReverseLink` does the op-
1528 posite by returning the TDC channel by knowing the RPC channel. Finally, `Mask` returns the mask
1529 associated to a given RPC channel.

```

1530
typedef map<Uint,Uint> MappingData;

class Mapping {
    private:
        bool          CheckIfNewLine(char next);
        bool          CheckIfTDCCh(Uint channel);
        string         FileName;
        MappingData   Link;
        MappingData   ReverseLink;
        MappingData   Mask;
        int           Error;

1531
    public:
        Mapping();
        Mapping(string baseName);
        ~Mapping();

        void SetFileName(const string filename);
        int Read();
        Uint GetLink(Uint tdcchannel);
        Uint GetReverse(Uint rpcchannel);
        Uint GetMask(Uint rpcchannel);
};

1532

```

Source Code B.4: Description of C++ object `Mapping` used as a parser for the channel mapping and mask file.

B.4 Description of GIF++ setup within the Offline Analysis tool

In the previous section, the tool input files have been discussed. The dimension file information is stored in a map hosted by the `IniFile` object. But this information is then used to create a series of new objects that helps defining the GIF++ infrastructure directly into the Offline Analysis. Indeed, from the `RPC`, to the more general `Infrastructure`, every element of the GIF++ infrastrucutre is recreated for each data analysis based on the information provided in input. All this information about the infrastructure will be used to assign each hit signal to a specific strip channel of a specific detector, and having a specific active area. This way, rate per unit area calculation is possible.

1541

B.4.1 RPC objects

1543 `RPC` objects have been developped to represent physical active detectors in GIF++ at the moment
 1544 of data taking. Thus, there are as many `RPC` objects created during the analysis than there were
 1545 active `RPCs` tested during a run. Each `RPC` hosts the information present in the corresponding INI
 1546 slot group, as shown in B.3, and organises it using a similar architecture. This can be seen from
 1547 Source Code B.5.

1548 To make the object more compact, the lists of gap labels, of gap active areas and strip active
 1549 areas are stored into `vector` dynamical containers. `RPC` objects are always contructed thanks to the
 1550 dimension file information stored into the `IniFILE` and their ID, using the format `TtSs`. Using the
 1551 `RPC` ID, the constructor calls the methods of `IniFILE` to initialise the `RPC`. The other constructors
 1552 are not used but exist in case of need. Finally, some getters have been written to access the different
 1553 private parameters storing the detector information.

```

1554
1554 class RPC{
1554     private:
1554         string          name;           //RPC name as in webDCS database
1554         Uint            nGaps;          //Number of gaps in the RPC
1554         Uint            nPartitions;    //Number of partitions in the RPC
1554         Uint            nStrips;        //Number of strips per partition
1554         vector<string> gaps;          //List of gap labels (BOT, TOP, etc...)
1554         vector<float>  gapGeo;         //List of gap active areas
1554         vector<float>  stripGeo;       //List of strip active areas
1554
1554     public:
1554         RPC();
1554         RPC(string ID, IniFile* geofile);
1554         RPC(const RPC& other);
1554         ~RPC();
1554         RPC& operator=(const RPC& other);
1554
1554         string GetName();
1554         Uint GetNGaps();
1554         Uint GetNPartitions();
1554         Uint GetNStrips();
1554         string GetGap(Uint g);
1554         float GetGapGeo(Uint g);
1554         float GetStripGeo(Uint p);
1554     };

```

1556 *Source Code B.5: Description of C++ objects RPC that describe each active detectors used during data taking.*

1557 B.4.2 Trolley objects

1558 Trolley objects have been developped to represent physical active trolleys in GIFT++ at the moment
 1559 of data taking. Thus, there are as many trolley objects created during the analysis than there were
 1560 active trolleys hosting tested RPCs during a run. Each Trolley hosts the information present in the
 1561 corresponding INI trolley group, as shown in B.2, and organises it using a similar architecture. In
 1562 addition to the information hosted in the INI file, these object have a dynamical container of RPC
 1563 objects, representing the active detectors the active trolley was hosting at the time of data taking.
 1564 This can been seen from Source Code B.6.

1565 Trolley objects are always contructed thanks to the dimension file information stored into the
 1566 IniFILE and their ID, using the format Tt. Using the Trolley ID, the constructor calls the methods
 1567 of IniFILE to initialise the Trolley. Retrieving the information of the RPC IDs via SlotsID, a new
 1568 RPC is constructed and added to the container RPCs for each character in the ID string. The other
 1569 constructors are not used but exist in case of need. Finally, some getters have been written to access
 1570 the different private parameters storing the trolley and detectors information.

```

1571
class Trolley{
    private:
        Uint          nSlots; //Number of active RPCs in the considered trolley
        string        SlotsID; //Active RPC IDs written into a string
        vector<RPC*> RPCs;   //List of active RPCs

    public:
        //Constructors, destructor and operator =
        Trolley();
        Trolley(string ID, IniFile* geofile);
        Trolley(const Trolley& other);
        ~Trolley();
        Trolley& operator=(const Trolley& other);

        //Get GIFTrolley members
        Uint  GetNSlots();
        string GetSlotsID();
        Uint   GetSlotID(Uint s);

        //Manage RPC list
        RPC*  GetRPC(Uint r);
        void  DeleteRPC(Uint r);

        //Methods to get members of RPC objects stored in RPCs
        string GetName(Uint r);
        Uint   GetNGaps(Uint r);
        Uint   GetNPartitions(Uint r);
        Uint   GetNStrips(Uint r);
        string GetGap(Uint r, Uint g);
        float  GetGapGeo(Uint r, Uint g);
        float  GetStripGeo(Uint r, Uint p);
    };

```

Source Code B.6: Description of C++ objects `Trolley` that describe each active trolley used during data taking.

1574 B.4.3 Infrastructure object

1575 The `Infrastructure` object has been developped to represent the GIFT++ bunker area dedicated to
 1576 CMS RPC experiments. With this very specific object, all the information about the CMS RPC
 1577 setup within GIFT++ at the moment of data taking is stored. It hosts the information present in the
 1578 corresponding INI general group, as shown in B.1, and organises it using a similar architecture. In
 1579 addition to the information hosted in the INI file, this object have a dynamical container of `Trolley`
 1580 objects, representing the active tolleys in GIFT++ area. This can be seen from Source Code B.7.

1581 The `Infrastructure` object is always contructed thanks to the dimension file information stored
 1582 into the `IniFILE`. Retrieving the information of the trolley IDs via `TrolleysID`, a new `Trolley` is
 1583 constructed and added to the container `Trolleys` for each character in the ID `string`. By extension,
 1584 it is easy to understand that the process described in Section B.4.2 for the construction of RPCs
 1585 takes place when a trolley is constructed. The other constructors are not used but exist in case of
 1586 need. Finally, some getters have been written to access the different private parameters storing the
 1587 infrastructure, tolleys and detectors information.

```

1588
class Infrastructure {
    private:
        Uint             nTrolleys;   //Number of active Trolleys in the run
        string          TrolleysID;  //Active trolley IDs written into a string
        vector<Trolley*> Trolleys;  //List of active Trolleys (struct)

    public:
        //Constructors and destructor
        Infrastructure();
        Infrastructure(IniFile* geofile);
        Infrastructure(const Infrastructure& other);
        ~Infrastructure();
        Infrastructure& operator=(const Infrastructure& other);

        //Get Infrastructure members
        Uint  GetNTrolleys();
        string GetTrolleysID();
        Uint   GetTrolleyID(Uint t);

1589
        //Manage Trolleys
        Trolley* GetTrolley(Uint t);
        void     DeleteTrolley(Uint t);

        //Methods to get members of GIFTrolley objects stored in Trolleys
        Uint  GetNSlots(Uint t);
        string GetSlotsID(Uint t);
        Uint   GetSlotID(Uint t, Uint s);
        RPC*  GetRPC(Uint t, Uint r);

        //Methods to get members of RPC objects stored in RPCs
        string GetName(Uint t, Uint r);
        Uint   GetNGaps(Uint t, Uint r);
        Uint   GetNPartitions(Uint t, Uint r);
        Uint   GetNStrips(Uint t, Uint r);
        string GetGap(Uint t, Uint r, Uint g);
        float  GetGapGeo(Uint t, Uint r, Uint g);
        float  GetStripGeo(Uint t, Uint r, Uint p);
    };
}

```

Source Code B.7: Description of C++ object *Infrastructure* that contains the full information about CMS RPC experiment in GIF++.

1591 B.5 Handeling of data

1592 As discussed in Appendix A.4.2, the raw data as a `TTree` architecture where every entry is related to
 1593 a trigger signal provided by a muon or a random pulse, whether the goal of the data taking was to
 1594 measure the performance of the detector or the noise/gamma background respectively. Each of these
 1595 entries, referred also as events, contain a more or less full list of hits in the TDC channels to which
 1596 the detectors are connected. To this list of hits corresponds a list of time stamps, marking the arrival
 1597 of the hits within the TDC channel.

1598 The infrastructure of the CMS RPC experiment within GIF++ being defined, combining the
 1599 information about the raw data with the information provided by both the mapping/mask file and the
 1600 dimension file allows to build new physical objects that will help in computing efficiency or rates.

B.5.1 RPC hits

1602 The raw data stored in the ROOT file as output of the GIFT++ DAQ, is readout by the analysis tool
1603 using the structure `RAWData` presented in Source Code B.9 that differs from the structure presented
1604 in Appendix A.4.2 as it is not meant to hold all of the data contained in the ROOT file. In this sense,
1605 this structure is in the case of the offline analysis tool not a dynamical object and will only be storing
1606 a single event contained in a single entry of the `TTree`.

```

1607
class RPCHit {
    private:
        Uint Channel;           //RPC channel according to mapping (5 digits)
        Uint Trolley;           //0, 1 or 3 (1st digit of the RPC channel)
        Uint Station;            //Slot where is held the RPC in Trolley (2nd digit)
        Uint Strip;              //Physical RPC strip where the hit occurred (last 3
    ↵  digits)
        Uint Partition;          //Readout partition along eta segmentation
        float TimeStamp;         //Time stamp of the arrival in TDC

    public:
        //Constructors, destructor & operator =
        RPCHit();
        RPCHit(Uint channel, float time, Infrastructure* Infra);
        RPCHit(const RPCHit& other);
        ~RPCHit();
        RPCHit& operator=(const RPCHit& other);

        //Get RPCHit members
        Uint GetChannel();
        Uint GetTrolley();
        Uint GetStation();
        Uint GetStrip();
        Uint GetPartition();
        float GetTime();
};

typedef vector<RPCHit> HitList;
typedef struct GIFHitList { HitList rpc[NTROLLEYS][NSLOTS][NPARTITIONS]; }
    ↵  GIFHitList;

bool SortHitbyStrip(RPCHit h1, RPCHit h2);
bool SortHitbyTime(RPCHit h1, RPCHit h2);

```

1609 *Source Code B.8: Description of C++ object RPCHit.*

```
1610 struct RAWData{  
    int iEvent; //Event i  
    int TDCNHits; //Number of hits in event i  
    int QFlag; //Quality flag list (1 flag digit per TDC)  
    vector<UInt> *TDCCh; //List of channels giving hits per event  
    vector<float> *TDCTS; //List of the corresponding time stamps  
};
```

Source Code B.9: Description of C++ structure RAWData.

1612 Each member of the structure is then linked to the corresponding branch of the ROOT data tree,
1613 as shown in the example of Source Code B.10, and using the method `GetEntry(int i)` of the ROOT
1614 class `TTree` will update the state of the members of `RAWData`.

```

1615     TTree* dataTree = (TTree*)dataFile.Get("RAWData");
1616     RAWData data;
1617
1618     dataTree->SetBranchAddress("EventNumber", &data.iEvent);
1619     dataTree->SetBranchAddress("number_of_hits", &data.TDCNHits);
1620     dataTree->SetBranchAddress("Quality_flag", &data.QFlag);
1621     dataTree->SetBranchAddress("TDC_channel", &data.TDCCh);
1622     dataTree->SetBranchAddress("TDC_TimeStamp", &data.TDCTS);

```

1617 *Source Code B.10: Example of link in between RAWData and TTree.*

1618 The data is then analysed entry by entry and to each element of the TDC channel list, a `RPCHit` is
1619 constructed by linking each TDC channel to the corresponding RPC channel thanks to the `Mapping`
1620 object. The information carried by the RPC channel format allows to easily retrieve the trolley and
1621 slot from which the hit was recorded (see section B.3.2). Using these 2 values, the readout partition
1622 can be found by knowing the strip channel and comparing it with the number of partitions and strips
1623 per partition stored into the `Infrastructure` object.

1624 Thus `RPCHit` objects are then stored into 3D dynamical list called `GIFHitList` (Source Code B.9)
1625 where the 3 dimensions refer to the 3 layers of the readout in `GIF++` : in the bunker there are *trolleys*
1626 (τ) holding detectors in *slots* (s) and each detector readout is divided into 1 or more pseudo-rapidity
1627 *partitions* (p). Using these 3 information allows to assign an address to each readout partition and
1628 this address will point to a specific hit list.

1629

1630 **B.5.2 Clusters of hits**

1631 All the hits contained in the ROOT file have been sorted into the different hit lists through the
1632 `GIFHitList`. At this point, it is possible to start looking for clusters. A cluster is a group of adjacent
1633 strips getting hits within a time window of 25 ns. These strips are then assumed to be part of the same
1634 physical avalanche signal generated by a muon passing through the chamber or by the interaction of
1635 a gamma stopping into the electrodes of the RPCs.

1636 To keep the cluster information, `RPCCluster` objects have been defined as shown in Source
1637 Code B.11. Using the information of each individual `RPCHit` taken out of the hit list, it stores
1638 the cluster size (number of adjacent strips composing the cluster), the first and last hit, the center for
1639 spatial reconstruction and finally the start and stop time stamps as well as the time spread in between
1640 the first and last hit.

```

1641
class RPCCluster{
    private:
        Uint ClusterSize; //Size of cluster #ID
        Uint FirstStrip; //First strip of cluster #ID
        Uint LastStrip; //Last strip of cluster #ID
        float Center; //Center of cluster #ID ((first+last)/2)
        float StartStamp; //Time stamp of the earliest hit of cluster #ID
        float StopStamp; //Time stamp of the latest hit of cluster #ID
        float TimeSpread; //Time difference between earliest and latest hits
                           //of cluster #ID

    public:
        //Constructors, destructor & operator =
        RPCCluster();
        RPCCluster(HitList List, Uint cID, Uint cSize, Uint first, Uint firstID);
        RPCCluster(const RPCCluster& other);
        ~RPCCluster();
        RPCCluster& operator=(const RPCCluster& other);

        //Get Cluster members
        Uint GetID();
        Uint GetSize();
        Uint GetFirstStrip();
        Uint GetLastStrip();
        float GetCenter();
        float GetStart();
        float GetStop();
        float GetSpread();
};

typedef vector<RPCCluster> ClusterList;

//Other functions to build cluster lists out of hit lists
void BuildClusters(HitList &cluster, ClusterList &clusterList);
void Clusterization(HitList &hits, TH1 *hcSize, TH1 *hcMult);

```

Source Code B.11: Description of C++ object cluster.

To investigate the hit list of a given detector partition, the function `Clusterization()` defined in `include/Cluster.h` needs the hits in the list to be time sorted. This is achieved by calling function `sort()` of library `<algorithm>` using the comparator `SortHitbyTime(RPCHit h1, RPCHit h2)` defined in `include/RPCHit.h` that returns `true` if the time stamp of hit `h1` is lower than that of `h2`. A first isolation of strips is made only based on time information. All the hits within the 25 ns window are taken separately from the rest. Then, this sub-list of hits is sorted this time by ascending strip number, using this time the comparator `SortHitbyStrip(RPCHit h1, RPCHit h2)`. Finally, the groups of adjacent strips are used to construct `RPCcluster` objects that are then stored in a temporary list of clusters that is at the end of the process used to know how many clusters were reconstructed and to fill their sizes into an histogram that will allows to know the mean size of muon or gamma clusters.

1656 B.6 DAQ data Analysis

1657 All the ingredients to analyse GIF++ data have been defined. This section will focus on the different
1658 part of the analysis performed on the data, from determining the type of data the tool is dealing with

1659 to calculating the rate in each detector or reconstructing muon or gamma clusters.

1660 B.6.1 Determination of the run type

1661 In GIF++, both the performance of the detectors in detecting muons in an irradiated environment and
 1662 the gamma background can be independantly measured. These corresponds to different run types
 1663 and thus, to different TDC settings giving different data to look at.

1664
 1665 In the case of performance measurements, the trigger for data taking is provided by the coïncidence
 1666 of several scintillators when muons from the beam passing through the area are detected. Data
 1667 is collected in a 600 ns wide window around the arrival of muons in the RPCs. The expected time
 1668 distribution of hits is shown in Figure B.1a. The muon peak is clearly visible in the center of the
 1669 distribution and is to be extracted from the gamma background that composes the flat part of the
 1670 distribution.

1671 On the other hand, gamma background or noise measurements are focussed on the non muon
 1672 related physics and the trigger needs to be independant from the muons to give a good measurement
 1673 of the gamma/noise distribution as seen by the detectors. The trigger is then provided by a pulse
 1674 generator at a frequency of 300 Hz whose pulse is not likely to be on time with a muon. In order
 1675 to increase the integrated time without increasing the acquisition time too much, the width of the
 1676 acquisition windows are increased to 10 μ s. The time distribution of the hits is expected to be flat, as
 1677 shown by Figure B.1b.

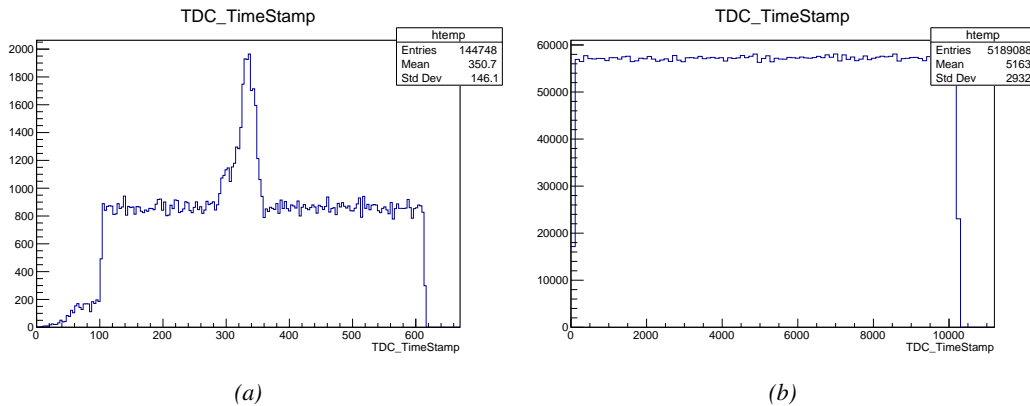


Figure B.1: Example of expected hit time distributions in the cases of efficiency (Figure B.1a) and noise/gamma rate per unit area (Figure B.1b) measurements as extracted from the raw ROOT files. The unit along the x-axis corresponds to ns. The fact that "the" muon peak is not well defined in Figure B.1a is due to the contribution of all the RPCs being tested at the same time that don't necessarily have the same signal arrival time. Each individual peak can have an offset with the ones of other detectors. The inconsistency in the first 100 ns of both time distributions is an artefact of the TDCs and are systematically rejected during the analysis.

1678 The ROOT files include a TTree called RunParameters containing, among other things, the in-
 1679 formation related to the type of run. The run type can then be accessed as described by Source
 1680 Code B.12 and the function IsEfficiencyRun() is then used to determine if the run file is an effi-
 1681 ciency run or, on the contrary, another type of run (noise or gamma measurement).

```

1682     TTree* RunParameters = (TTree*)dataFile.Get("RunParameters");
1683     TString* RunType = new TString();
1684     RunParameters->SetBranchAddress("RunType", &RunType);
1685     RunParameters->GetEntry(0);

```

1684 *Source Code B.12: Access to the run type contained in TTree* RunParameters.*

1685 Finally, the data files will have a slightly different content whether it was collected before or after
 1686 October 2017 and the upgrade of the DAQ software that brought a new information into the ROOT
 1687 output. This is discussed in Appendix A.4.3 and implies that the analysis will differ a little depending
 1688 on the data format. Indeed, as no information on the data quality is stored, in older data files, the cor-
 1689 rections for missing events has to be done at the end of the analysis. The information about the type
 1690 of data format is stored in the variable **bool** `isNewFormat` by checking the list of branches contained
 1691 in the data tree via the methods `TTree::GetListOfBranches()` and `TCollection::Contains()`.

1692 **B.6.2 Beam time window calculation for efficiency runs**

1693 Knowing the run type is important first of all to know the width of the acquisition window to be used
 1694 for the rate calculation and finally to be able to seek for muons. Indeed, the peak that appears in the
 1695 time distribution for each detectors is then fitted to extract the most probable time window in which
 1696 the tool should look for muon hits. The data outside of this time window is then used to evaluate the
 1697 noise or gamma background the detector was subjected to during the data taking. Computing the
 1698 position of the peak is done calling the function `SetBeamWindow()` defined in file `src/RPCHit.cc` that
 1699 loops a first time on the data. The data is first sorted in a 3D array of 1D histograms (`GIFH1Array`, see
 1700 `include/types.h`). Then the location of the highest bin is determined using `TH1::GetMaximumBin()`
 1701 and is used to define a window in which a gaussian fit will be applied to compute the peak width.
 1702 This window is a 80 ns defined by Formula B.1 around the central bin.

$$t_{center}(ns) = \text{bin} \times \text{width}_{\text{bin}}(ns) \quad (\text{B.1a})$$

$$[t_{low}; t_{high}] = [t_{center} - 40; t_{center} + 40] \quad (\text{B.1b})$$

1703 Before the fit is performed, the average number of noise/gamma hits per bin is evaluated using
 1704 the data outside of the fit window. Excluding the first 100 ns, the average number of hits per bin
 1705 due to the noise or gamma is defined by Formula B.2 after extracting the amount of hits in the time
 1706 windows $[100; t_{low}]$ and $[t_{high}; 600]$ thanks to the method `TH1::Integral()`. This average number
 1707 of hits is then subtracted to every bin of the 1D histogram, in order to *clean* it from the noise or
 1708 gamma contribution as much as possible to improve the fit quality. Bins where $\langle n_{\text{hits}} \rangle$ is greater
 1709 than the actual bin content are set to 0.

$$\Delta t_{noise}(ns) = 600 \overbrace{-t_{high} + t_{low}}^{-80ns} - 100 = 420ns \quad (\text{B.2a})$$

$$\langle n_{\text{hits}} \rangle = \text{width}_{\text{bin}}(ns) \times \frac{\sum_{t=100}^{t_{low}} + \sum_{t=t_{high}}^{600}}{\Delta t_{noise}(ns)} \quad (\text{B.2b})$$

1710 Finally, the fit parameters are extracted and saved for each detector in 3D arrays of **float**
 1711 (`muonPeak`, see `include/types.h`), a first one for the mean arrival time of the muons, `PeakTime`,

1712 and a second one for the width of the peak, `PeakWidth`. The width is defined as 6σ of the gaussian
 1713 fit. The same settings are applied to every partitions of the same detector. To determine which one
 1714 of the detector's partitions is directly illuminated by the beam, the peak height of each partition is
 1715 compared and the highest one is then used to define the peak settings.

1716 **B.6.3 Data loop and histogram filling**

1717 3D arrays of histogram are created to store the data and display it on the DQM of GIF++ webDCS
 1718 for the use of shifters. These histograms, presented in section B.2.1.1, are filled while looping on
 1719 the data. Before starting the analysis loop, it is necessary to control the entry quality for the new
 1720 file formats featuring `QFlag`. If the `QFlag` value for this entry shows that 1 TDC or more have a
 1721 `CORRUPTED` flag, then this event is discarded. The loss of statistics is low enough to be neglected.
 1722 `QFlag` is controled using the function `IsCorruptedEvent()` defined in `src/utils.cc`. As explained
 1723 in Appendix A.4.3, each digit of this integer represent a TDC flag that can be 1 or 2. Each 2 is
 1724 the sign of a `CORRUPTED` state. Then, the data is accessed entry by entry in the ROOT `TTree` using
 1725 `RAWData` and each hit in the hit list is assigned to a detector channel and saved in the corresponding
 1726 histograms. In the first part of the analysis, in which the loop over the ROOT file's content is
 1727 performed, the different steps are:

1728 **1- RPC channel assignment and control:** a check is done on the RPC channel extracted thanks
 1729 to the mapping via the method `Mapping::GetLink()`. If the channel is not initialised and is 0, or if
 1730 the TDC channel was greater than 5127, the hit is discarded. This means there was a problem in the
 1731 mapping. Often a mapping problem leads to the crash of the offline tool.

1732 **2- Creation of a `RPCHit` object:** to easily get the trolley, slot and partition in which the hit has
 1733 been assigned, this object is particularly helpful.

1734 **3- General histograms are filled:** the hit is filled into the time distribution and the general hit
 1735 distribution histograms, and if the arrival time is within the first 100 ns, it is discarded and nothing
 1736 else happens and the loop proceeds with the next hit in the list.

1737 **4- Multiplicity counter:** the hit multiplicity counter of the corresponding detectors incremented.

1738 **5-a- Efficiency runs - Is the hit within the peak window? :** if the peak is contained in the peak
 1739 window previously defined in section B.6.2, the hit is filled into the beam hit profile histogram of
 1740 the corresponding chamber, added into the list of muon hits and increments the counter of *in time*
 1741 hits. The term *in time* here refers to the hits that are likely to be muons by arriving in the expected
 1742 time window. If the hit is outside of the peak window, it is filled into the noise profile histogram
 1743 of the corresponding detector, added into the list of noise/gamma hits and increments the counter of
 1744 noise/gamma hits.

1745 **5-b- Noise/gamma rate runs - Noise histograms are filled:** the hit is filled into the noise profile
 1746 histogram of the corresponding detector, added into the list of noise/gamma hits and increments the
 1747 counter of noise/gamma hits.

1748

1749 After the loop on the hit list of the entry is over, the next step is to clusterize the 3D lists filled
 1750 in the previous steps. A 3D loop is then started over the active trolley, slot and RPC partitions to
 1751 access these objects. Each `NoiseHitList` and `MuonHitList`, in case of efficiency run, are clusterized
 1752 as described in section B.5.2. There corresponding cluster size and multiplicity histograms are filled
 1753 at the end of the clustering process. Then, the efficiency histogram is filled in case of efficiency run.
 1754 The selection is simply made by checking whether the RPC detected signals in the peak window
 1755 during this event. Nevertheless, it is useful to highlight that at this level, it is not possible yet to
 1756 discriminate in between a muon hit and noise or gamma hit. Thus, `MuonCSize_H`, `MuonCMult_H`
 1757 and `Efficiency0_H` are subjected to noise and gamma contamination. This contamination will be
 1758 estimated and corrected at the moment the results will be written into output CSV files. Finally, the
 1759 loop ends on the filling of the general hit multiplicity histogram.

1760 **B.6.4 Results calculation**

1761 As mentioned in section B.2.1, the analysis of DAQ data provides the user with 3 CSV files and
 1762 a ROOT file associated to each and every ROOT data file. The fourth CSV file is provided by the
 1763 extraction of the CEAN main frame data monitored during data taking and will be discussed later.
 1764 After looping on the data in the previous part of the analysis macro, the output files are created and a
 1765 3D loop on each RPC readout partitions is started to extract the histograms parameters and compute
 1766 the final results.

1767

1768 **B.6.4.1 Rate normalisation**

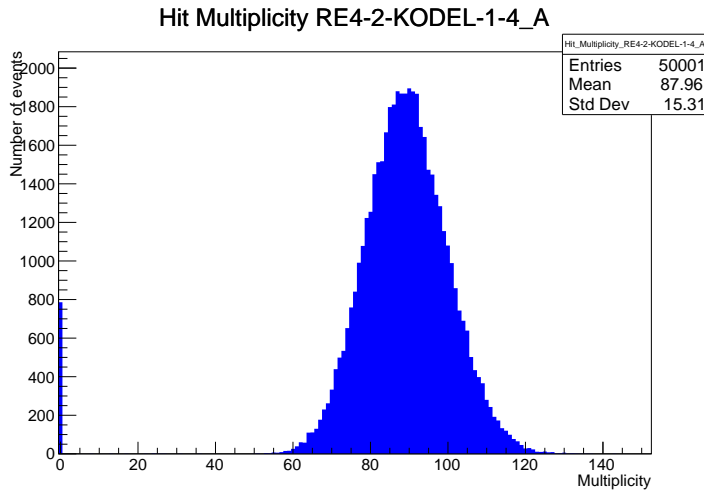


Figure B.2: The effect of the quality flag is explained by presenting the reconstructed hit multiplicity of a data file without `Quality_flag`. The artificial high content of bin 0 is the effect of corrupted data.

1769 To analyse old data format files, not containing any quality flag, it is needed to estimate the amount
 1770 of corrupted data via a fit as the corrupted data will always fill events with a fake "0 multiplicity".
 1771 Indeed, as no hits were stored in the DAQ ROOT files, these events artificially contribute to fill
 1772 the bin corresponding to a null multiplicity, as shown in Figure B.2. In the case the mean of the

hit multiplicity distribution is high, the contribution of the corrupted data can easily be evaluated for later correction by comparing the level of the bin at multiplicity 0 and of a skew fit curve that should indicate a value consistent with 0. A skew fit has been chosen over a Poisson fit as it was giving better results for lower mean multiplicity values. Nevertheless, for low irradiation cases, as explained in Appendix A.4.3, the hit multiplicity distribution mean is, on the contrary, rather small and the probability to record events without hits can't be considered small anymore, leading to a difficult and non-reliable estimation of the corruption. As can be seen in Source Code B.13, conditions have been applied to prevent bad fits and wrong corruption estimation in cases where :

- The difference in between the data for multiplicity 1 and the corresponding fit value should be lower than 1% of the total amount of data : $\frac{|n_{m=1} - sk(1)|}{N_{tot}} < 0.01$ where $n_{m=1}$ is the number of entries with multiplicity 1, $sk(1)$ the value of the skew fit, as defined by Formula 5.3, for multiplicity 1 and N_{tot} the total number of entries.

- The amount of data contained in the multiplicity 0 bin should not exceed 40% : $\frac{n_{m=0}}{N_{tot}} \leq 0.4$ where $n_{m=0}$ is the number of entries with multiplicity 0. This number has been determined to be the maximum to be able to separate the excess of data due to corruption from the hit multiplicity distribution.

Those 2 conditions need to be fulfilled to estimate the corruption of old data format files. If the fit was successful, the level of corruption is written in `Offline-Corrupted.csv` and the number of corrupted entries, refered as the integer `nEmptyEvent`, is subtracted from the total number of entries when the rate normalisation factor is computed as explicit in Source Code B.13. Note that for new data format files, the number of corrupted entries being set to 0, the definition of `rate_norm` stays valid.

```

1795 if(!isNewFormat){
    TF1* GaussFit = new TF1("gaussfit","[0]*exp(-0.5*((x-[1])/[2])**2)",0,Xmax);
    GaussFit->SetParameter(0,100);
    GaussFit->SetParameter(1,10);
    GaussFit->SetParameter(2,1);
    HitMultiplicity_H.rpc[T][S][p]->Fit(GaussFit,"LIQR","",0.5,Xmax);

    TF1* SkewFit = new TF1("skewfit","[0]*exp(-0.5*((x-[1])/[2])**2) / (1 +
→   exp(-[3]*(x-[4])))",0,Xmax);
    SkewFit->SetParameter(0,GaussFit->GetParameter(0));
    SkewFit->SetParameter(1,GaussFit->GetParameter(1));
    SkewFit->SetParameter(2,GaussFit->GetParameter(2));
    SkewFit->SetParameter(3,1);
    SkewFit->SetParameter(4,1);
    HitMultiplicity_H.rpc[T][S][p]->Fit(SkewFit,"LIQR","",0.5,Xmax);

    double fitValue = SkewFit->Eval(1,0,0,0);
    double dataValue = (double)HitMultiplicity_H.rpc[T][S][p]->GetBinContent(2);
    double difference = TMath::Abs(dataValue - fitValue);
    double fitTOdataVSentries_ratio = difference / (double)nEntries;
    bool isFitGOOD = fitTOdataVSentries_ratio < 0.01;

    double nSinglehit = (double)HitMultiplicity_H.rpc[T][S][p]->GetBinContent(1);
    double lowMultRatio = nSinglehit / (double)nEntries;
    bool isMultLOW = lowMultRatio > 0.4;

    if(isFitGOOD && !isMultLOW){
        nEmptyEvent = HitMultiplicity_H.rpc[T][S][p]->GetBinContent(1);
        nPhysics = (int)SkewFit->Eval(0,0,0,0);
        if(nPhysics < nEmptyEvent)
            nEmptyEvent = nEmptyEvent-nPhysics;
    }
}

double corrupt_ratio = 100.*(double)nEmptyEvent / (double)nEntries;
outputCorrCSV << corrupt_ratio << '\t';

float rate_norm = 0.;
float stripArea = GIFTraffic->GetStripGeo(tr,sl,p);

if(IsEfficiencyRun(RunType)){
    float noiseWindow = BMTDCWINDOW - TIMEREJECT - 2*PeakWidth.rpc[T][S][p];
    rate_norm = (nEntries-nEmptyEvent)*noiseWindow*1e-9*stripArea;
} else
    rate_norm = (nEntries-nEmptyEvent)*RDMNOISEWDW*1e-9*stripArea;

```

Source Code B.13: Definition of the rate normalisation variable. It takes into account the number of non corrupted entries and the time window used for noise calculation, to estimate the total integrated time, and the strip active area to express the result as rate per unit area.

B.6.4.2 Rate and activity

At this point, the strip rate histograms, `StripNoiseProfile_H.rpc[T][S][p]`, only contain an information about the total number of noise or rate hits each channel received during the data taking. As described in Source Code B.14, a loop on the strip channels will be used to normalise the content of the rate distribution histogram for each detector partitions. The initial number of hits recorded for a given bin will be extracted and 2 values will be computed:

- 1804 ● the strip rate, defined as the number of hits recorded in the bin normalised like described in
 1805 the previous section, using the variable `rate_norm`, and

- 1806 ● the strip activity, defined as the number of hits recorded in the bin normalised to the average
 1807 number of hits per bin contained in the partition histogram, using the variable `averageNhit`.
 1808 This value provides an information on the homogeneity of the detector response to the gamma
 1809 background or of the detector noise. An activity of 1 corresponds to an average response.
 1810 Above 1, the channel is more active than the average and bellow 1, the channel is less active.

```

int nNoise = StripNoiseProfile_H.rpc[T][S][p]->GetEntries();
float averageNhit = (nNoise>0) ? (float)(nNoise/nStripsPart) : 1.;

for(Uint st = 1; st <= nStripsPart; st++) {
    float stripRate =
        StripNoiseProfile_H.rpc[T][S][p]->GetBinContent(st)/rate_norm;
    float stripAct =
        StripNoiseProfile_H.rpc[T][S][p]->GetBinContent(st)/averageNhit;

    StripNoiseProfile_H.rpc[T][S][p]->SetBinContent(st,stripRate);
    StripActivity_H.rpc[T][S][p]->SetBinContent(st,stripAct);
}

```

1812 *Source Code B.14: Description of the loop that allows to set the content of each strip rate and strip activity
 channel for each detector partition.*

1813 On each detector partitions, which are readout by a single FEE, all the channels are not processed
 1814 by the same chip. Each chip can give a different noise response and thus, histograms using a chip
 1815 binning are used to investigate chip related noise behaviours. The average values of the strip rate
 1816 or activity grouped into a given chip are extracted using the using the function `GetChipBin()` and
 1817 stored in dedicated histograms as described in Source Codes B.15 and B.16 respectively.

```

float GetChipBin(TH1* H, Uint chip){
    Uint start = 1 + chip*NSTRIPSCHIP;
    int nActive = NSTRIPSCHIP;
    float mean = 0.;

    for(Uint b = start; b <= (chip+1)*NSTRIPSCHIP; b++) {
        float value = H->GetBinContent(b);
        mean += value;
        if(value == 0.) nActive--;
    }

    if(nActive != 0) mean /= (float)nActive;
    else mean = 0.;

    return mean;
}

```

1820 *Source Code B.15: Function used to compute the content of a bin for an histogram using chip binning.*

```

1821   for(UInt ch = 0; ch < (nStripsPart/NSTRIPSCHIP); ch++) {
1822     ChipMeanNoiseProf_H.rpc[T][S][p]->
1823       SetBinContent(ch+1,GetChipBin(StripNoiseProfile_H.rpc[T][S][p],ch));
1824     ChipActivity_H.rpc[T][S][p]->
1825       SetBinContent(ch+1,GetChipBin(StripActivity_H.rpc[T][S][p],ch));
1826   }

```

Source Code B.16: Description of the loop that allows to set the content of each chip rate and chip activity bins for each detector partition knowing the information contained in the corresponding strip distribution histograms.

The activity variable is used to evaluate the homogeneity of the detector response to background or of the detector noise. The homogeneity h_p of each detector partition can be evaluated using the formula $h_p = \exp(-\sigma_p^R / \langle R \rangle_p)$, where $\langle R \rangle_p$ is the partition mean rate and σ_p^R is the rate standard deviation calculated over the partition channels. The more homogeneously the rates are distributed and the smaller will σ_p^R be, and the closer to 1 will h_p get. On the contrary, if the standard deviation of the channel's rates is large, h_p will rapidly get to 0. This value is saved into histograms as shown in Source Code B.17 and could in the future be used to monitor through time, once extracted, the evolution of every partition homogeneity. This could be of great help to understand the apparition of eventual hot spots due to ageing of the chambers subjected to high radiation levels. The monitored homogeneity information could then be combined with a monitoring of the activity of each individual channel in order to have a finer information. Monitoring tools have been suggested and need to be developed for this purpose.

```

1835   float MeanPartSDev = GetTH1StdDev(StripNoiseProfile_H.rpc[T][S][p]);
1836   float strip_homog = (MeanPartRate==0)
1837     ? 0.
1838     : exp(-MeanPartSDev/MeanPartRate);
1839   StripHomogeneity_H.rpc[T][S][p]->Fill("exp -#left(#frac{\#sigma_{Strip}
1840     \rightarrow Rate}{\#mu_{Strip Rate}}\#right)",strip_homog);
1841   StripHomogeneity_H.rpc[T][S][p]->GetYaxis()->SetRangeUser(0.,1.);

1842   float ChipStDevMean = GetTH1StdDev(ChipMeanNoiseProf_H.rpc[T][S][p]);
1843   float chip_homog = (MeanPartRate==0)
1844     ? 0.
1845     : exp(-ChipStDevMean/MeanPartRate);
1846   ChipHomogeneity_H.rpc[T][S][p]->Fill("exp -#left(#frac{\#sigma_{Chip}
1847     \rightarrow Rate}{\#mu_{Chip Rate}}\#right)",chip_homog);
1848   ChipHomogeneity_H.rpc[T][S][p]->GetYaxis()->SetRangeUser(0.,1.);

```

Source Code B.17: Storage of the homogeneity into dedicated histograms.

1838 B.6.4.3 Strip masking tool

The offline tool is automatically called at the end of each data taking to analyse the data and offer the shifter DQM histograms to control the data quality. After the histograms have been published online in the DQM page, the shifter can decide to mask noisy or dead channels that will contribute to bias the final rate calculation by editing the mask column of `ChannelsMapping.csv` as can be seen in Figure B.3.

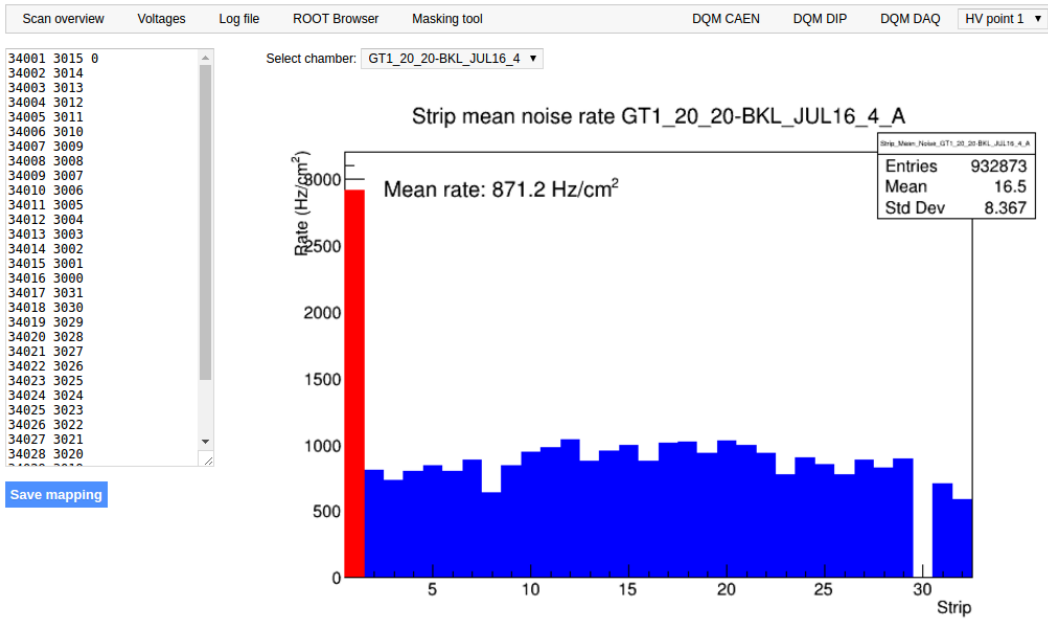


Figure B.3: Display of the masking tool page on the webDCS. The window on the left allows the shifter to edit ChannelsMapping.csv. To mask a channel, it only is needed to set the 3rd field corresponding to the strip to mask to 0. It is not necessary for older mapping file formats to add a 1 for each strip that is not masked as the code is versatile and the default behaviour is to consider missing mask fields as active strips. The effect of the mask is directly visible for noisy channels as the corresponding bin turns red. The global effect of masking strips will be an update of the rate value showed on the histogram that will take into consideration the rejected channels.

1844 From the code point of view, the function `GetTH1Mean()` is used to retrieve the mean rate par-
 1845 tition by partition after the rates have been calculated strip by strip and filled into the histograms
 1846 `StripNoiseProfile_H.rpc[T][S][p]`, as described through Source Code B.18.

1847 Once the mask for each rejected channel has been updated, the shifter can manually run the of-
 1848 fline tool again to update the DQM plots, now including the masked strips, as well the rate results
 1849 written in the output CSV file `Offline-Rate.csv`. If not done during the shifts, the strip masking
 1850 procedure needs to be carefully done by the person in charge of data analysis on the scans that were
 1851 selected to produce the final results.

```

1852   float GetTH1Mean(TH1* H) {
1853     int nBins = H->GetNbinsX();
1854     int nActive = nBins;
1855     float mean = 0.;
1856
1857     for(int b = 1; b <= nBins; b++) {
1858       float value = H->GetBinContent(b);
1859       mean += value;
1860       if(value == 0.) nActive--;
1861     }
1862
1863     if(nActive != 0) mean /= (float)nActive;
1864     else mean = 0.;
1865
1866     return mean;
1867   }

```

Source Code B.18: The function `GetTH1Mean()` is used to return the mean along the y-axis of `TH1` histograms containing rate information. In order to take into account masked strips whose rate is set to 0, the function looks for masked channels and decrement the number of active channels for each null value found.

1855 B.6.4.4 Output CSV files filling

1856 All the histograms have been filled. Parameters will then be extracted from them to compute the
 1857 final results that will later be used to produce plots. Once the results have been computed, the very
 1858 last step of the offline macro is to write these values into the corresponding CSV outputs. Aside of
 1859 the file `Offline-Corrupted.csv`, 2 CSV files are being written by the macro `offlineAnalysis()`,
 1860 `Offline-Rates.csv` and `Offline-L0-EffCl.csv` that respectively contain information about noise
 1861 or gamma rates, cluster size and multiplicity, and about level 0 reconstruction of the detector effi-
 1862 ciency, muon cluster size and multiplicity. Details on the computation and file writing are respec-
 1863 tively given in Sources Codes B.19 and B.20.

1864 **Noise/gamma background variables** are computed and written in the output file for each detector
 1865 partitions. A detector average of the hit and cluster rate is also provided, as shown through Sources
 1866 Code B.19. The variables that are written for each partition are:

- 1867 • The mean partition hit rate per unit area, `MeanPartRate`, that is extracted from the histogram
`StripNoiseProfile_H` as the mean value along the y-axis, as described in section B.6.4.3. No
 1868 error is recorded for the hit rate as this is considered a single measurement. No statistical error
 1869 can be associated to it and the systematics are unknown.
- 1870
- 1871 • The mean cluster size, `cSizePart`, is extracted from the histogram `NoiseCSize_H` and it's
 1872 statistical error, `cSizePartErr`, is taken to be 2σ of the total distribution.
- 1873 • The mean cluster multiplicity per trigger, `cMultPart`, is extracted from the histogram `NoiseCMult_H`
 1874 and it's statistical error, `cMultPartErr`, is taken to be 2σ of the total distribution. It is impor-
 1875 tant to point to the fact that this variable gives an information that is dependent on the buffer
 1876 window width used for each trigger for the calculation.
- 1877 • The mean cluster rate per unit area, `ClustPartRate`, is defined as the mean hit rate normalised

1878 to the mean cluster size and it's statistical error, `ClustPartRateErr`, is then obtained using the
 1879 relative statistical error on the mean cluster size.

```

for (UInt tr = 0; tr < GIFInfra->GetNTrolleys(); tr++) {
  UInt T = GIFInfra->GetTrolleyID(tr);

  for (UInt sl = 0; sl < GIFInfra->GetNSlots(tr); sl++) {
    UInt S = GIFInfra->GetSlotID(tr,sl) - 1;

    float MeanNoiseRate = 0.;
    float ClusterRate = 0.;
    float ClusterSDev = 0.;

    for (UInt p = 0; p < GIFInfra->GetNPartitions(tr,sl); p++) {
      float MeanPartRate = GetTH1Mean(StripNoiseProfile_H.rpc[T][S][p]);
      float cSizePart = NoiseCSIZE_H.rpc[T][S][p]->GetMean();
      float cSizePartErr = (NoiseCSIZE_H.rpc[T][S][p]->GetEntries()==0)
        ? 0.
        : 2*NoiseCSIZE_H.rpc[T][S][p]->GetStdDev() /
          sqrt(NoiseCSIZE_H.rpc[T][S][p]->GetEntries());
      float cMultPart = NoiseCMult_H.rpc[T][S][p]->GetMean();
      float cMultPartErr = (NoiseCMult_H.rpc[T][S][p]->GetEntries()==0)
        ? 0.
        : 2*NoiseCMult_H.rpc[T][S][p]->GetStdDev() /
          sqrt(NoiseCMult_H.rpc[T][S][p]->GetEntries());
      float ClustPartRate = (cSizePart==0) ? 0.
        : MeanPartRate/cSizePart;
      float ClustPartRateErr = (cSizePart==0) ? 0.
        : ClustPartRate * cSizePartErr/cSizePart;

      outputRateCSV << MeanPartRate << '\t'
        << cSizePart << '\t' << cSizePartErr << '\t'
        << cMultPart << '\t' << cMultPartErr << '\t'
        << ClustPartRate << '\t' << ClustPartRateErr << '\t';

      RPCarea += stripArea * nStripsPart;
      MeanNoiseRate += MeanPartRate * stripArea * nStripsPart;
      ClusterRate += ClustPartRate * stripArea * nStripsPart;
      ClusterSDev += (cSizePart==0)
        ? 0.
        : ClusterRate*cSizePartErr/cSizePart;
    }

    MeanNoiseRate /= RPCarea;
    ClusterRate /= RPCarea;
    ClusterSDev /= RPCarea;

    outputRateCSV << MeanNoiseRate << '\t'
      << ClusterRate << '\t' << ClusterSDev << '\t';
  }
}

```

1881 *Source Code B.19: Description of rate result calculation and writing into the CSV output Offline-Rate.csv. Are saved into the file for each detector, the mean partition rate, cluster size and cluster mutiplicity, along with their errors, for each partition and as well as a detector average.*

1882 **Muon performance variables** are computed and written in the output file for each detector parti-
 1883 tions as shown through Sources Code B.20. The variables that are written for each partition are:

- 1884 ● The muon efficiency, `eff`, extracted from the histogram `Efficiency0_H`. It is reminded that
1885 this offline tool doesn't include any tracking algorithm to identify muons from the beam and
1886 only relies on the hits arriving in the time window corresponding to the beam time. The con-
1887 tent of the efficiency histogram is thus biased by the noise/gamma background contribution
1888 into this window and is thus corrected by estimating the muon data content in the peak re-
1889 gion knowing the noise/gamma content in the rate calculation region. Both time windows
1890 being different, the choice was made to normalise the noise/gamma background calculation
1891 window to it's equivalent beam window in order to have comparable values using the variable
1892 `windowRatio`. Finally, to estimate the data ratio in the peak region, the variable `DataRatio`
1893 is defined as the ratio in between the estimated mean cluster multiplicity of the muons in the
1894 peak region, `MuonCM`, and of the total mean cluster multiplicity in the peak region, `PeakCM`.
1895 `MuonCM` is itself defined as the difference in between the total mean cluster multiplicity in the
1896 peak region and the normalised mean noise/gamma cluster multiplicity calculated outside of
1897 the peak region. The statistical error related to the efficiency, `eff_err`, is computed using a
1898 binomial distribution, as the efficiency measure the probability of "success" and "failure" to
1899 detect muons.
- 1900 ● The mean muon cluster size, `MuonCS`, is calculated using the total mean cluster size and multi-
1901 plicity in the peak region, respectively extracted from histograms `MuonCSize_H` and `MuonCMult_H`,
1902 the noise/gamma background mean cluster size and normalised multiplicity, extracted from
1903 `NoiseCSize_H` and `NoiseCMult_H`, and of the estimated muon cluster multiplicity `MuonCM` pre-
1904 viously explicated. The associated statistical error, `MuonCM_err`, is calculated using the propa-
1905 gation of errors of the mentioned variables.
- 1906 ● The mean muon cluster multiplicity in the peak region, `MuonCM`, explicated above whose sta-
1907 tistical error, `MuonCM_err`, is the sum of statistical error associated to the total mean clus-
1908 ter multiplicity in the peak reagion, `PeakCM_err`, and of the mean noise/gamma cluster size,
1909 `NoiseCM_err`.

1910 In addition to these 2 CSV files, the histograms are saved in ROOT file `Scan00XXXX_HVY_Offline.root`
1911 as explained in section B.2.1.1.

1912

```

for (UInt tr = 0; tr < GIFInfra->GetNTrolleys(); tr++) {
    UInt T = GIFInfra->GetTrolleyID(tr);
    for (UInt sl = 0; sl < GIFInfra->GetNSlots(tr); sl++) {
        UInt S = GIFInfra->GetSlotID(tr,sl) - 1;
        for (UInt p = 0; p < GIFInfra->GetNPartitions(tr,sl); p++) {
            float noiseWindow =
                BMTDCWINDOW - TIMEREJECT - 2*PeakWidth.rpc[T][S][p];
            float peakWindow = 2*PeakWidth.rpc[T][S][p];
            float windowRatio = peakWindow/noiseWindow;

            float PeakCM = MuonCMult_H.rpc[T][S][p]->GetMean();
            float PeakCS = MuonCSize_H.rpc[T][S][p]->GetMean();
            float NoiseCM = NoiseCMult_H.rpc[T][S][p]->GetMean() *windowRatio;
            float NoiseCS = NoiseCSize_H.rpc[T][S][p]->GetMean();
            float MuonCM = (PeakCM<NoiseCM) ? 0. : PeakCM-NoiseCM;
            float MuonCS = (MuonCM==0 || PeakCM*PeakCS<NoiseCM*NoiseCS)
                ? 0.
                : (PeakCM*PeakCS-NoiseCM*NoiseCS) / MuonCM;
            float PeakCM_err = (MuonCMult_H.rpc[T][S][p]->GetEntries()==0.)
                ? 0.
                : 2*MuonCMult_H.rpc[T][S][p]->GetStdDev() /
                    sqrt(MuonCMult_H.rpc[T][S][p]->GetEntries());
            float PeakCS_err = (MuonCSize_H.rpc[T][S][p]->GetEntries()==0.)
                ? 0.
                : 2*MuonCSize_H.rpc[T][S][p]->GetStdDev() /
                    sqrt(MuonCSize_H.rpc[T][S][p]->GetEntries());
            float NoiseCM_err = (NoiseCMult_H.rpc[T][S][p]->GetEntries()==0.)
                ? 0.
                : windowRatio*2*NoiseCMult_H.rpc[T][S][p]->GetStdDev() /
                    sqrt(NoiseCMult_H.rpc[T][S][p]->GetEntries());
            float NoiseCS_err = (NoiseCSize_H.rpc[T][S][p]->GetEntries()==0.)
                ? 0.
                : 2*NoiseCSize_H.rpc[T][S][p]->GetStdDev() /
                    sqrt(NoiseCSize_H.rpc[T][S][p]->GetEntries());
            float MuonCM_err = (MuonCM==0) ? 0. : PeakCM_err+NoiseCM_err;
            float MuonCS_err = (MuonCS==0 || MuonCM==0) ? 0.
                : (PeakCS*PeakCM_err + PeakCM*PeakCS_err +
                    NoiseCS*NoiseCM_err + NoiseCM*NoiseCS_err +
                    MuonCS*MuonCM_err) / MuonCM;

            float DataRatio = MuonCM/PeakCM;
            float DataRatio_err = (MuonCM==0) ? 0.
                : DataRatio*(MuonCM_err/MuonCM + PeakCM_err/PeakCM);
            float eff = DataRatio*Efficiency0_H.rpc[T][S][p]->GetMean();
            float eff_err = DataRatio*2*Efficiency0_H.rpc[T][S][p]->GetStdDev() /
                sqrt(Efficiency0_H.rpc[T][S][p]->GetEntries()) +
                Efficiency0_H.rpc[T][S][p]->GetMean()*DataRatio_err;

            outputEffCSV << eff << '\t' << eff_err << '\t'
                << MuonCS << '\t' << MuonCS_err << '\t'
                << MuonCM << '\t' << MuonCM_err << '\t';
        }
    }
}

```

1913

Source Code B.20: Description of efficiency result calculation and writing into the CSV output Offline-L0-EffCl.csv. Are saved into the file for each detector, the efficiency, corrected taking into account the background in the peak window of the time profile, muon cluster size and muon cluster multiplicity, along with their errors, for each partition and as well as a detector average.

1914

1915 B.7 Current data Analysis

1916 Detectors under test at GIF++ are connected both to a CAEN HV power supply and to a CAEN
1917 ADC that reads the currents inside of the RPC gaps bypassing the supply cable. During data tak-
1918 ing, the webDCS records into a ROOT file called `Scan00XXXX_HVY_CAEN.root` histograms with the
1919 monitored parameters of both CAEN devices. Are recorded for each RPC channels (in most cases,
1920 a channel corresponds to an RPC gap):

- 1921 • the effective voltage, HV_{eff} , set by the webDCS using the PT correction on the CAEN power
1922 supply,
- 1923 • the applied voltage, HV_{app} , monitored by the CAEN power supply, and the statistical error
1924 related to the variations of this value through time to follow the variation of the environmental
1925 parameters defined as the RMS of the histogram divided by the square root of the number of
1926 recorded points,
- 1927 • the monitored current, I_{mon} , monitored by the CAEN power supply, and the statistical error
1928 related to the variations of this value through time to follow the variation of the environmental
1929 parameters defined as the RMS of the histogram divided by the square root of the number of
1930 recorded points,
- 1931 • the corresponding current density, J_{mon} , defined as the monitored current per unit area,
1932 $J_{mon} = I_{mon}/A$, where A is the active area of the corresponding gap,
- 1933 • the ADC current, I_{ADC} , recorded through the CAEN ADC module that monitors the dark
1934 current in the gap itself. First of all, the resolution of such a module is better than that of
1935 CAEN power supplies and moreover, the current is not read-out through the HV supply line
1936 but directly at the chamber level giving the real current inside of the detector. The statistical
1937 error is defined as the RMS of the histogram distribution divided by the square root of the
1938 number of recorded points.

1939 Once extracted through a loop over the element of GIF++ infrastructure via the C++ macro
1940 `GetCurrent()`, these parameters, organised in 9 columns per detector HV supply line, are written in
1941 the output CSV file `Offline-Current.csv`. The macro can be found in the file `Current.cc`.